NASA
National
Aeronautics and
Space
Administration

EFFECT OF VIBRATION ON RETENTION CHARACTERISTICS OF SCREEN ACQUISITION SYSTEMS

Final Report
October 1977
by J. R. Tegart and A. C. Park

MARTIN MARIETTA CORPORATION
Denver Division

1. Report No. NASA CR-135264	2. Government Accession No.	3. Recipient's Catalog No.
4. Title and Subtitle Effect of Vibration on Retention Character- istics of Screen Acquisition Systems		5. Report Date October 1977
		6. Performing Organization Code
7. Author(s) J. R. Tegart, A. C. Park		8. Performing Organization Report No. MCR-77-253
9. Performing Organization Name and Address Martin Marietta Corporation P. O. Box 179 Denver, Colorado 80201		10. Work Unit No.
		11. Contract or Grant No. NAS3-20097
		13. Type of Report and Period Covered
12. Sponsoring Agency Name and Address NASA Lewis Research Center Cleveland, Ohio		Final Report May 1976 to June 1977
		14. Sponsoring Agency Code

15. Supplementary Notes

Project Manager, John C. Aydelott, NASA Lewis Research Center,
Cleveland, Ohio

16. Abstract

An analytical and experimental investigation of the effect of vibration
on the retention characteristics of screen acquisition systems was per-
formed. Vibration contributes to the pressure differential acting on a
surface tension device, which could lead to gas ingestion through the
fine-mesh screen. A survey was conducted to establish the range of the
vibration environments to be expected. Analytical methods to predict
the pressure differential due to vibration and the screen response were
developed. An extensive test program, considering the many variables
that influence the screen response, was performed. Through a direct
evaluation of the test data the effect of factors such as weave orien-
tation, vibration orientation, screen support method, screen mesh,
liquid flow and liquid subcooling was determined. Prediction of the
effect of random and sine vibration for certain conditions was
possible.

17. Key Words (Selected by Author(s)) Vibration effects Screen acquisition systems Screen performance analysis	18. Distribution Statement Unclassified - Unlimited	
19. Security Classif. (of this report) Unclassified	20. Security Classif. (of this page) Unclassified	21. No. of Pages 164 22. Price

FOREWORD

Page intentionally left blank

TABLE OF CONTENTS

LIST OF FIGURES

LIST OF TABLES

An analytical and experimental investigation of the effect of vibration on the retention characteristics of screen acquisition systems was performed. The functioning of surface tension devices using fine-mesh screens requires that the pressure differential acting on the screen be less than its pressure retention capability. When exceeded, screen breakdown will occur and gas-free expulsion of propellant will no longer be possible. Vibration, inherent in any spacecraft operational environment, is a means by which that pressure differential is increased.

In order to establish the range of the vibration environments to be expected, a survey was conducted. This survey considered present and future applications of surface tension devices and the vibration environments that they would experience.

An analytical approach to predicting the effect of vibration was developed. This approach considers the transmission of the vibration to the screens of the device and the coupling of the liquid and the screen in establishing the screen response. A method of evaluating the transient response of the gas/liquid interface within the screen was also developed. Also considered was a hydrostatic model, developed under previous studies.

A test program that would verify the analytical models and evaluate the effects of vibration was performed. A total of 551 vibration tests were performed, considering the many variables that effect the screen response. The pressure differential due to the vibration and the acceleration of the screen were measured during the tests.

Through a direct evaluation of the test results, an understanding of many of the factors influencing the vibration response was gained. The pressure differential data allowed the harmonics, waveforms and amplitudes to be studied. It was found that the screen responds to the positive peak pressure (lowering the liquid pressure with respect to the gas on the opposite side of the screen) due to the vibration. The effects of screen weave orientation, vibration orientation, screen support method, screen mesh, liquid flow, single and dual screen elements, and liquid subcooling were evaluated. The hydrostatic model is capable of predicting the effect of low frequency sine vibration and the effect of random vibration by using empirical coefficients for specific screen support methods and vibration spectra. Limited verification of the structural dynamics model was achieved.

Continued investigation of the effects of vibration, considering both empirical and theoretical based approaches, is recommended.

I. INTRODUCTION

The application of surface tension systems to propellant acquisition and control has increased significantly in recent years. These applications include both high- and low-g environments, and boost and orbital mission phases. Most of these recent applications have employed fine-mesh screen systems, as opposed to sheet-metal vane devices, due to the high adverse accelerations encountered during the missions. Proper design of these fine-mesh screen devices requires a delicate balance between the bubble point of the screen and the pressure losses in the system. To preclude gas ingestion into the controlled liquid region, i.e., screen breakdown, and assure delivery of single-phase liquid to the propulsion system, the bubble point of the screen must exceed the pressure differential imposed on the device during all phases of the mission.

The pressure differential is composed of many contributions. Gravity forces produce hydrostatic pressures. Propellant flow produces viscous losses and changes in the velocity head. Vibration is another means by which the pressure differential can be increased.

A surface tension device will be subjected to some form of vibration. It could be from a booster or from the main engines and attitude control engines of a space vehicle, even the movement of a crew can produce vibration. Vibration accelerates the liquid mass within a surface tension device in much the same way as a steady acceleration. However, due to the periodic nature of the vibration, interaction between the liquid, screen and surface tension device structure influences the pressure differential produced.

Previous investigations have shown that vibration can contribute significantly to the pressure differential acting on a surface tension device and have attempted to characterize the effect. Table I-1 summarizes the important prior studies. A large part of this work (Ref. I 1, I-3 and I-4) has been performed on a screen acquisition/expulsion device (tank plus screen system) to determine the impact of sine and random vibrations on expulsion capability. Initial tests performed by Orton were run with a spherical liner made of pleated screen and encased in an outer shell of plexiglass (Ref. I-1). These tests were conducted with both sine and random vibrations in the horizontal and vertical axes. Results showed good agreement with a hydrostatic model for vibration (see Chapter III for a discussion of this modeling technique) when applied to random and low frequency sine tests. Failure to correlate at higher sinusoidal frequencies was attributed to resonant conditions, i.e., attenuation and amplification of input. However, instrumentation was not placed on the device and a quantitative evaluation was not obtained.

Similar tests were run by Martin Marietta using a cylindrical dual-screen-liner system (Ref. I-3). Accelerometers were located on the plexiglass tank at various positions. Again, good correlation was obtained during

1

ORIGINAL PAGE IS OF POOR QUALITY

Table I-1. Prior Studies

ORGANIZATION/AUTHOR	STUDY OR REPORT TITLE (DATE PERFORMED)	TEST ARTICLE	FINE MESH SCREEN(S) TESTED	TEST FLUID	VIBRATION	RESULTS AND CONCLUSIONS	COMMENTS
G. F. Orton (Ref. 1-1)	Simulated Flight Vibration Testing of a Surface Tension Propellant Expulsion Screen (1971)	Spherical Plexiglas tank with pleated screen liner.	239 x 1370 D.T.	Isopropyl Alcohol	Sine 5-400 Hz Random 50-2000 Hz Vertical & Horizontal Axis	Hydrostatic correlation for random and low frequency sine.	Failure to correlate at higher frequencies due to resonant conditions - attenuation and amplification of input. Suggest using +1σ value instead of rms for random.
McDonnell Douglas Astronautics (Ref. 1-2)	Study and Design of a Cryogenic Propellant Acquisition System (1972)	Screen coupons with variable liquid height above screen.	250 x 1370 D.T. 200 x 1400 D.T. 200 x 600 D.T. 325 x 325 Sq. 850 x 155 Rombute	Isopropyl Alcohol	Sinusoidal Only 5-1000 Hz Frequency Range Vertical and Horizontal Axis	Majority of data follows a hydrostatic correlation. However, a significant amount deviates from this approach making results inconclusive.	No accelerometer data available. Resonant frequency of test system undetermined. No instrumentation on test article.
Martin Marietta (Ref. 1-3)	Final Report Acquisition Expulsion System for Earth Orbital Propulsion System Study. Volume III Cryogenic Test (1973)	Cylindrical Plexiglas tank with dual screen liner.	325 x 2300 D.T. and 250 x 1370 D.T.	Methanol	Sine 5-2000 Hz Random 20-2000 Hz Vertical and Horizontal Axis	Outflow and non-outflow tests gave hydrostatic correlation during random and sinusoidal tests. Deviations noted during sinusoidal testing coincided with measured resonance points.	Accelerometers located on Plexiglas tank at various positions.
Martin Marietta (Ref. 1-4)	SS/RCS Surface Tension Propellant Acquisition/Expulsion Tankage Technology (1975)	Spherical Plexiglas compartmented tank with fine mesh screen channel system.	324 x 2300 D.T.	Freon 113	Sine 5-1000 Hz Random 20-1000 Hz Vertical Axis Only	Outflow and non-outflow tests indicated hydrostatic correlation.	No unexpected effects were detected during tests.
Martin Marietta ?? Program (Ref. 1-5)	The Effect of Vibration on Surface Tension Devices (1974)	Rectangular Plexiglas channel with vertical screen partition.	325 x 2300 D.T.	Methanol	Sine 5-2000 Hz Random 3-7000 Hz Vertical Axis	Performance of test article agrees with hydrostatic correlation, except for sine input near harmonic frequencies of test article.	Preliminary assessment limited in scope prior to contract NAS8-30592.
Martin Marietta (Ref. 1-6)	Acquisition System Environmental Effects Study (1975)	Rectangular Plexiglas channel with vertical screen partition.	325 x 2300 D.T. 200 x 1400 D.T. 80 x 700 D.T.	Isopropyl Alcohol Methanol	Sine 5-2000 Hz Random 5-2000 Hz	Performance predictable by hydrostatic theory for wide band random vibration using rms levels. Hydrostatic correlation using sine vibration peak input level for frequencies not close to resonance.	Harmonic frequency analytically calculated - good agreement with test accelerometer data. Effect on screen predicted to be amplitude dependent implying reaction of screen system may be dependent on rigidity.

2

random and sine tests based on hydrostatic theory except at certain discrete frequencies during sinusoidal inputs. However, these deviations coincided with resonance points indicated by accelerometer readouts where the amplified g-level was high enough to produce screen instability based on hydrostatic theory. In contrast, some periods of resonance were observed at higher frequencies when screen instability was not observed, indicating a time or amplitude dependency. A spherical compartmented tank with a fine-mesh screen channel system was also tested by Martin Marietta during a subscale verification test program (Ref. I-4). Results showed no unexpected vibration effects on the system during a series of outflow and non-outflow tests.

In contrast, some tests have been performed on discrete screen elements. McDonnell Douglas (Ref. I-2) subjected individual screen coupons with variable liquid column heights to sine vibration. A total of five different screens were tested. Although a large part of the data was correlated by hydrostatic analysis, a significant amount deviated from this approach. These deviations were attributed to resonance conditions of the system. However, since accelerometers were not located on the test article, evaluation of screen dynamics was not possible and results were inconclusive.

The most significant prior study was performed by Martin Marietta (Ref. I-6). The effect of vibration on the capillary stability of a screen and the resultant hydrostatic pressure head due both to the rigid-body motion and screen dynamics were investigated during this work. Extensive vibration testing of a vertical, transparent channel was conducted for both random and sinusoidal vibration environments. Accelerometers were located on the channel and screen to allow a quantitative evaluation of test results. With the exception of the sinusoidal vibration at frequencies near the screen resonance, gas ingestion across the screen was found to occur when the total hydrostatic head computed from the sum of the input g-level and the static earth gravity was approximately equal to the screen bubble point.

The effective level for sine vibration was the peak value while that for random vibration was the rms value. For sine vibrations near the natural frequency of the systems, a departure from the hydrostatic effect due to the large accelerations and amplitudes was noted. A comparison of calculated and experimental data for the natural frequency of the system showed good agreement. The analysis considered screen, perforated plate, liquid, and accelerometer masses.

This program continued the investigation of the effects of vibration on the retention capability of fine-mesh screens. Using what has been learned from the previous studies, this program made an in-depth study of the many factors that can influence the response of the screen to vibration.

First, a survey was performed to establish the range of the vibration environment to be expected for typical surface tension device applications. This survey is presented in Chapter II. Then an analytical method was

3

developed that considers in detail the response of the screen of a surface tension device to vibration. The previously successful hydrostatic model was also considered as discussed in Chapter III. An experimental program that considered the many factors that effect the response of a screen device to vibration, such as screen mesh, screen support method, screen orientation and liquid flow, was devised. A test model with differential pressure and acceleration instrumentation was built and tested (Chapter IV).

The results of the testing, and the data analysis and correlation are presented in Chapter V. The conclusions and recommendations can be found in Chapter VI.

A survey was performed to establish the range of the vibration environment
to be expected for present and future applications, within the U.S. space
program, of liquid acquisition systems using fine-mesh woven screens. For
each application the available information on the configuration, opera-
tional environment and other pertinent parameters were documented. Groups
of systems with similar requirements were established and the range of
vibrational effects to be expected for each group was determined. This
information was used to define the regimes of interest for the analytical
and experimental efforts that followed.

This information is presented in three parts. First, the present and
future applications of surface tension devices are presented along with
available descriptions and mission requirements. Next the data collected
on the vibrational environments of space vehicles and spacecraft is pre-
sented. Finally, the data is compiled and grouped to define the regimes
of interest.

A.   Present and Future Applications of Surface Tension Devices

Surface tension devices have "come of age" and are now flight operational
and being considered for numerous near-future applications. It can be
presumed that surface tension devices will be strong contenders for the
acquisition system of any future liquid propulsion system.

The most prominent of the current applications for surface tension devices
is the Space Shuttle Orbiter. A surface tension device is used to supply
propellant during the start of the Orbital Maneuvering System (OMS) engines
(Figure II-1). The device must also be capable of supplying the thrusters
of the Reaction Control System (RCS). The OMS performs the large ΔV
translational maneuvers of the Space Shuttle Orbiter. The configuration
and the operational environment for the OMS acquisition system is presented
in Table II-1, as is the data for all the applications presented in this
section.

Surface tension devices are also used in the tanks of the Space Shuttle
RCS (Figures II-2 and II-3). This system controls the orbiter attitude and
accomplishes small ΔV translational maneuvers. The system must function
during a boost abort, on-orbit and during the initial phases of atmospheric
entry.

A surface tension device was used in the tanks of the Viking orbiter main
propulsion system (Figure II-4). This propulsion system performed the mid-
course corrections, Mars orbit insertion and the orbital trims. The sur-
face tension device was comprised of sheet metal vanes that took advantage
of the liquid surface tension in positioning the propellant over the tank
outlet. This program was only concerned with surface tension devices using
fine-mesh screen, but the Viking system was of interest because it is repre-
sentative of the environment for similar future spacecraft.

5

ONS PROPELLANT TANK

ALL SCREEN 165x800
PLAIN DUTCH SINGLE WEAVE

GAGING PROBE

COMMUNICATION SCREEN
(3 REMOVABLE TITANIUM PANELS)

GALLERY VENT LINE

VENT & DRAIN

GALLERY
(4 PLCS)
PLEATED SCREEN ON TANK
WALL SIDE OF GALLERY

GALLERY
DEFLECTION
PAD

COLLECTOR
FLAT GAS ARRESTOR SCREEN
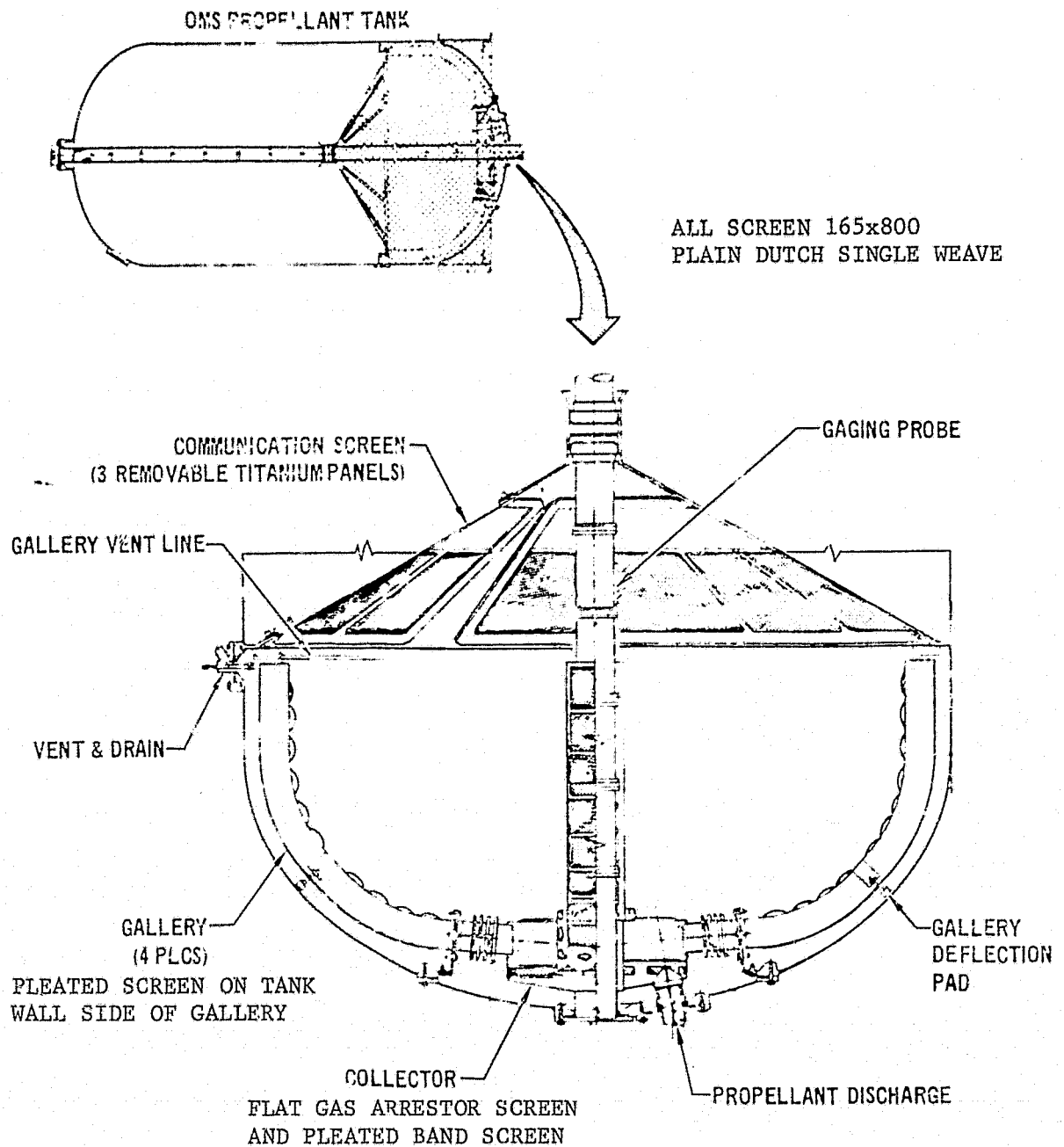AND PLEATED BAND SCREEN

PROPELLANT DISCHARGE

Figure II-1. Space Shuttle Orbital Maneuvering System
Acquisition Device (from Ref. II-1)

Table II-1. Configuration and Operational Environment

Spacecraft/ Vehicle	System	Accelerations, g	Fluids				Configuration	
			Type	State °C (°F)	Quantity, kg (lbm)	Flowrate, kg/sec (lbm/sec)	Tank, cm (in.)	Acquisition Device
Space Shuttle	Orbital Maneuvering System (Ref II-1)	Boost 3.3 Axial 0.3 Lateral	Fuel MMH	Subcooled 4.4–37.8 (40–100)	2221 (4896)	6.56 (14.46) Maximum	Cylindrical with Ellipti-cal Domes 240 (94.1) Long by 125 (49.1) Diameter 2 Pods, 2 Tanks Each	Propellant reservoir with conical screen bulkhead, 4 gallery legs and collector manifold. 165x800 Plain Dutch single weave screen. (See Figure II-1)
		Orbit +0.077 Axial 0.040 Omni-directional	Oxidizer N_2O_4	Subcooled 4.4–37.8 (40–100)	3688 (8130)	10.60 (23.36) Maximum		
	Reaction Control System (Ref II-2)	Boost 3.3 Axial 0.3 Lateral	Fuel MMH	Subcooled 4.4–37.8 (40–100)	422 (930)	3.68 (8.12) Maximum	Spherical 99 (39) Diameter 2 Tanks in each OMS Pod 2 Tanks in Nose	Compartmented tank with channel network in each compartment. Entry collector and sump, and abort duct for aft tank device. (See Figures II-2 and II-3)
		Orbit Aft Tank 0.040 Omnidirectional Fwd Tank 0.075 Omnidirectional Entry 2.5 Lateral	Oxidizer N_2O_4	Subcooled 4.4–37.8 (40–100)	675 (1488)	5.87 (12.95) Maximum		
Viking	Orbiter Main Propulsion System (Ref II-3)	0.158 Axial 2.0x10⁻⁴ Omnidirectional	Fuel MMH	Subcooled 13–29 (55–85)	561.6 (1238)	0.209 (0.460) Maximum	Cylindrical with Hemi-spherical Domes 137.2 (54.0) Long by 92.7 (36.5) Diameter	12 sheet metal vanes radially located on standpipe. (See Figure II-4)
			Oxidizer N_2O_4	Subcooled 13–29 (55–85)	799.2 (1762)	0.297 (0.655) Maximum		
Agena (Ref II-4)	Primary & Secondary Propulsion Systems	Axial 6 Max Tangential (Impulsive) 2.5x10⁻³ Max Centrifugal (Steady) 2.1x10⁻³ Max Translational (Impulsive) 6.5x10⁻³ Max	Fuel UDMH/ H_2(A200 Oil) (New)	Subcooled 4.4–32.2 (40–90)	~1800 (~4000)	Primary 7.3 (16) Secondary 0.04 (0.09)	Cylindrical, Hemispheri-cal Domes 152 (60) Diameter, 142 (56) Long	Propellant sump with retention screens and sponge assembly. Gas arrester assembly over outlets. Sump refills during primary burns, sponge assembly can refill in low-g for secondary burns. (See Figure II-5)
	Primary-Orbit Injection Secondary-Orbit Adjust		Oxidizer High Density Acid or IRFNA	Subcooled 4.4–32.2 (40–90)	~4500 (~10,000)	Primary 19 (42) Secondary 0.11 (0.24)	Cylindrical, Hemispheri-cal Domes (Upper Inverted) 153 (60) Diameter 196 (77) Long	
Transtage (Ref II-5)	Main Engines (2)	3.0 Max Axial	Fuel MMH	7.2–26.7 (45–80)	3550 (7820)	4.01 (8.83)	Cylindrical, Ellipsoidal Fwd Dome, Conical Aft Dome 118.1 (46.5) Diameter 421.6 (166.0) Long	Trap assembly with 2 check valves on barrier, screen gas arrestor (60 mesh), screen barrier to control ullage location (200 mesh and 20 mesh). (See Figure II-6 and II-7)
			Oxidizer N_2O_4	7.2–26.7 (45–80)	7100 (15,650)	8.01 (17.66)	Cylindrical, Ellipsoidal Fwd Dome, Conical Aft Dome 155.7 (61.3) Diameter 357.4 (140.7) Long	
	Attitude Control (12 Thrusters)	0.03 Max Omnidirectional	Mono-Propellant Hydrazine	7.2–26.7 (45–80)	121 (267)	0.54 (1.2) Maximum	Cylindrical, Hemispheri-cal Domes 72.1 (28.4) Diameter 89.9 (35.4) Long	Ethylene Propylene Rubber Diaphragm
Viking	Lander RCS/Deorbit (12 Thrusters)	Deorbit 0.02 Axial Entry 17 Axial Deorbit & Entry 0.06 Lateral	Mono-Propellant Hydrazine	Subcooled 7.2–32.2 (45–90)	85.3 (188)	0.15 (0.32) Maximum	Two Spherical 56.1 (22.1) Diameter	Elastomeric Diaphragm (EPT-10)
Interim Upper Stage	Reaction Control System (12 Thrusters)	Solids 10.0 Axial RCS ~0.1 Axial ~0.02 Lateral	Mono-Propellant Hydrazine	Subcooled 7.2–37.8 (45–100)	110 (243)	0.20 (0.44) Maximum	Two Spherical 56.1 (22.1) Diameter	Elastomeric Diaphragm
Centaur D-1S (Ref II-6)	Main Engine	Axial 2.51 Max Attitude Control 1.9x10⁻⁴ Max	Fuel Liquid Hydrogen	Saturated -251 (-420)	2371 (5229)	4.89 (10.8)	Cylindrical, Conospherical Fwd Dome, Common Bulkhead Aft Dome 305 (120) Diameter	Current Vehicle – Settling Rockets Proposed for Future Vehicles Start basket that can be refilled, through valves, passively cooled by wicking, throttled propellant used in subcooler heat exchanger.
			Oxidizer Liquid Oxygen	Saturated -183 (-297)	11,554 (25,450)	25.9 (57.1)	Ellipsoidal 432 (170) Diameter	
Space Storable Propulsion Module (Ref II-7 & II-8)	Main Engine & Attitude Control	Main Engine 0.048–0.19 Attitude Control 7x10⁻⁴ Max	Fuel or Mono-Propellant Hydrazine	Subcooled 4.4–37.8 (40–100)	283 (614)	Mono-Mode 0.29 (0.64) Biprop-Mode 0.24 (0.52)	Spherical 82.3 (32.4) Diameter	Sheet metal vane type surface tension device (similar to device in Viking Orbiter).
			Oxidizer Fluorine	Saturated -218 to -173 (-360 to -280)	353 (778)	0.47 (1.04)		

Table II-1. Configuration and Operational Environment (concl)

Spacecraft/ Vehicle	System	Accelerations, g	Fluids				Configuration	
			Type	State °C (°F)	Quantity, kg (lbm)	Flowrate, kg/sec (lbm/sec)	Tank, cm (in.)	Acquisition Device
Cryogenic Space Shuttle Orbiter (Ref II-9)	Integrated Supply for Orbit Maneuvering & Attitude Control	Boost 3 Axial; On-Orbit 0.070 Translational 0.086 Rotational Maximum; Entry 2.3 Lateral	Fuel Liquid Hydrogen	Saturated -251 (-420)	3900 (8600)	2.7 (6) Maximum	Spherical 358 (141) Diameter Vacuum Jacketed, 2 Tanks	Dual screen liner concept, total liner with channels, re-entry tank. (See Figure II-8)
			Oxidizer Liquid Oxygen	Saturated -183 (-297)	18,000 (40,000)	13 (29) Maximum	Spherical 242 (95.3) Diameter Vacuum Jacketed, 2 Tanks	
Cryogenic Space Shuttle Orbiter (Ref II-10)	Integrated Supply for: Orbiter Maneuvering Attitude Control Life Support Electrical Power	Boost 3 Axial; On-Orbit 0.045 Omnidirectional; Entry 0.08 Axial 1.15 Lateral	Fuel Liquid Hydrogen	Saturated -251 (-420)	4720 (10,400)	4.5 (10) Maximum	Cylindrical Hemispherical Domes 366 (144) Diameter 782 (308) Long	Screen device within start tank supplies engine until propellant in main tank is settled. Refill and vent valves are then opened to continue supply and refill start tank. (See Figure II-9)
			Oxidizer Liquid Oxygen	Saturated -183 (-297)	17,900 (39,500)	23 (50) Maximum	Cylindrical Hemispherical Domes 244 (96) Diameter 250 (98.4) Long	
Communications Satellite	Attitude Control	On-Orbit 1×10^{-5} Max Omnidirectional	Mono-Propellant Hydrazine	4.4-60 (40-140)	~59 (~130) Per Tank	0.014 (0.03) Maximum	Cylindrical Hemispherical Domes 244 (96) Diameter 250 (98.4) Long	Total Communication Surface Tension Device
Space Tug (Ref II-12)	Main Engines & Fuel Cell	Boost 3.3 Axial 0.68 Lateral; Main Engine 0.26-2.91; Reaction Control 0.005-0.05	Fuel Hydrogen	Saturated -253 (-423)	3230 (7130)	2.1 (4.7) Maximum	Spherical 57.2 (22.5) Diameter	Propellant settling with idle mode thrust or a surface tension device. (Ref II-13 & II-14) (See Figures II-10 & II-11)
			Oxidizer Oxygen	Saturated -183 (-297)	19,400 (42,800)	12.8 (28.2) Maximum	Ellipsoidal 365.8 (144.0) Diameter 258.6 (101.8) Long	
	Auxiliary Propulsion System		Mono-Propellant Hydrazine	Subcooled 4.4-79 (40-175)	92.5 (204) Per Tank	0.05-0.5 (0.1-1.2)	Spherical 56.9 (22.4) Diameter 3 Tanks	Total communication surface tension device.
	Integrated Auxiliary Propulsion System (Ref II-15)		Fuel Hydrogen	Saturated -253 (-423)	4.5 (10.0)	0.094 (0.21) Maximum	Spherical 50.8 (20.0) Diameter	Two compartments separated by screen barrier, screen covered acquisition tubes within compartments. (See Figure II-12) Tank refilled from main tank.
			Oxidizer Oxygen	Saturated -183 (-297)	9.1 (20.1)	0.31 (0.069) Maximum		
Three Axis Stabilized Vehicle (Ref II-16)	Orbit Adjust Propulsion System & Refill of Reaction Control System Tanks	Axial $+2 \times 10^{-2}$ -4.4×10^{-5}; Lateral 1.3×10^{-5}	Mono-Propellant Hydrazine	Subcooled 4.4-49 (40-120)	2059 (4540) Maximum	Orbit Adjust 0.54 (1.2) Maximum; Transfer 0.09 (0.2) Maximum	Spherical 157 (62) Diameter	Four galleries with 150x150 mesh screen windows. 400x400 mesh gas barrier at outlet. Galleries fill by capillary pumping at orbit injection. (See Figure II-13)

UPPER COMPARTMENT FLOW
CHANNEL NETWORK - FLAT
325x2300 DTDW

TRAP SCREEN -
FLAT 50x250
PDSW

COLLECTOR
PLEATED
325x2300
DTDW

ABORT
DUCT

PLENUM (BARRIER PENETRATION)
PLEATED 325x2300 DTDW

LOWER COMPARTMENT
CHANNEL NETWORK -
FLAT 325x2300 DTDW

SUMP
FLAT 325x2300 DTDW AND
FLAT 165x800 DTSW
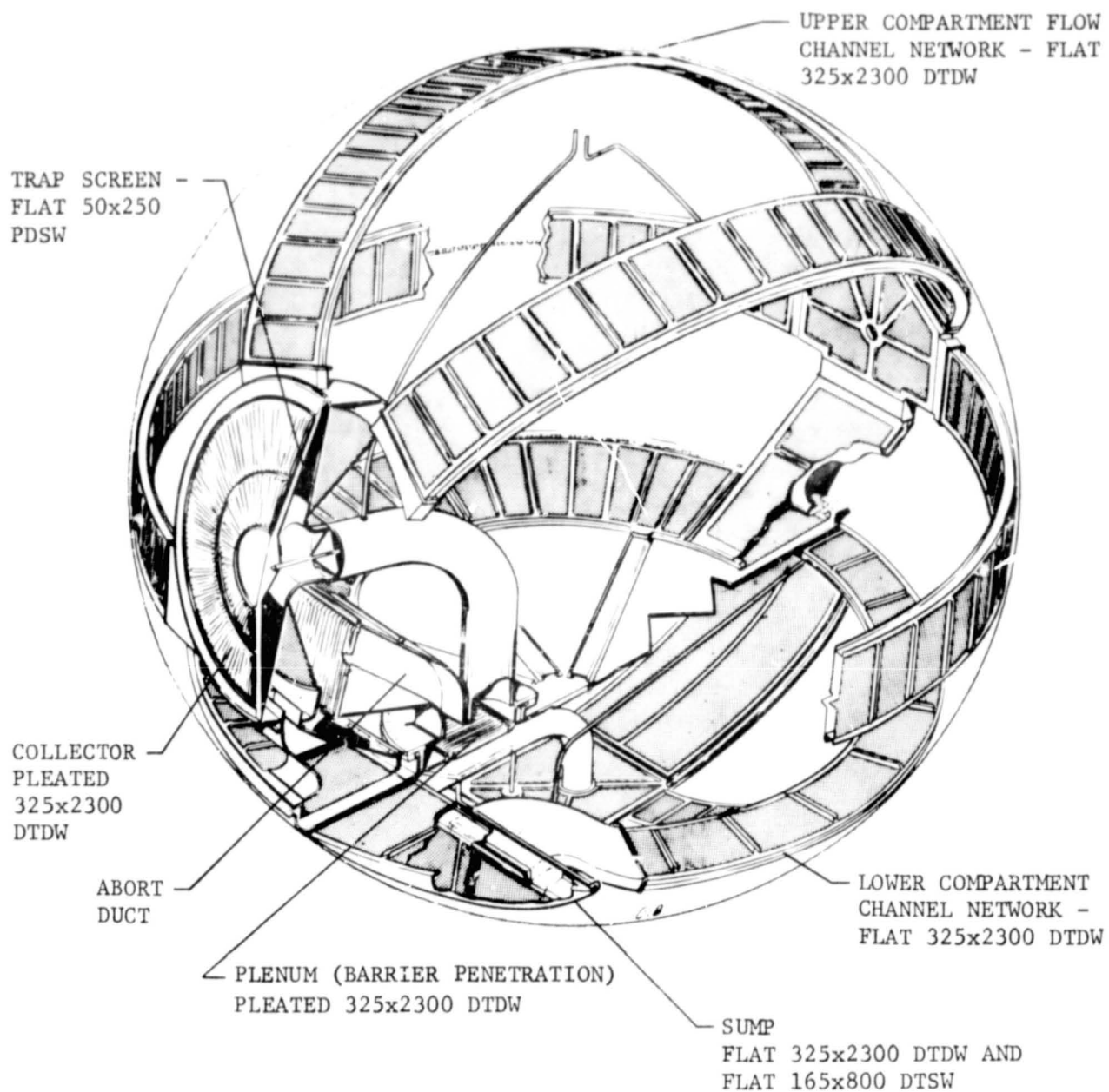
Figure II-2. Space Shuttle Reaction Control System
Acquisition Device for Aft Tanks

UPPER COMPARTMENT FLOW
CHANNEL NETWORK –
FLAT 325x2300 DTDW

BARRIER

PLENUM
(BARRIER PENETRATION)
FLAT 165x800 DTSW

LOWER COMPARTMENT
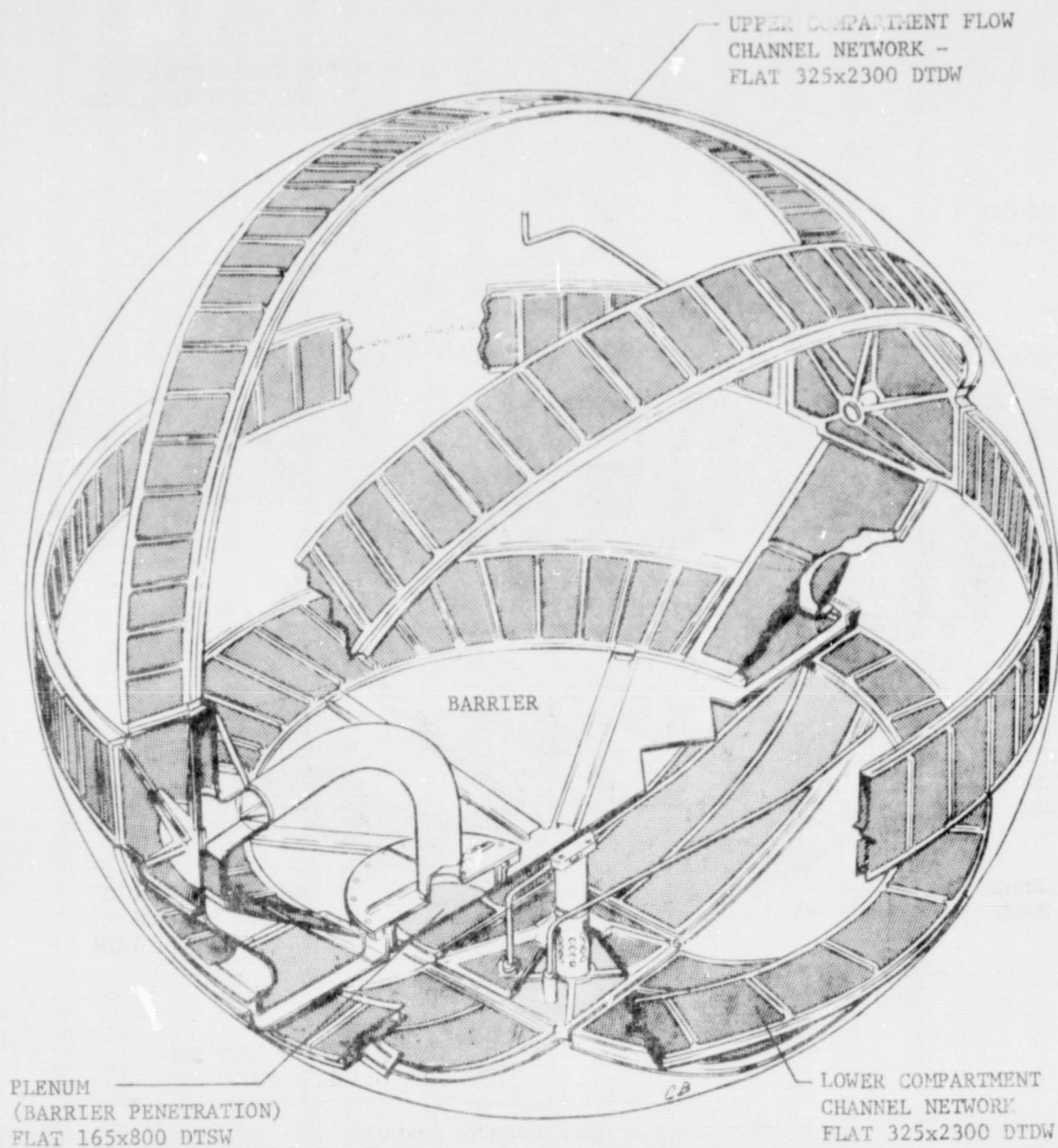CHANNEL NETWORK
FLAT 325x2300 DTDW

Figure II-3. Space Shuttle Reaction Control System
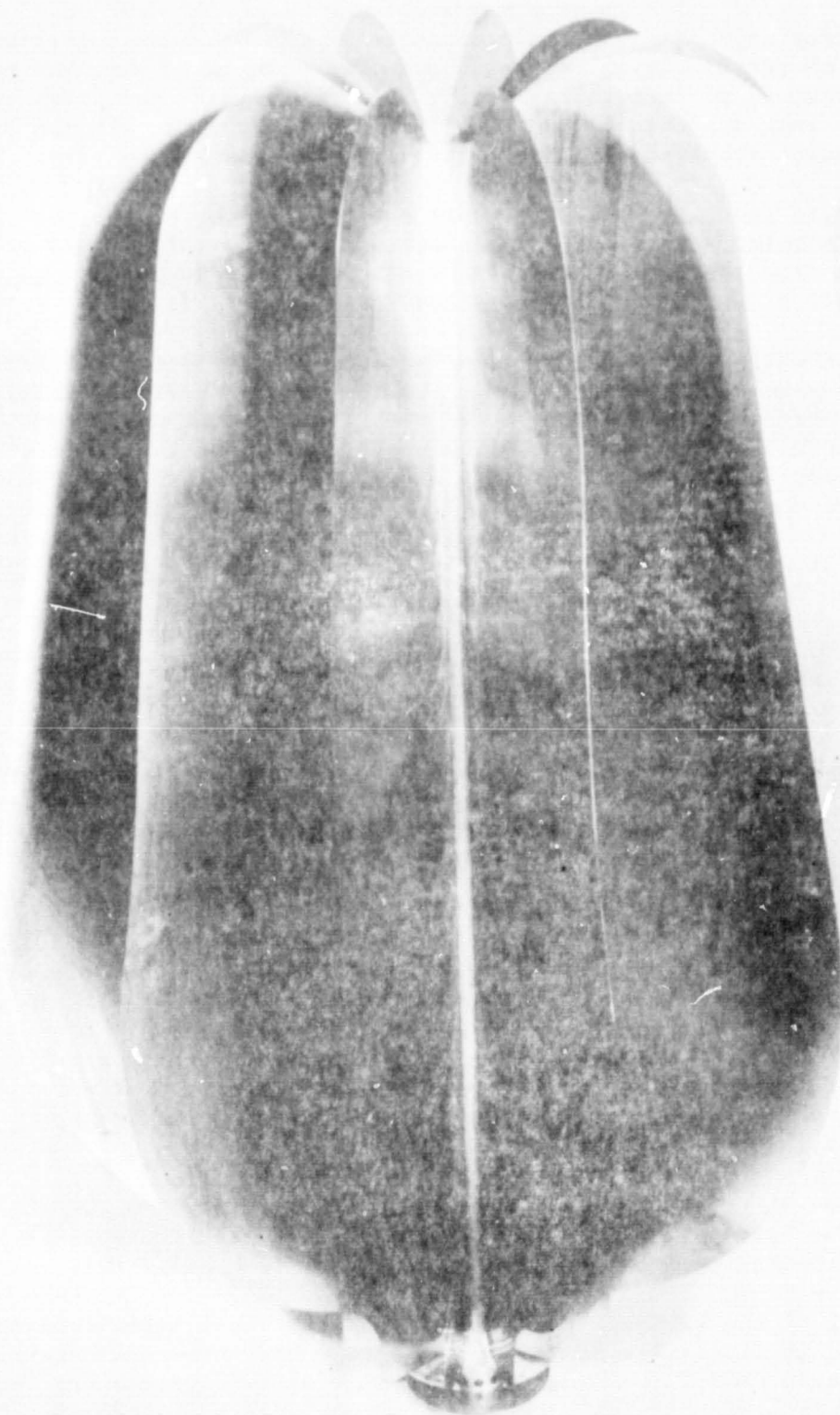Acquisition Device for Forward Tanks

10

Figure II-4. Viking Orbiter Surface Tension Device

11

The surface tension device for the Agena main engine has been operational for a number of years, having completed over 250 missions. Recently the device was improved so that it can supply both the primary and secondary propulsion systems and this device has flown six times. The details of this newer device are listed in Table II-1 and shown in Figure II-5.

The Transtage is another application that has been flight proven, having successfully completed 24 missions. A screen barrier within a trap prevents bubbles from leaving the tank and another barrier keeps the pressurization diffuser clear of propellant (Figures II-6 and II-7).

Next, some current systems, in which surface tension devices could have been used but were not, are presented. Future systems, having similar missions to these current systems, would also have similar requirements. The Viking deorbit system was mounted on the aeroshell of the lander. This system took the lander out of Mars orbit and controlled attitude up until terminal descent began (Table II-1). The aeroshell was jettisoned when the parachute was opened. Propellants were settled while the terminal descent propulsion system (mounted on the lander) operated, so the system did not require propellant acquisition.

The Interim Upper Stage, as it is presently defined, has solid main motors and a liquid attitude control system. The requirements for the attitude control system are listed in Table II-1.

A surface tension device has been suggested to replace settling rockets for an improved version of the Centaur. Since cryogenic propellants are involved, control of the thermodynamic state of the liquid within the surface tension device and the liquid delivered to the engine pumps are important factors (Table II-1).

A future system being developed by the Jet Propulsion Laboratory is a Space Storable Propulsion Module that is being considered as an orbiter of Mercury, Jupiter, Venus and Saturn and for a Mars surface sample return mission. Depending on the ΔV required, the engine can operate either in the monopropellant or bipropellant mode. A sheet metal vane device (similar to the Viking orbiter device) is currently baselined for this application. The long term compatibility of screen material with fluorine is a concern (Table II-1).

The application of surface tension devices to a future cryogenic Space Shuttle Orbiter has been evaluated. The criteria and the concepts from two such studies are listed in Table II-1 (Figures II-8 and II-9).

The capability of the propulsion systems of earth orbital satellites continues to grow (Ref. II-11). Many satellites are now three-axis stabilized (rather than spin stabilized) so propellant acquisition systems are required. The requirements listed in Table II-1 are for an Intelsat V communications satellite, now being developed.
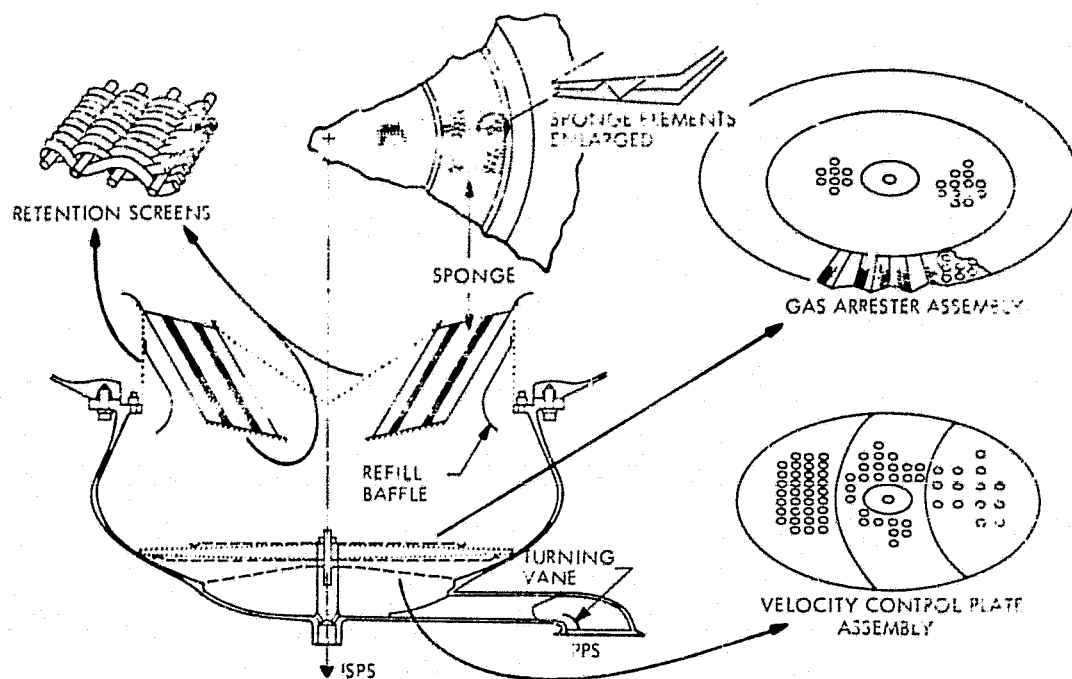
```
Upper Retention Screen    -   14 x 88
Lower Retention Screen    -   24 x 110
Gas Arrester Screen       -   120 x 120
Velocity Control Screen   -   84 x 84
```

Figure II-5. Surface Tension Device for Agena (from Ref. II-4)

CHECK VALVE

VORTEX BAFFLES

CHECK VALVE

FLOW

CHECK VALVE

A

FLOW

A

PRINCIPAL
FLOW PATHS

GAS BAFFLE

VORTEX BAFFLES

VORTEX BAFFLES

SCREEN
(60 MESH)

VIEW A-A
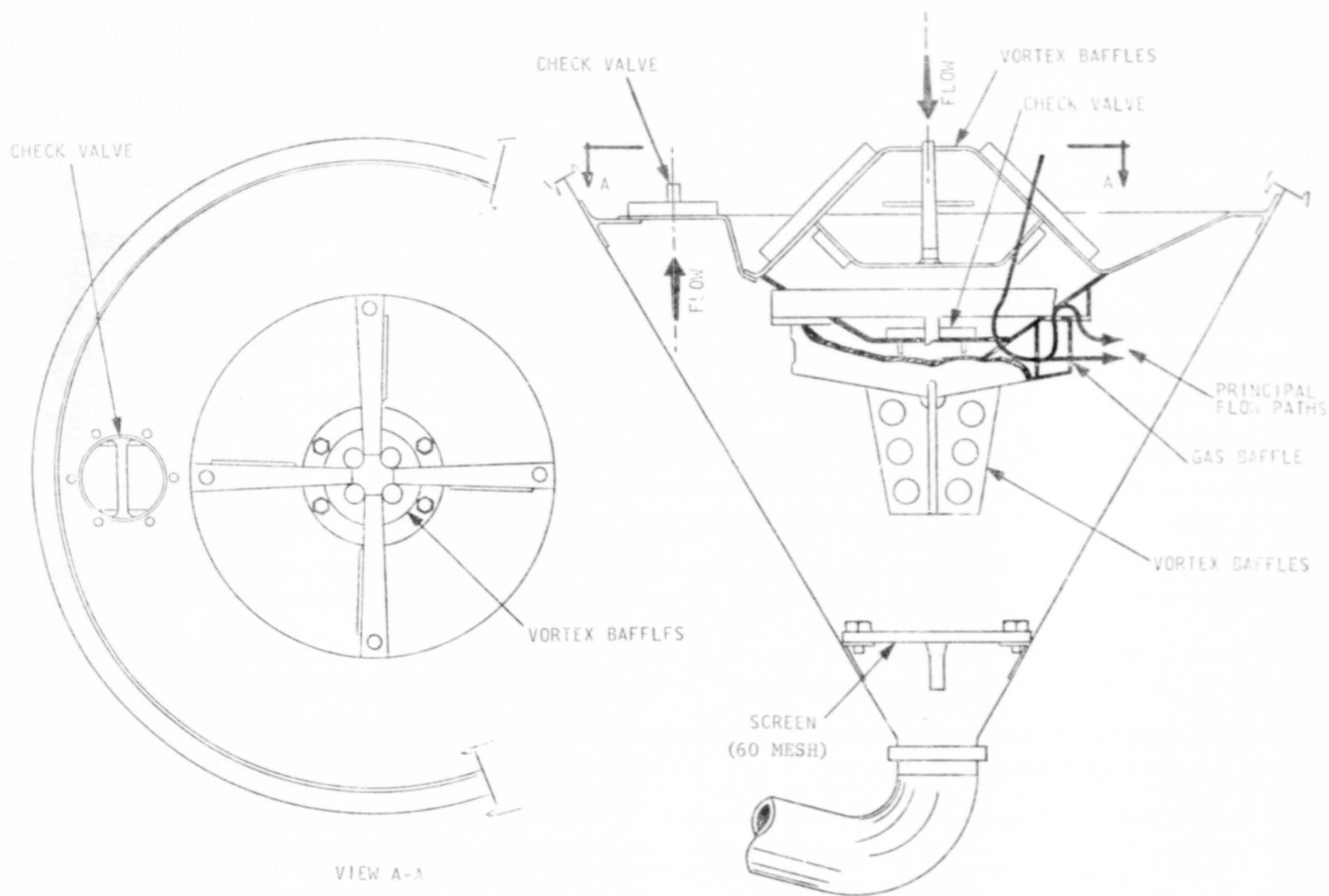
Figure II-6. Trap Assembly, Transtage Main Tanks

14

PRESSURIZATION
DIFFUSER

PRESSURIZATION INLET

MANHOLE COVER

CAPILLARY
BARRIER

SCREEN - 200 MESH BACKED
UP WITH 20 MESH,
CIRCULAR DISK
(4 LAYERS TOTAL)

SCREEN BAFFLES (2)
-20 MESH
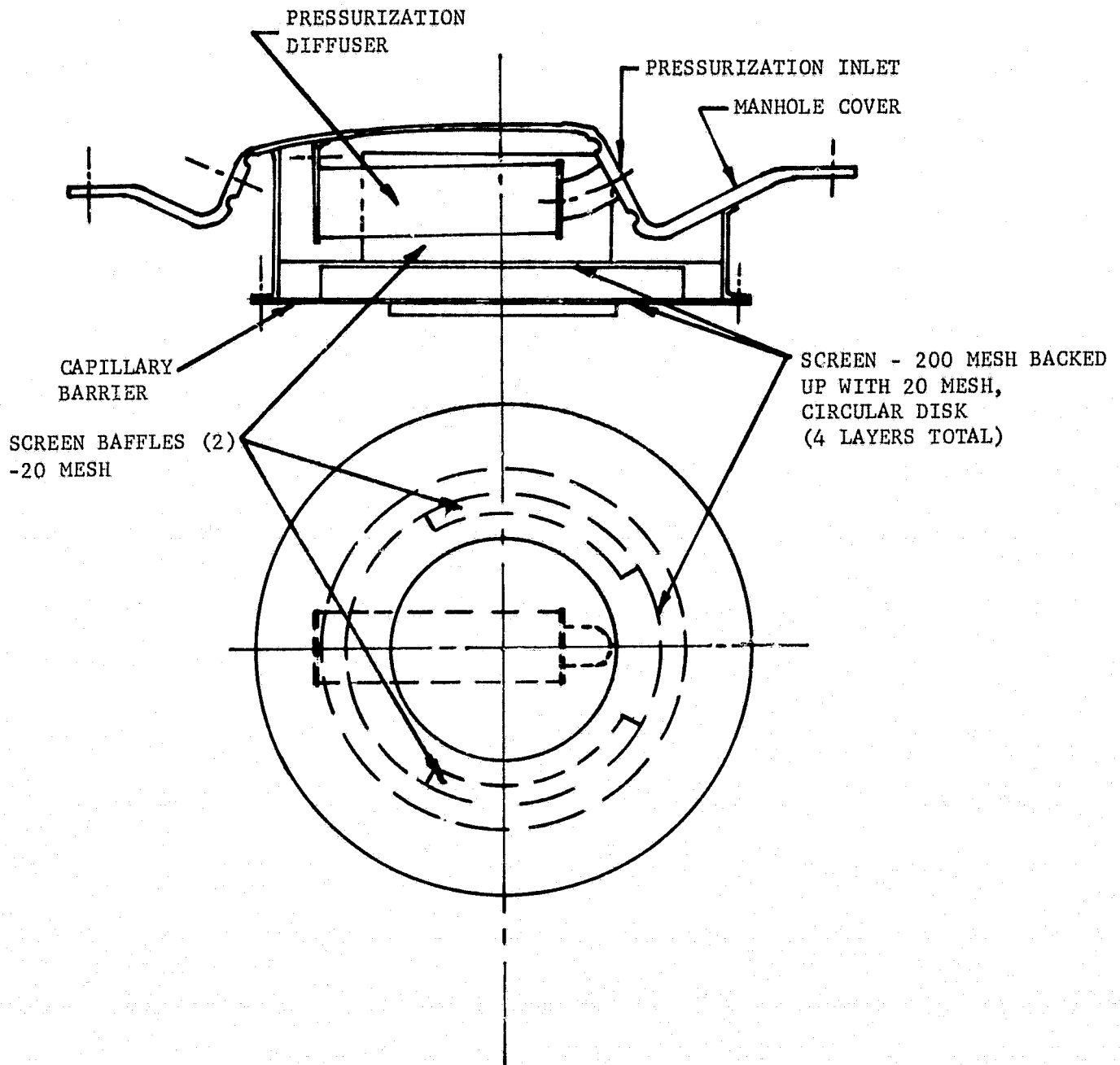
Figure II-7. Pressurization Inlet Capillary Barrier
Transtage Main Tanks

15

Pressurization/Vent Line

Multilayer Insulation

Vacuum Jacket

Liner
Suspension Cable

Girth Ring

Tank
Suspension
Cable

Capillary Liner

Flow
Channel

Channel Manifold

Pressure Vessel

Outflow Line
Reentry Tank

Fill/Drain Line

Figure II-8. Dual Screen Liner Concept for Cryogenic Orbiter (from Ref. II-9)

Figure II-9. Start Tank Concept for Cryogenic Orbiter (from Ref. II-10)

16

The Space Tug is a spacecraft that would be carried in the cargo bay of the Space Shuttle to deploy and retrieve payloads to orbits beyond the capability of the Shuttle. It is unmanned, has a cryogenic propulsion system and was to replace the Interim Upper Stage now being developed. Current plans consider a manned orbit-to-orbit shuttle instead of the Space Tug.

The Space Tug, as it was defined (Ref. II-12), made use of the idle mode thrust from the main engine to settle propellants before an engine burn. However, the use of a surface tension device has been studied (Ref. II-13, II-14 and II-15). One concept (Table II-1 and Figure II-10) has a screen trap at the tank outlet and uses a screen liner to form a vapor annulus that can be vented in low-g. Another concept (Figure II-11) uses a surface tension device within a start tank. Fill and vent valves allow the start tank to refill during the engine burn.

The third approach is an integrated system, permitting the auxiliary propulsion system (APS) to be supplied from the main tanks. A reservoir tank with a surface tension device (Figure II-12) supplies propellant to the APS thrusters. During main propulsion system (MPS) and APS translational burns the reservoir tank is refilled by opening a vent valve. The APS is used to settle the main tank propellant prior to MPS burns.

Another current application for surface tension devices is the orbit adjust propulsion system of a classified space vehicle (Figure II-13). This system is presently operational, having performed six successful missions.

Another surface tension device is presently operational in the RCA Satcom (Ref. II-17). The device is of the sheet metal vane type. Two satellites are now in orbit and each has four tanks. The criteria for this system are similar to those for a "communications satellite" presented in Table II-1.

B. Vibration Environment

The most important aspect of this survey was to identify the vibration environments that could be experienced by a surface tension device. For this reason the survey concentrated on this parameter, somewhat independent of the applications.

The usual sources of space vehicle vibration are acoustic noise, aerodynamic noise and mechanically induced excitation. During the launch and ascent phase of the mission there are many significant vibration sources: wind loads, propellant sloshing, transonic buffeting, supersonic flight, operation of engines, turbopumps and auxiliary equipment, Pogo interaction and aeroelastic interaction (Ref. II-18). Once in space, the primary source of vibration becomes the mechanical excitation of the spacecraft engine and any other operating machinery.

The vibrations produce a spectrum of frequency dependent accelerations. The sinusoidal and random components of the spectrum are used to define the environment. Rather than consider all the detailed variations with frequency, an envelope defines the magnitudes of the vibration as they are

17

75 R

PRESSURIZATION & VENT LINE

OBLATE ELLIPSOIDAL TANK

1.0

A A

105

TANK WALL

WICKING CHANNEL

SCREEN LINER

75 R

SECTION A-A
1:6

18°

TRAP

TO APS

TO PPS ENGINE

NOTE: All dimensions are in inches.

ASSEMBLY
1:15

48

1 LAYER 80 x 700/ PERF. PLATE

2 LAYERS 200 x 1400/ PERF. PLATE

5½

14

TRAP DETAIL
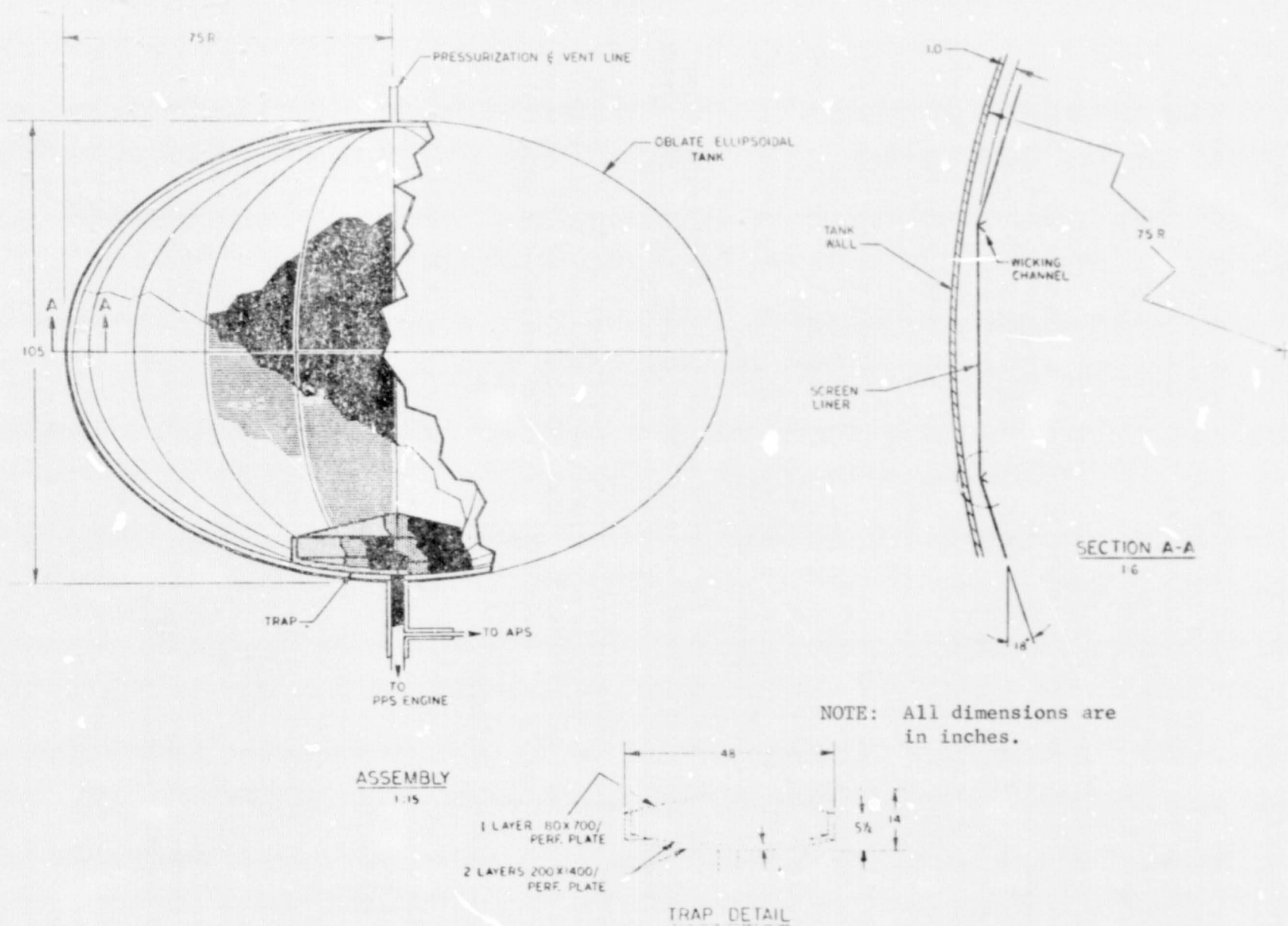
Figure II-10   Trap with Liner for Space Tug Oxidizer Tank (from Ref II-13)
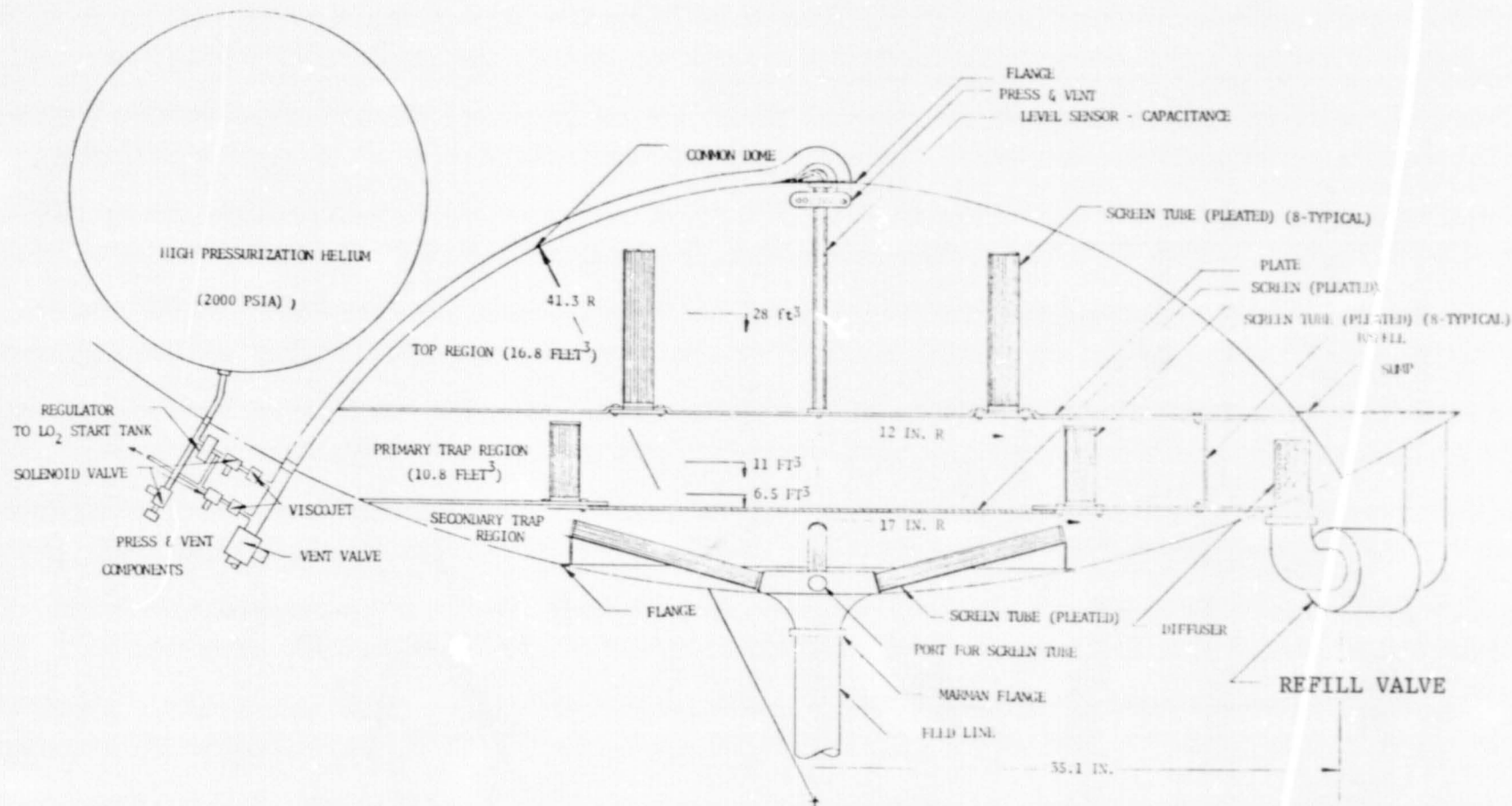
Figure II-11. Start Tank with Surface Tension Device
for Space Tug Fuel Tank (from Ref. II-14)

INLET VENT

ACQUISITION TUBES

325 X 2300 MESH SCREEN
5 PLACES

50.8-CM (20-IN.) DIAMETER

165 X 800 MESH SCREEN

LOWER COMPARTMENT

BLEED LINE

PUMP

TO ACCUMULATOR

LH$_2$ RESERVOIR SHOWN
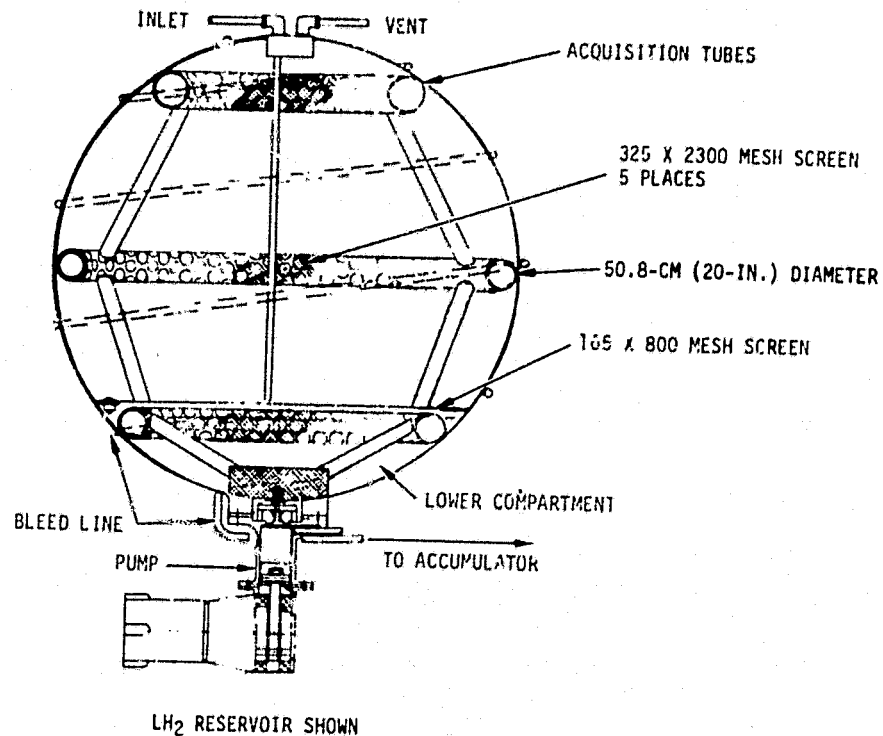
Figure II-12. Integrated APS Zero-G Reservoir
for Space Tug (Ref. II-15)

UPPER RECEIVER
ASSEMBLY

GALLERIES

SCREEN
WINDOWS

LOWER
RECEIVER
ASSEMBLY

FILTER GAS
ARRESTER SCREEN

FEED OUTLET

Figure II-13. Surface Tension Device for
Orbit Adjust Propulsion System
(from Ref. II-16)

20

used in acceptance tests. Sinusoidal amplitude is specified in terms of the peak or RMS value of the sine wave at a given frequency. Random vibration is defined with the power spectral density as a function of frequency. Power spectral density (in units of g^2/Hz) is defined as the limiting mean-square value of a random variable, in this case, acceleration per unit bandwidth. An overall RMS g-level is defined for any given random vibration spectrum and is equal to the square root of the area under the spectral density versus frequency curve.

The largest magnitude vibration is usually produced during launch and ascent, due to the acoustic coupling of the high thrust engines. Using the Space Shuttle as an example, the vibration environments specified for the OMS and RCS acquisition systems are compared in Figure II-14 (Ref. II-1 and II-2). The structure of the tank and acquisition system is designed for the launch environment, the "worst-case" condition. Neither the OMS nor the RCS devices are fully operational during launch, so the boost vibration environment is not considered for their functional design. The devices do operate in the vibration environment produced by the OMS engines (OMS roll control is the case where the RCS maintains attitude if one of the two OMS engines should fail). The RCS operates during atmospheric entry until aerodynamic control is possible, so that vibration environment must also be considered.

This situation is typical of payload/booster vibration environments. The booster produces the significant vibration environment that is specified for the structural design of the payload. This is usually not the "worst-case" condition for the operation of a surface tension device in the payload because they are not functional during launch. Either the device is completely 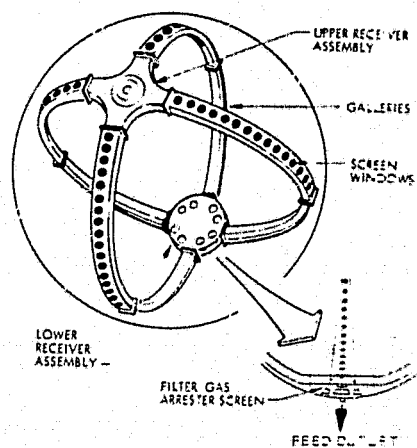submerged in propellant or breakdown of the screen has already been accepted as a consequence of the acceleration environment. Therefore, the in-space vibration environment, where the surface tension device is functional, is the prime concern.

The Viking spacecraft is another example of the varied vibration environments that can be encountered (Figures II-15 and II-16). Launch, trans-Mars injection, Mars orbit, entry and terminal descent environments were specified (Ref. II-19 and II-20).

The vibration environments that were collected fall into four general categories: (1) the environments produced by space boosters during the lift-off and ascent phase of the mission, (2) the environments produced by liquid upper stages and spacecraft main engines, (3) the environments produced by solid rocket motors, and (4) the environments produced by small thrusters and other miscellaneous disturbances.

1.   Space Boosters - The vibration environments specified for the payload on the space boosters presently in use, are shown in Figures II-17 and II-18 (Ref. II-21) (the environment for the Titan III/Centaur is shown above in Figure II-15). The levels shown are for flight acceptance testing, which envelop the actual predicted or measured flight vibration environment. Qualification levels are 1.5 to 2.0 times the flight acceptance level. These levels are typical, the actual vibration level experienced by the spacecraft propulsion system may vary, dependent on its location and mounting in the spacecraft.

21
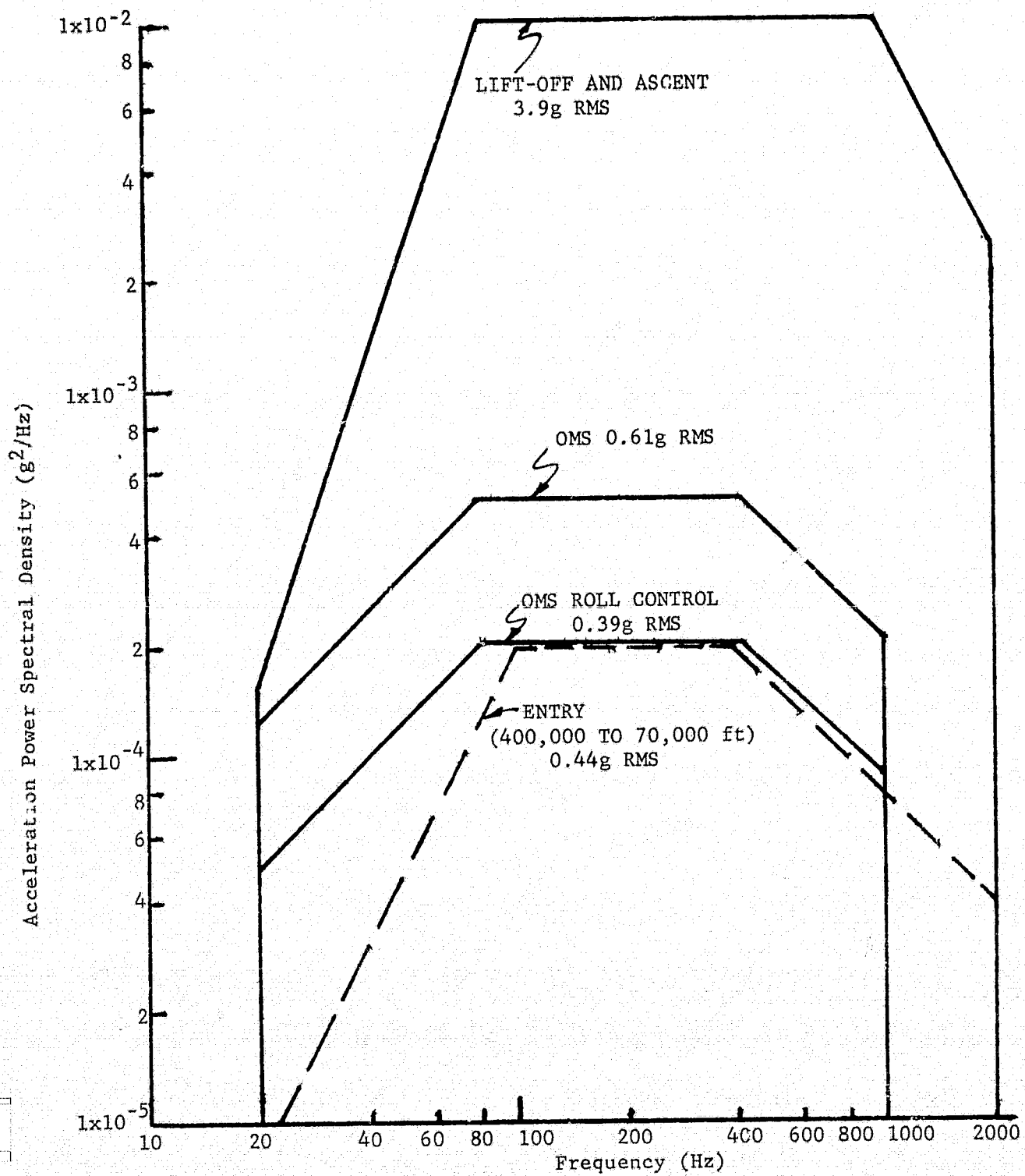
Figure II-14. Space Shuttle Random Vibration Environments
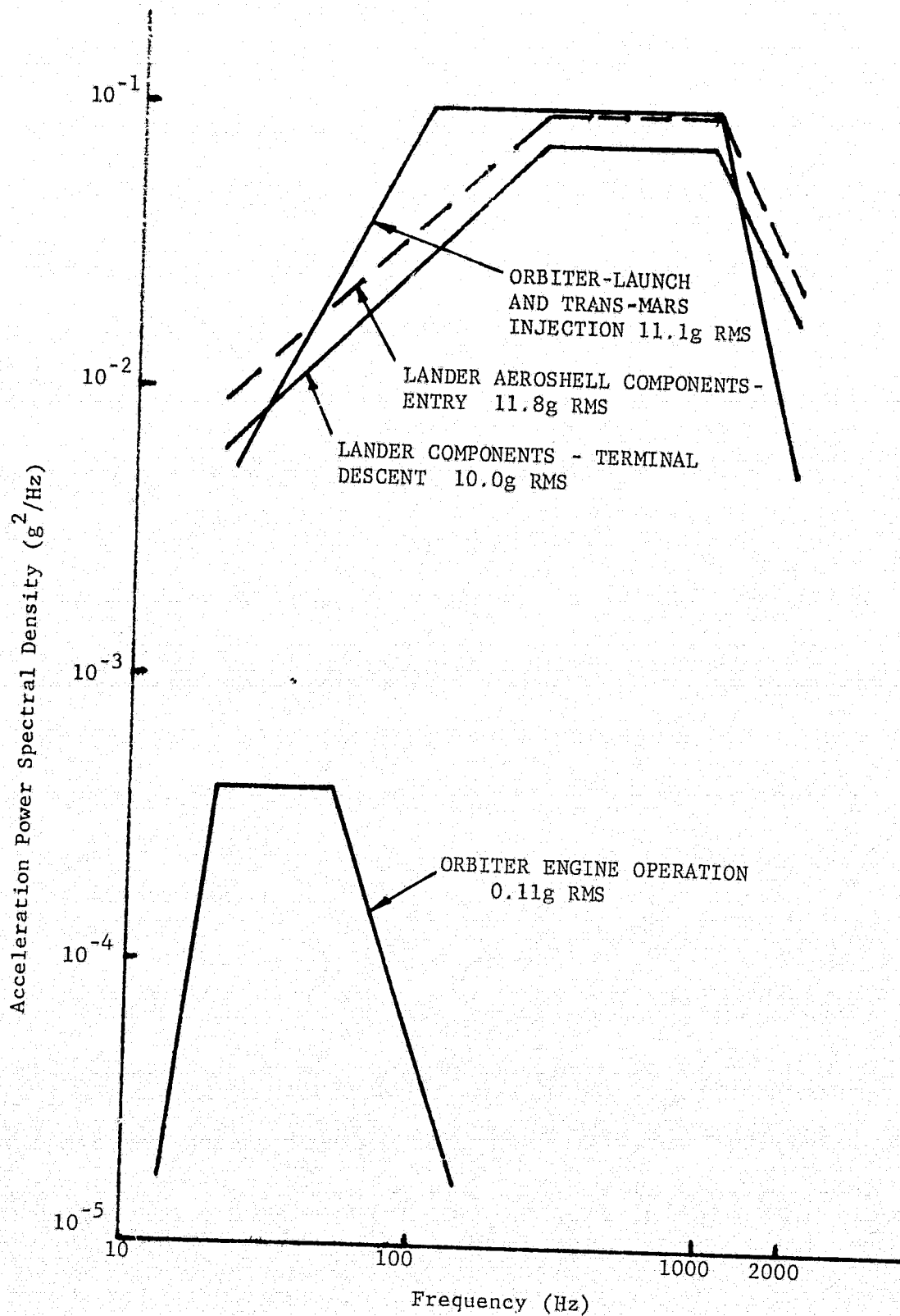
Figure II-15. Viking Random Vibration Environment

The figure's y-axis is labeled "Acceleration Power Spectral Density (g^2/Hz)" with values 10^{-1}, 10^{-2}, 10^{-3}, 10^{-4}, 10^{-5}. The x-axis is labeled "Frequency (Hz)" with values 10, 100, 1000, 2000.

Labels within the figure:

ORBITER-LAUNCH AND TRANS-MARS INJECTION 11.1g RMS

LANDER AEROSHELL COMPONENTS-ENTRY 11.8g RMS

LANDER COMPONENTS - TERMINAL DESCENT 10.0g RMS

ORBITER ENGINE OPERATION 0.11g RMS

23
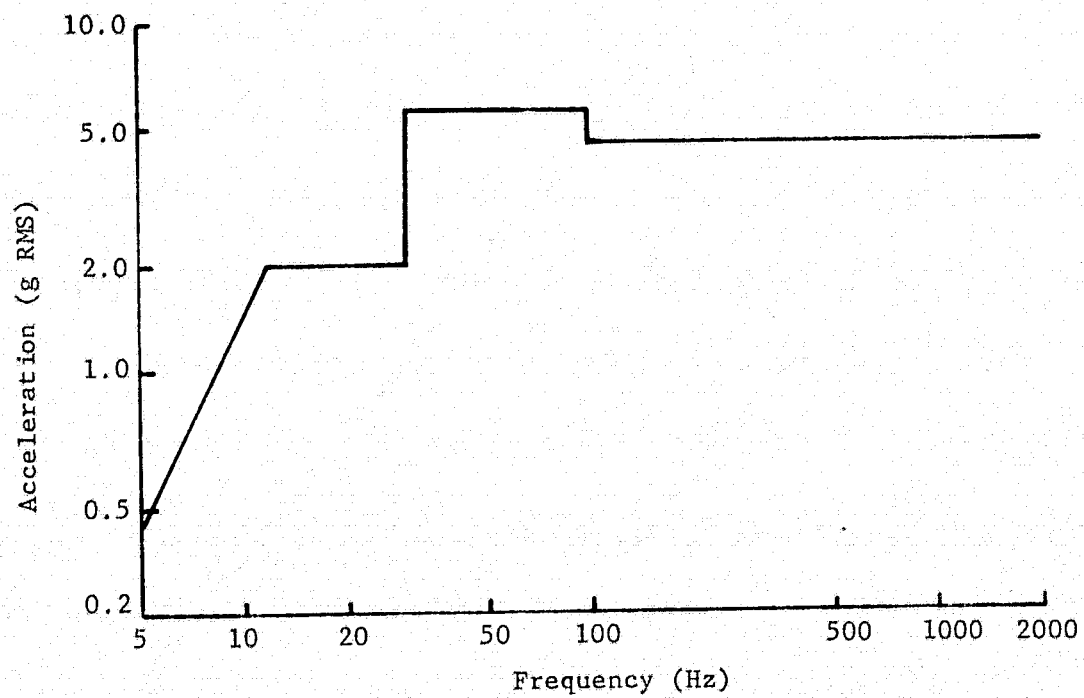
Figure II-16. Viking Orbiter Launch Sinusoidal Vibration
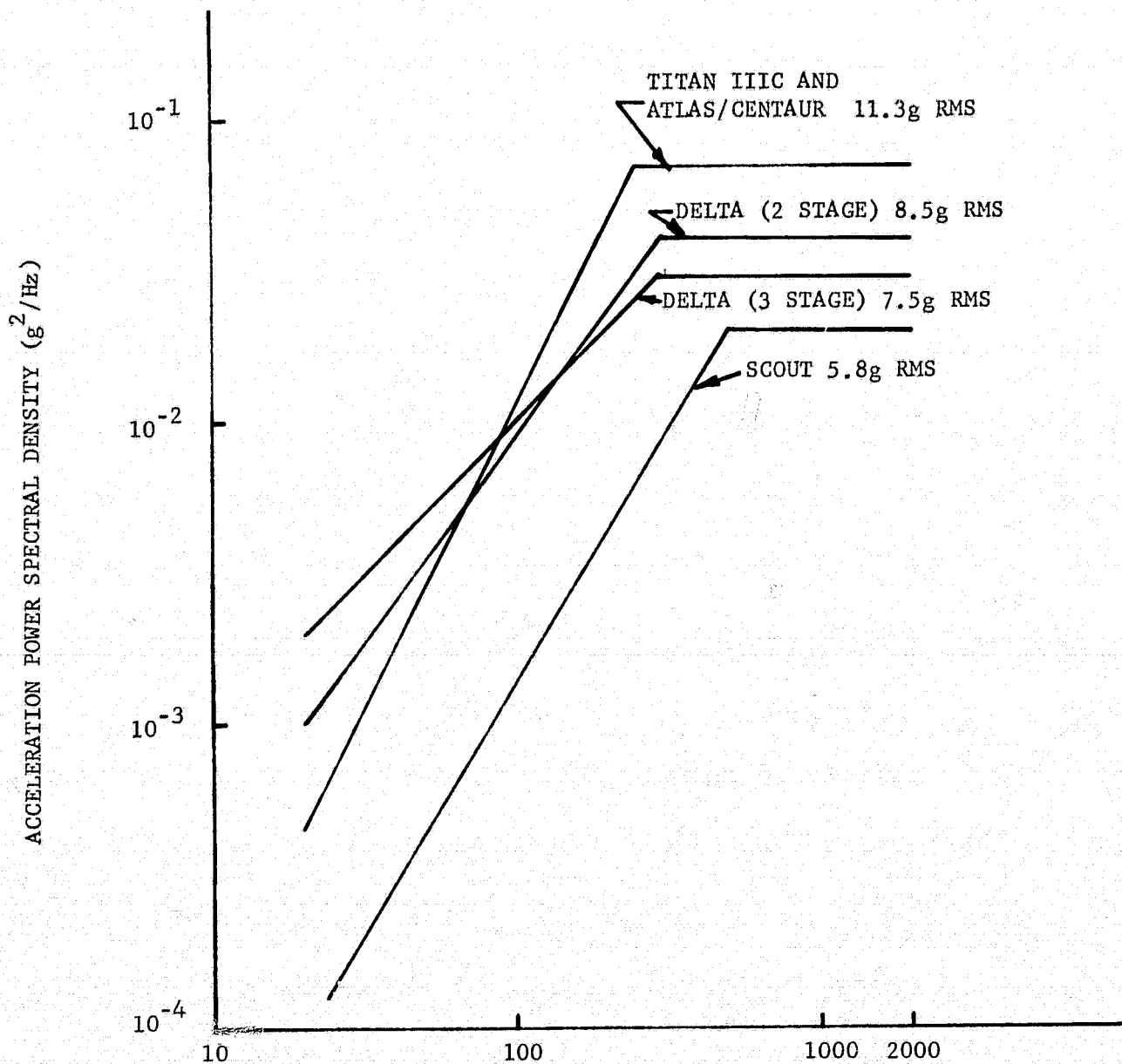
Figure II-17.   Random Vibration Acceptance
                Levels, Space Boosters

THRUST AXIS ————————
LATERAL AXIS — — — — —
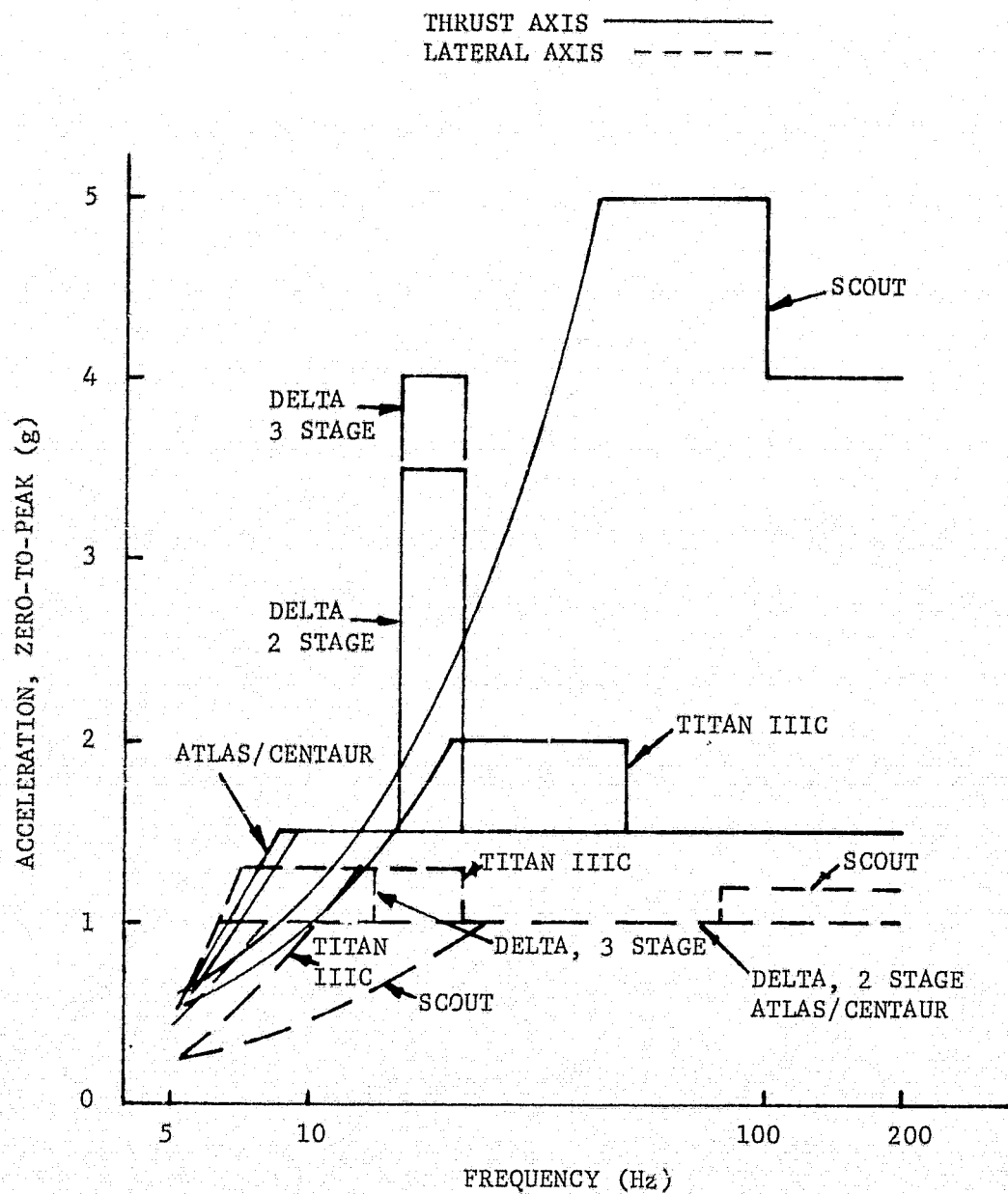
Figure II-18. Sinusoidal Vibration Flight Acceptance
Levels, Space Boosters

The Saturn V environment is representative of the environment for future large cryogenic boosters, such as a single stage to orbit booster. Reference II-22 presents a summary of the environments measured on the Saturn V. Figure II-19 shows the influence of the propellant volume on the vibration spectrum.
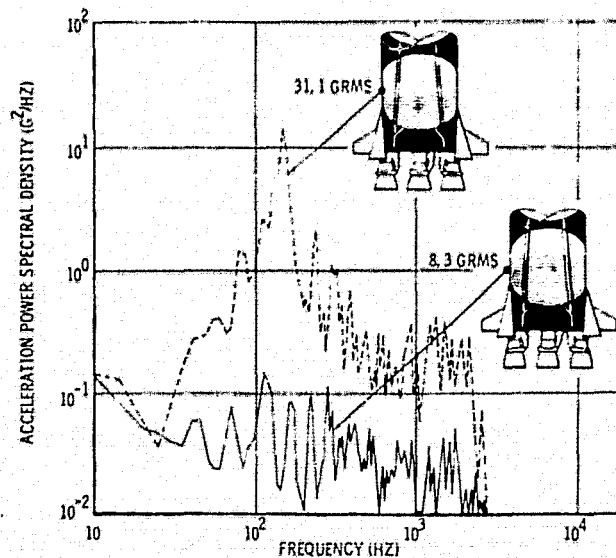
Figure II-19. Effect of Liquid Level in a Tank
on the Vibration Environment during
Static Firing

2. Spacecraft Main Engines - The vibration environment produced by the Agena and Transtage engines is shown in Figure II-20 (Ref. II-23 and II-24). The environment for both descent and ascent of the Lunar Module is shown in Figure II-21 (Ref. II-25).

3. Solid Rocket Motors - The vibration environment produced by solid rocket motors is of interest because liquid propulsion systems are also found on space vehicles with solid rocket motors. The Interim Upper Stage, with solid main engines and liquid attitude control, is a good example. Solids are also used as "kick stages" for spacecraft with liquid propulsion systems.

Acoustic pressure oscillations within the motor chamber of a solid rocket have been shown to cause a severe sinusoidal vibration environment (Ref. II-26 and II-27). Oscillatory burning produced high amplitude, narrow frequency band vibration with characteristics that vary rapidly with time. Accelerations exceeding 300g have been measured on the motor and 150 g at

27
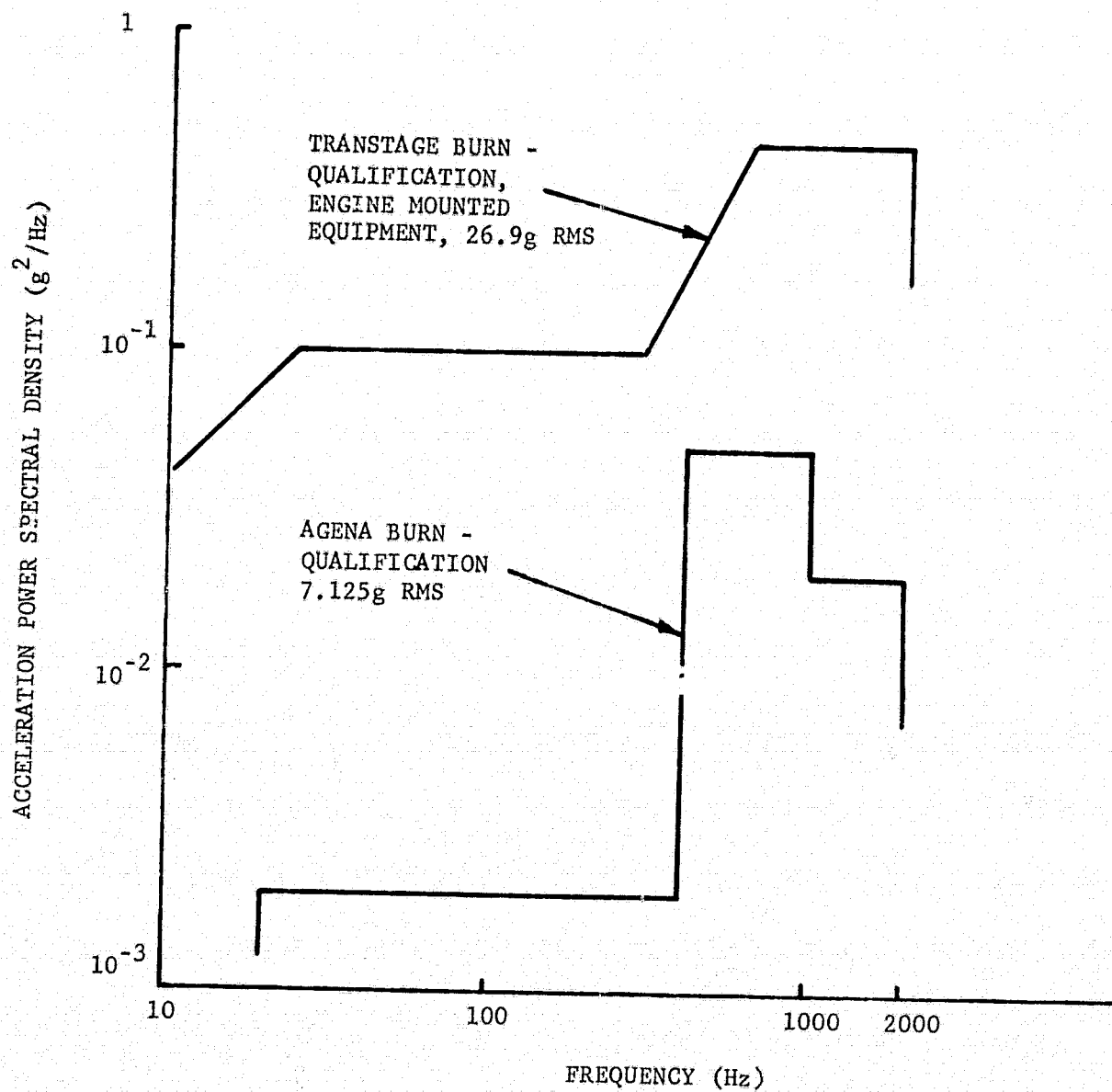
Figure II-20. Upper Stage Engines
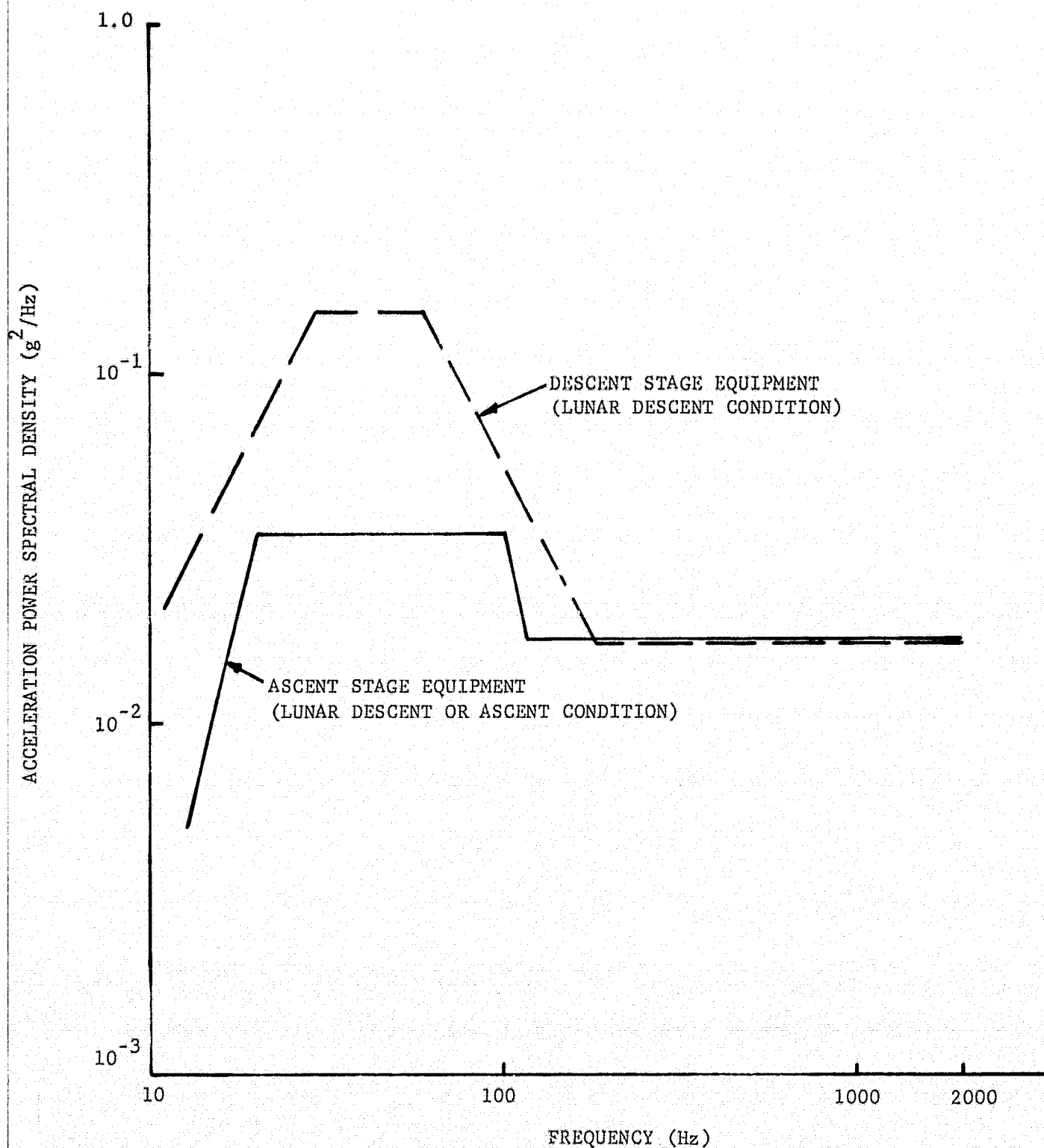
Figure II-21. Lunar Module Primary Structure
Random Vibration Criteria

29

a forward mounting adapter (Ref. II-26). However, these rocket motors are the fairly large engines of the Minuteman and Poseidon missiles.

With a somewhat smaller rocket motor (Nike, Ref. II-28), another unusual vibration environment was discovered. Oscillatory burning caused significant vibration in the frequency range of 10 to 12.4 KHz. Vibration levels of 31.5g RMS were measured in the first 1.2 seconds of burning, but then dropped to 7.4g RMS.

Rocket motors currently used for "kick stages" apparently burn with very little oscillation and do not produce a significant vibration environment. Specifications for the interface with the spacecraft require vibrations less than 2g, zero-to-peak. A g-level of 0.018 was measured from 10 to 250 Hz for a Thiokol TE-M-616-1 motor (Ref. II-29). Measurements made on a Thiokol TE-M-604 were all less than 10^{-5} g^2/Hz over 5 to 3000 Hz, and this appears to be typical of spacecraft solid motors (Ref. II-30). A TE-M-364-19 rocket motor for FLTSATCOM produced a maximum vibration of 3.16g peak-to-peak along a lateral axis over the frequency range of 0 to 5 KHz (Ref. II-31).

4. <u>Small Thrusters</u> - Very little information is available on the in-space vibration environment produced by small thrusters and other small disturbances. A number of government agencies and aerospace companies were contacted and they confirmed this fact. The Shock and Vibration Information Center performed a literature search on this subject and they could not find anything.

During the Skylab missions some measurements of the spacecraft disturbances produced by crew motion were made (Ref. II-32). Shown in Figure II-22 is one of the more severe force spectra produced by the flapping of the astronauts' arms. The force can be converted to an acceleration for a given spacecraft mass. Accelerations as large at 10^{-3}g with a frequency spectrum of about one to several thousand Hertz were experienced as the Skylab coasted in space. These disturbances have been referred to as "G-Jitter" and could have a significant impact on processes or experiments that were intended to be performed in zero-g (Ref. II-33).

C.   Compilation of Survey Results

The survey of the applications for surface tension acquisition systems included all the currently operational spacecraft using surface tension devices. They are:

Agena - Screen trap in main tanks.
Transtage - Screen trap and ullage barrier in main tanks.
Viking Orbiter - Vane device in main tanks.
Three Axis Stabilized Vehicle - Screen galleries in orbit adjust tank.
RCA Satcom - Vane device in attitude control tanks.

Surface tension devices presently being actively developed for flight systems consisted of the following:
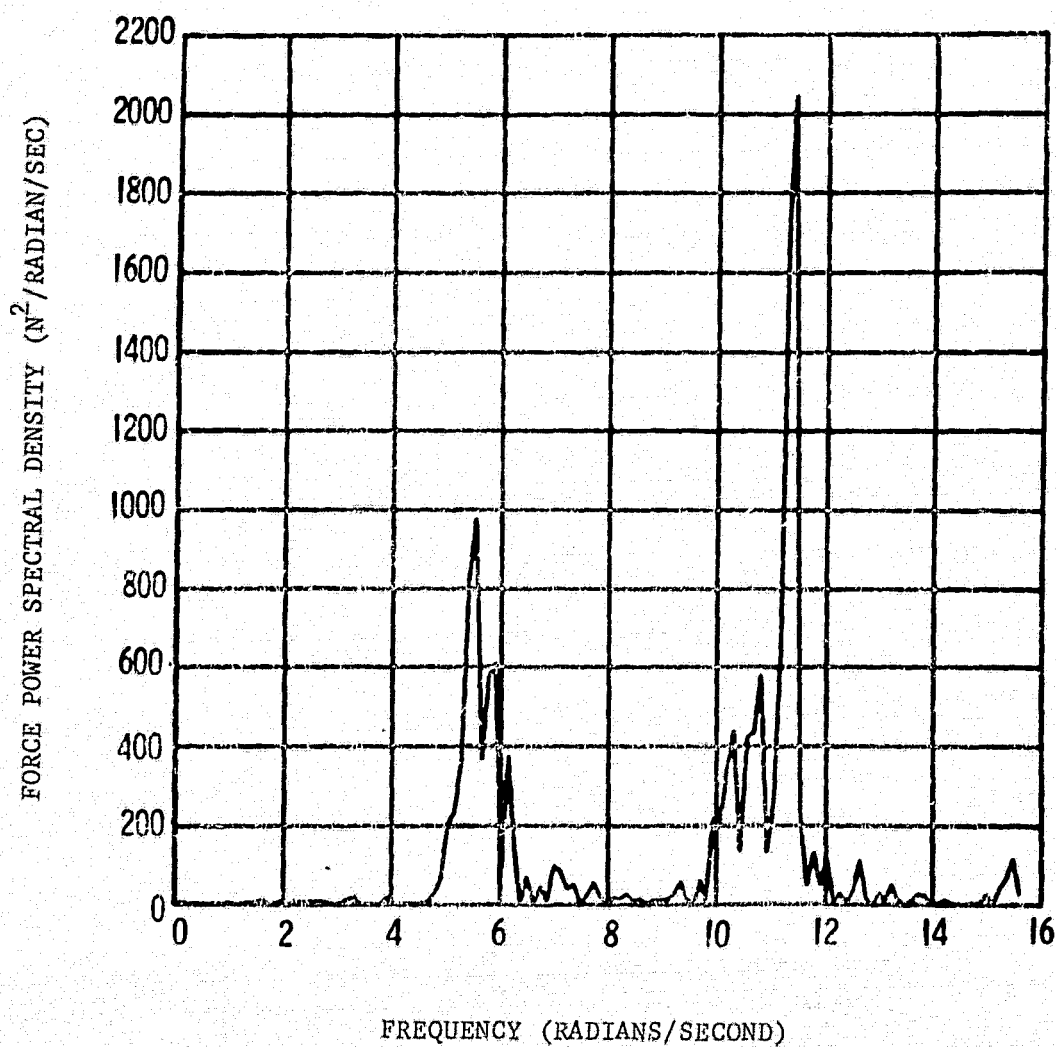
Figure II-22. Power Spectral Density
Due to Arm Flapping
(From Ref. II-32)

Space Shuttle Reaction Control System - Screen channels with barrier in RCS tanks.

Space Shuttle Orbital Maneuvering System - Screen traps in OMS tanks.

Intelsat V Communications Satellite - Screen channels in attitude control system tanks.

Future applications include such systems as communications satellites, Space Tug and a cryogenic Space Shuttle. This survey was intended to consider only applications of surface tension devices using fine-mesh screen within the U.S. Space Program. Some spacecraft falling outside those limits have been added because they are representative of future systems and contributed to the depth of the survey.

A similar survey was recently performed (Ref. II-34), except that it was directed toward flow transients. The data from that survey was reviewed to insure that this survey was complete. Another recent survey of potential receivers for in-orbit supply, provides a comprehensive list of future spacecraft, as envisioned by the NASA (Ref. II-35). The more significant systems listed in that survey have been included in this survey. The scope of possible future spacecraft continues to grow. Large space stations for in-space manufacturing, solar energy collection, observation and communication are considered to be feasible future objectives within the next 25 years (Ref. II-36 and II-37).

Based on the results of this survey, the potential for surface tension device applications is unlimited. The possible applications cover a wide range of sizes, flow rates and acceleration environments. The fluids of interest are primarily N_2O_4, MMH, oxygen, hydrogen and hydrazine. The screens being used ranged from a 60 x 60 square weave to a 325 x 2300 Dutch twill.

In many cases the vibration environment specified for the applications collected in the first part of this survey was available. In other cases the information was not available or only the environment for a portion of the mission, when vibration was a maximum (such as boost), was specified. Therefore, a wide ranging search for information on vibration environments was conducted, since this was the most significant parameter of the survey. The Shock and Vibration Information Center of the Naval Research Laboratory, and various NASA centers and aerospace companies were contacted during the survey.

The vibration environments were found to fall into four general categories, based on the source of the vibration. The categories are: (1) space boosters during lift-off and ascent operation, (2) main engines of upper stages and spacecraft, (3) solid rocket motors, and (4) small thrusters and miscellaneous disturbances.

The environments produced by space boosters were found to be well documented. Some representative data was found for liquid main engines and solid rockets. Essentially no data could be found on the in-space operation of small

thrusters, but some data on disturbances such as crew movement was found. Since the structural design of the spacecraft is usually the reason for the vibration specification, there has been little interest in low level vibration sources.

To summarize the vibration environments, they are of two types: random and sinusoidal. Random vibration is specified over a frequency range of 10 to 2,000 Hz. The amplitude is stated in g RMS, based on the power spectral density. Amplitudes ranging from 0.11g RMS for a main engine to 11.3 g RMS for a booster were found. Sinusoidal vibrations range in frequency from 5 to 2,000 Hz with amplitudes up to 5g zero-to-peak.

Care must be taken in using this collected data since the vibration level is a function of factors such as the location in the spacecraft and liquid levels. The environments presented are only typical of what may actually be experienced. In addition, some environments presented are as actually measured, some are acceptance test levels and some have safety factors applied to make the qualification test levels.

III.   VIBRATIONAL EFFECTS ANALYSIS

Analytical models to predict the retention characteristics of a screen acquisition system in any given vibration environment were developed. Two different analytical approaches were considered. One was to use the rather simple hydrostatic model that was developed under previous vibration studies. The second approach integrates two models, a structural dynamics model and a bubble growth model, to consider in more detail the factors involved in the response of the screen to vibration. In this chapter these two approaches are discussed.

A.   Hydrostatic Model

Past studies have shown that the effects of vibration on the retention capability of a screen can be predicted with a simple hydrostatic model (see Chapter I, Introduction, for a discussion of the previous vibration studies). The most recent and comprehensive of these studies (Ref. III-1) was used to define the state of development of the hydrostatic model. This model assumes the effect of the vibration to be hydrostatic in nature. The effect of the vibration is to create a pressure differential between the gas and liquid on opposite sides of the screen, with the liquid pressure being less than the gas pressure. This pressure differential has the form:

$$\Delta P_V = \rho g h \tag{1}$$

where the acceleration is due to the vibration and the height is a distance over which the vibration acts (a list of symbols can be found in Appendix B).

This model depends on test data to establish how the values of acceleration and height are defined. Data from previous tests (Ref. III-1) were correlated using this model when the acceleration was defined as the vibration amplitude input to the test model. For random vibration, it was the RMS level of the input. For sinusoidal vibration, the zero-to-peak amplitude was used at high frequencies (frequencies greater than 200 Hz). At lower frequencies, near the first harmonic of the structure, amplification must be taken into account. The height used was the length of screen exposed to the ullage, parallel to the direction of the vibration. The past verification of this model has been limited to fairly rigid screen specimens.

The model is applied to test data by predicting the contribution of vibration to the pressure differentials acting on the screen when screen breakdown occurs. At the point the retention capability of the screen is exceeded, the pressure differentials within the test system are related as follows:

$$\Delta P_c \geq \Delta P_v + \Delta P_s + \Delta P_f. \tag{2}$$

The pressure differentials due to vibration, hydrostatic head and flow must exceed the retention capability of the screen when breakdown occurs. The retention capability of the screen is measured by the standard bubble point test. The hydrostatic pressure differential due to one-g and the flow losses

(if present) can be calculated from established theory. Therefore, the value of ΔP_v can be determined. Considering now the hydrostatic model (Equation (1)), the values of acceleration and height that yield the proper value for ΔP_v can be determined. Empirical coefficients can also be applied to the model to account for various structural and screen support effects.

The hydrostatic model is applied to the design of surface tension devices in much the same way. If the model has been empirically verified for the surface tension device configuration of interest, the values of acceleration, height and coefficients are used to predict the value of ΔP_v for the specified vibration environment. This value is then used in conjunction with the other pressure differentials acting on the device to predict its performance.

B.   Screen Dynamics Approach

This approach to the analysis of the effects of vibration considers in detail all aspects of the system response. The approach is outlined in Figure III-1. It consists of two analytical models; a structural dynamics model and a bubble growth model. The input vibration is defined at the tank support structure, so the transmission of the vibration to the surface tension device must be considered. For the purpose of this study, the input was considered to be directly applied to the surface tension device, so an analysis of transmission of the vibration (box shown in dashed lines in Figure III-1) was not required.

The structural dynamics model predicts the pressure due to the vibration, taking into account the screen, its support structure, the liquid mass and liquid flow. The bubble growth model evaluates the pressure retention capability of the screen to determine if screen breakdown will occur due to the oscillating pressure of the vibration. This model considers the screen geometry, liquid properties and the steady pressure differentials acting on the screen. These two models are discussed in the following sections.

1.   Structural Dynamics Model - Our development of a structural dynamics model to predict the oscillatory pressure environment in screen liquid acquisition systems is centered on a simple analog, namely a single degree-of-freedom elemental model applicable to a controlled set of test specimens. It is expected that knowledge gained from tests on the controlled specimens can be used to qualify this elemental approach and yield a prediction of the characteristic system parameters, i.e., mass, damping and stiffness. We expected that such insight, in conjunction with a continuously expanding test program, would then lend itself to gradual extensions of the elemental model to encompass more complex screen configurations. Additionally, it was anticipated that the expanded model would be useful in estimating the pressure environment in flight article hardware. The following text details development of the single degree-of-freedom elemental model.

a.   Basic Equation of Motion - Consider a liquid/container system with a single compliant screen element as shown in Figure III-2. If we assume a linear single degree-of-freedom is representative of this system we have the basic equation

36
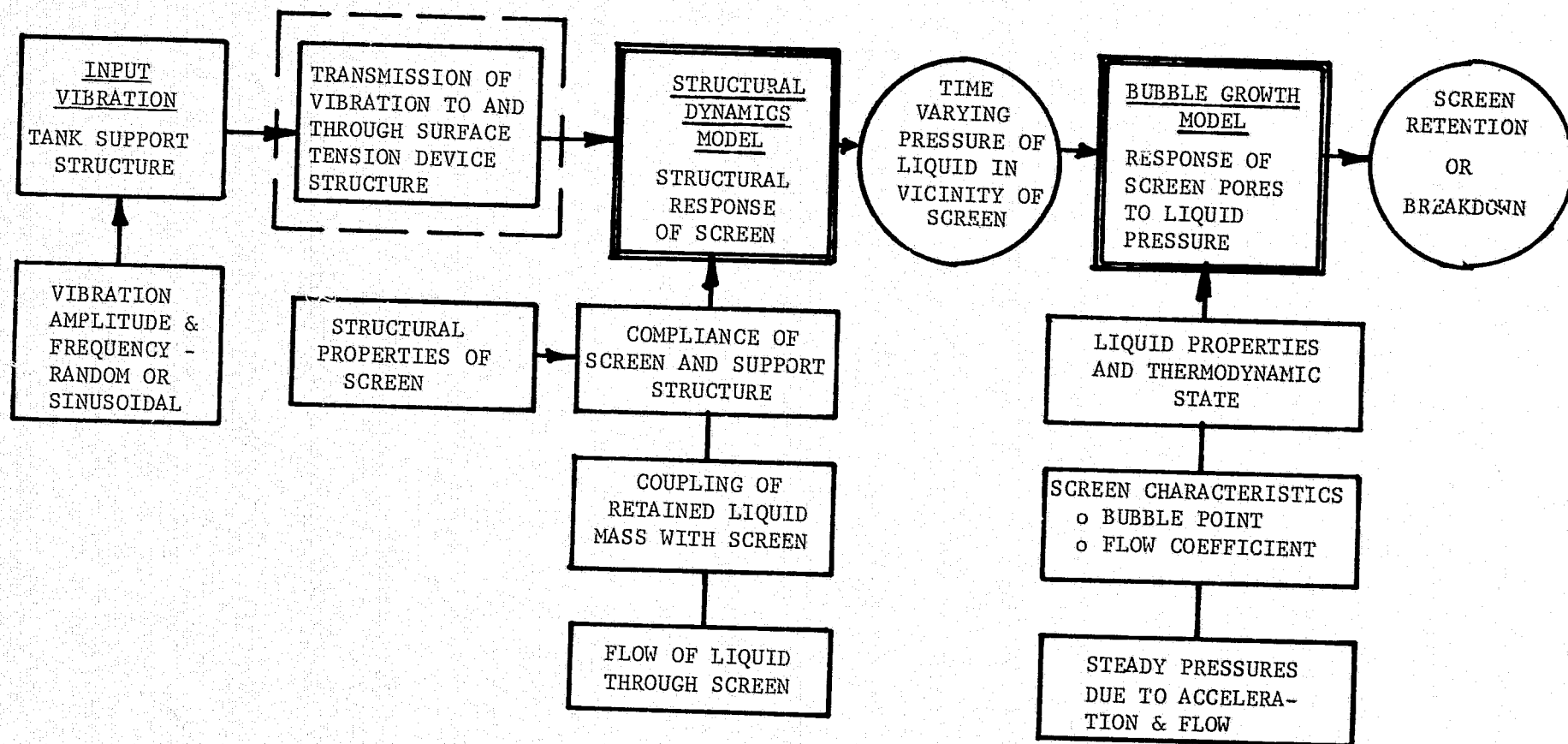
Figure III-1. Screen Dynamics Approach

The flow chart consists of the following boxes and connections:

- **INPUT VIBRATION** — TANK SUPPORT STRUCTURE
  - fed by: VIBRATION AMPLITUDE & FREQUENCY - RANDOM OR SINUSOIDAL
- **TRANSMISSION OF VIBRATION TO AND THROUGH SURFACE TENSION DEVICE STRUCTURE**
- **STRUCTURAL DYNAMICS MODEL** — STRUCTURAL RESPONSE OF SCREEN
  - fed by: COMPLIANCE OF SCREEN AND SUPPORT STRUCTURE
    - fed by: STRUCTURAL PROPERTIES OF SCREEN
    - COUPLING OF RETAINED LIQUID MASS WITH SCREEN
    - FLOW OF LIQUID THROUGH SCREEN
- **TIME VARYING PRESSURE OF LIQUID IN VICINITY OF SCREEN**
- **BUBBLE GROWTH MODEL** — RESPONSE OF SCREEN PORES TO LIQUID PRESSURE
  - fed by: LIQUID PROPERTIES AND THERMODYNAMIC STATE
    - SCREEN CHARACTERISTICS
      - o BUBBLE POINT
      - o FLOW COEFFICIENT
    - STEADY PRESSURES DUE TO ACCELERATION & FLOW
- **SCREEN RETENTION OR BREAKDOWN**

q_0 = screen center displacement coord.
q_1 = oscillatory vibration response coord.
q_2 = liquid outflow coord.

Figure III-2. Elemental Liquid/Container System

$$m\ddot{q} + c\dot{q} + kq = F(t) \tag{3}$$

and, letting $\omega_o = \sqrt{k/m}$, the natural frequency

$\qquad Q = \sqrt{km}/c$, the amplification

yields

$$\ddot{q} + \frac{\omega_o}{Q}\dot{q} + \omega_o^2 q = F(t)/m \; . \tag{4}$$

Implementation of Equation (4) requires knowledge of the system governing parameters (m, c, k) and an estimate of the forcing function (F(t)). This knowledge allows evaluation of the response acceleration which can then be expressed as a pressure.

b.   Coordinate Transformation - A relationship between the screen center displacement coordinate, q_o, and the oscillatory vibration response coordinate, q_1, can be obtained from considerations of continuity for an (assumed) incompressible flow. Assume that the screen deflection shape is of the form

$$q(x,z) = q_o \sin \frac{\pi x}{b} \sin \frac{\pi z}{a}$$

(5)

$$\dot{q}(x,z) = \dot{q}_o \sin \frac{\pi x}{b} \sin \frac{\pi z}{a}$$
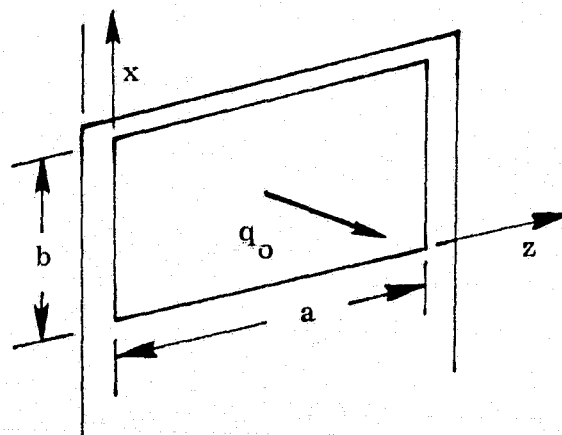
and, it follows that,

$$AB \; \dot{q}_1 = \dot{q}_o \iint_{area} \sin \frac{\pi x}{b} \sin \frac{\pi z}{a} \; dA = \frac{4ab}{\pi^2} \dot{q}_o .$$

(6)

c.   Mass Characteristics - The kinetic energy of the system as shown can be expressed in terms of the fluid mass density, ρ, the oscillatory vibration response coordinate, q_1, and the liquid outflow coordinate, q_2, as

$$T = \frac{\rho}{2} \iiint_{Vol} (\dot{q}_1 + \dot{q}_2)^2 \; dV$$

(7)

or

$$T = \frac{\rho}{2} ABL \; (\dot{q}_1 + \dot{q}_2)^2$$

(8)

and it follows, through application of Lagrange's equation, that the effective mass, expressed in terms of the oscillatory vibration response coordinate, q_1, is

39

$$\frac{d}{dt} \left(\frac{\partial T}{\partial \dot{q}_1} \right) = \rho \, ABL \, \ddot{q}_1 = M_{eff} \, \ddot{q}_1 \tag{9}$$

and $\quad M_{eff} = \rho \, ABL \, . \tag{10}$

Note that for steady flow, $\ddot{q}_2 = 0$. Alternatively, Equation (8) used in conjunction with Equation (6) yields the effective mass, expressed in terms of the screen center deflection coordinate, q_o, as

$$T = \frac{\rho}{2} \, ABL \left(\frac{4ab}{\pi^2 AB} \, \dot{q}_o + \dot{q}_2 \right)^2 \tag{11}$$

$$\frac{d}{dt} \left(\frac{\partial T}{\partial \dot{q}_o} \right) = \rho \, ABL \left(\frac{16a^2 b^2}{\pi^4 A^2 B^2} \right) \ddot{q}_o = M_{eff} \, \ddot{q}_o \tag{12}$$

and $\quad M_{eff} = \frac{16 \, \rho \, a^2 b^2 \, L}{\pi^4 \, AB} \, . \tag{13}$

Consideration must also be given the effective mass of the screen whose kinetic energy can be expressed in terms of the screen mass density, ρ_s, thickness, t_s, and screen center deflection coordinate, q_o, as

$$T = \rho_s \, \frac{t_s}{2} \iint_{area} \dot{q}_o^2 \, \sin^2 \frac{\pi x}{b} \, \sin^2 \frac{\pi z}{a} \, dA = \rho_s \, \frac{t_s ab}{8} \, \dot{q}_o^2 \tag{14}$$

$$\frac{d}{dt} \left(\frac{\partial T}{\partial \dot{q}_o} \right) = \rho_s \, \frac{t_s ab}{4} \, \ddot{q}_o = M_{eff} \, \ddot{q}_o \tag{15}$$

and $\quad M_{eff} = \rho_s \, \frac{t_s ab}{4} \, . \tag{16}$

Thus, it is observed that the effective mass of the moving screen is one-quarter of its actual mass and the ratio of effective screen mass to effective fluid mass is

$$\frac{(M_{eff})_{screen}}{(M_{eff})_{liquid}} = \frac{\pi^4 A^2 B^2 M_{screen}}{64 a^2 b^2 M_{liquid}} \ll 1 \qquad (17)$$

where M_{screen} and M_{liquid} are the total mass of screen and liquid, respectively. Equation (17) indicates that the effective screen mass can be neglected with little error.

d. Forcing Function Determination - Equations of Motion. - If the fluid mass of Figure III-2 is excited with a base acceleration $\ddot{X}$, the flow acceleration applies a net force

$$F(t) = - \rho ABh \ddot{X} \qquad (18)$$

and, making use of Equations (10) and (4), yields the equation of motion,

$$\ddot{q}_1 + \frac{\omega_o}{Q} \dot{q}_1 + \omega_o^2 q_1 = - \frac{h}{L} \ddot{X}. \qquad (19)$$

Determination of the applicable forcing functions for the other two directions of input excitation is not as straightforward. Reference to the sketch indicates the manner in which the pressure at the screen is determined as a function of base acceleration. For excitation in the Y-direction, ΔP_1, is likely to be zero when $\ddot{Y} > 0$ and ΔP_2 is likely to be zero when $\ddot{Y} < 0$. An approximate representation is then

$$F(t) = - \rho abc \ddot{Y}/2 \qquad (20)$$

and, making use of Equation (10) and Equation (4) yields, the equation of motion

$$\ddot{q}_1 + \frac{\omega_o}{Q} \dot{q}_1 + \omega_o^2 q_1 = - \frac{abc}{2 ABL} \ddot{Y}. \qquad (21)$$
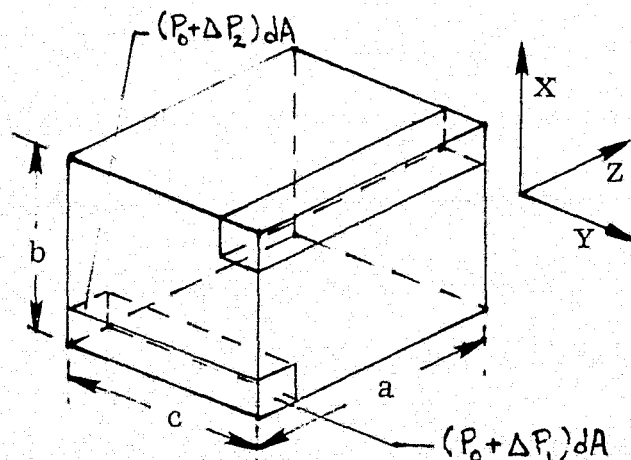
For excitation in the Z-direction, the distribution of the pressure varies linearly across the screen. Therefore, it seems appropriate to use the average value. Additionally, the excitation pressure does not go to zero when the acceleration changes sign but, rather, the reversal of the acceleration causes the same average screen differential pressure. Hence, the appropriate forcing function is

$$F(t) = - \frac{\rho a^2 b |\ddot{Z}|}{2} \tag{22}$$

and, making use of Equation (10) and Equation (4), yields the equation of motion

$$\ddot{q}_1 + \frac{\omega_o}{Q} \dot{q}_1 + \omega_o^2 q_1 = - \frac{a^2 b |\ddot{z}|}{2 ABL} . \tag{23}$$

Discussion to this point has evolved an equation of motion for base excited vibration of a fluid column subjected to a restoring force arising from a single compliant screen element. The peak flow acceleration follows under the assumption of large dynamic amplification ($Q \geq 10$):

for the X-direction $\qquad \ddot{q} \approx Q C_x \frac{h}{L} \ddot{X}_f$

for the Y-direction $\qquad \ddot{q} \approx \frac{Q C_y ab \ddot{Y}_f}{2AL}$ $\qquad$ (24a)

for the Z-direction $\qquad \ddot{q} \approx \frac{Q C_z a^2 b \ddot{Z}_{f/2}}{2ABL}$

for sinusoidal vibration input of modulus $\ddot{X}$, $\ddot{Y}$ and $\ddot{Z}$ at the system natural frequency, f. The constants C_x, C_y and C_z are included in Equation (24) to account for the fact that uniform flow may not exist and that the input excitation itself may be affected by bulk liquid response. For uniform flow, $C_x = C_y = C_z = 1$.

If random vibration input is considered, Equation (24a) becomes:

for the X-direction $\qquad \ddot{q} \approx \frac{C_x h}{L} \left\{ \frac{\pi}{2} Q f PSD_f \right\}^{\frac{1}{2}}$

for the Y-direction $\qquad \ddot{q} \approx \frac{C_y ab}{2AL} \left\{ \frac{\pi}{2} Q f PSD_f \right\}^{\frac{1}{2}}$ $\qquad$ (24b)

for the Z-direction $\qquad \ddot{q} \approx \frac{C_z a^2 b}{2ABL} \left\{ \frac{\pi}{2} Q f PSD_{f/2} \right\}^{\frac{1}{2}}$

where f is the natural frequency and PSD_f defines the acceleration spectral density at frequency, f.

e. Pressure Estimation - In a hydrostatic sense, the pressure at the screen element can be expressed as the sum of the static and dynamic contributions as

$$\Delta P_s = \rho g h$$

$$\Delta P_v = \rho g h \ddot{q} \qquad\qquad (25)$$

$$\Delta P_t = \Delta P_s + \Delta P_v$$

and it follows, for the three excitation directions, that:

for the X-direction
$$(\Delta P_t / \rho g)/h_s = 1 + QC_x \frac{h_s}{L} \ddot{X}_f$$

for the Y-direction
$$(\Delta P_t / \rho g)/h_s = 1 + \frac{QC_y \ ab \ \ddot{Y}_f}{2AL} \qquad (26a)$$

for the Z-direction
$$(\Delta P_t / \rho g)/h_s = 1 + \frac{QC_z \ a^2 b \ \ddot{Z}_{f/2}}{2ABL}$$

for sinusoidal input vibration, and

for the X-direction
$$(\Delta P_t / \rho g)/h_s = 1 + \frac{C_x h_s}{L} \left\{ \frac{\pi}{2} Qf \ PSD_f \right\}^{\frac{1}{2}}$$

for the Y-direction
$$(\Delta P_t / \rho g)/h_s = 1 + \frac{C_y \ ab}{2AL} \left\{ \frac{\pi}{2} Qf \ PSD_f \right\}^{\frac{1}{2}} \qquad (26b)$$

for the Z-direction
$$(\Delta P_t / \rho g)/h_s = 1 + \frac{C_z \ a^2 b}{2ABL} \left\{ \frac{\pi}{2} Qf \ PSD_{f/2} \right\}^{\frac{1}{2}}$$

for random input vibration where it has been assumed that $h \simeq h_s$, the true static head.

The extension of the above developed elemental model to what certainly must be required for complex screen/liquid configurations is not at all straightforward. In fact, its possible extension is predicted solely upon a building-block approach using test data from increasingly more complex systems.

2. **Bubble Growth Model** - The bubble growth model determines the time dependent response of a screen to pressure transients. Screen breakdown is actually the growth and detachment of a bubble from a screen pore. The model analyzes the growth of a gas bubble at the pore of a screen to determine its response to time varying pressure differentials. The model was developed under a prior study and was applied to evaluating the response of a screen to flow transients (Ref. III-2). During this program the model was refined and applied to the specific problem of the periodic pressure oscillations produced by vibration.

There has been some evidence (Ref. III-1 and III-2) that pressure transients exceeding the retention capability of screen can be applied to a screen without causing breakdown. The screen tends to act as an accumulator, reducing the effect of short duration pressure transients. The purpose of the bubble growth model was to analyze this effect, so that the screen response to transients could be predicted.

Preliminary analyses performed under this program (refer to Appendix A) indicated that a screen would not respond to the peak pressure of a sinusoidally oscillating pressure, as could be produced by vibration. The screen would actually be responding as if the periodic pressure was a steady pressure 80 to 90% of the peak value, even at low frequencies (< 50 Hz). The test data that was acquired during this program have shown that this is not the case (see Chapter V). The screen responds to the peak value of the pressure. Therefore, the predicted pressures of the structural dynamics model can be used directly and the time dependent effects considered by the bubble growth model are not significant.

The key factor influencing the preliminary predictions was the orifice coefficient for a screen pore. The derived values for this coefficient (see Appendix A) must be much larger (indicating more flow resistance) than is actually the case. Since it was concluded that the model was not applicable to the screen vibration problem, there was no effort to improve the coefficient values. The refinements added to the model during this program are presented in Appendix A.

An experimental investigation was performed to determine the effects of vibration on the retention capability of fine-mesh screens. The experimental program was composed to achieve this objective in two ways. First, the tests provided the data needed to verify the analytical models presented in Chapter III. Those models provide a means of predicting the effects of vibration. In addition, the tests were structured so that direct comparisons between various tests could be made, considering only one variable at a time. Through these direct comparisons the effects of vibration could also be established.

In this chapter the experimental investigation is described, including the approach, the test apparatus and the test matrix.

A.   Approach

Vibration was applied to screen specimens and the conditions under which screen breakdown occurred were established. In an actual spacecraft, the vibration is transmitted from the source to the tank wall and then to the surface tension device mounted within the tank. In this study it was assumed that the vibration transmitted to the surface tension device structure was known. Our primary concern was the transmission of the vibration from the screen support structure to the screen and the resulting screen response.

Therefore, the test model consisted of a screen specimen, with its actual support structure, rigidly mounted within a container. The vibration was applied to the container.

A flat rectangular screen specimen was selected since its response is readily analyzed and the results can be applied to any other screen configuration. The flat configuration for screen is found in most of the present and future surface tension devices, based on the survey presented in Chapter II. The screen is attached to the basic structure of the device and its span can be either unsupported, or supported in some manner by ribs or perforated plate.

The basic purpose of the screen of a surface tension device is to exclude gas from a controlled liquid region. Liquid can then be expelled gas-free from the controlled region. A portion of a surface tension device was simulated for the tests by forming a controlled region with the screen specimen and the container. This region could be between a single screen and the container wall or between two parallel screens. When the retention capability of the screen was exceeded (screen breakdown), gas entered the controlled liquid region.

Having defined the basic configuration of the test model, there are a number of parameters that can influence the response of the screen to an applied vibration. The parameters considered are discussed in the following paragraphs.

1. Test Liquids - Three test liquids were selected. Their properties of interest are listed in Table IV-1. All three liquids have a similar surface tension, but the density of the Freons is about twice that of the alcohol. This permitted a comparison of the influence of the liquid mass as it affected liquid pressure and the structural characteristics of the system. The alcohol has a high viscosity relative to that of the Freons, so viscous effects could also be compared.

The vapor pressures of the three liquids at ambient temperature cover a wide range. At atmospheric pressure ($\sim$ 8 N/cm^2 (12 psia) in Denver) and a temperature of 20°C (68°F) the isopropyl alcohol is subcooled by 61°C (110°F), the Freon 113 is subcooled by 22°C (39°F) and the Freon 11 is at its boiling point. Test conditions with a small amount of subcooling were produced by controlling the system pressure. For comparison, large amounts of subcooling were obtained with the Freon 113 and isopropyl alcohol.

Another consideration in the selection of the liquids was their compatibility and hazardous handling characteristics. A plastic window in the model was required so that screen breakdown could be observed. These liquids have sufficient compatibility with plastic for test purposes. The only hazard presented was the flammability of the alcohol. The vapors are not toxic.

2. Screen Mesh - Eight screen meshes were selected. The parameters for these screens are listed in Table IV-2. The screens cover the full range of fine-mesh screen that would be applied to surface tension devices. The 325 x 2300 Dutch twill is a practical limit for the smallest pore size. Screens that are coarser than 200 x 200 square weave have little retention capability. Between these two extremes was an assortment of representative meshes. The 325 x 2300, 165 x 800 Dutch twill and the 50 x 250 are used in the Space Shuttle Reaction Control System propellant acquisition device and the 165 x 800 plain Dutch is used in the Space Shuttle Orbital Maneuvering System device. All of the typical weaves were represented in the selection.

The bubble point of the screens is presented in four different ways in Table IV-2. First, the water column height corresponding to the differential pressure necessary to produce breakdown of the screen when it is wet with isopropyl alcohol is listed (the standard bubble point test). For the selected screens, there is a progression of the bubble point values from the coarsest to the finest, filling the entire range.

The last three columns of Table IV-2 list the height of the test liquids that could be supported in one-g by a vertically oriented screen. When the test liquid level is lowered on one side of the screen to the listed height (see Figure IV-1), gas just begins to pass through the pores at the top of the screen.

The length of the model was selected based on data in Table IV-1. Hydrostatic pressure was used to "preload" the screen when it was oriented as in Figure IV-1. As the exposed screen height is increased, the hydrostatic pressure acting on the screen is increased, which brings the screen closer to the bubble point. Varying the hydrostatic pressure therefore varies the

46

Table IV-1.   Properties of Test Liquids at 20°C (68°F)

Liquid	Surface Tension dynes/cm (lbf/ft)	Density gm/cm³ (lbm/ft³)	Viscosity Centipoise (lbm/ft sec)	Vapor Pressure N/cm² (psia)
Isopropyl Alcohol	21.7 (1.49×10^{-3})	0.786 (49.0)	2.50 (1.68×10^{-3})	0.42 (0.61)
Freon 113	19.3 (1.32×10^{-3})	1.58 (98.4)	0.70 (4.7×10^{-4})	3.7 (5.3)
Freon 11	19.0 (1.30×10^{-3})	1.49 (92.9)	0.45 (3.0×10^{-4})	8.8 (12.8)

47

Table IV-2. Screen Mesh

| Screen Mesh (wires per inch) | Weave | Wire Diameter mm (in.) | | Bubble Point at 20°C (68°F) | | | |
		Warp	Shute	cm (in.) of Water with Isopropanol	cm (in.) of Isopropanol/w Isopropanol	cm (in.) of F113 with F113	cm (in.) of F11 with F11
325 x 2300	Dutch twill	.038 (.0015)	.025 (.0010)	61.0 (24.0)	77.6 (30.5)	34.3 (13.5)	35.8 (14.1)
200 x 1400	Dutch twill	.071 (.0028)	.041 (.0016)	41.4 (16.3)	52.7 (20.7)	23.3 (9.2)	24.3 (9.6)
165 x 800	Dutch twill	.071 (.0028)	.051 (.0020)	19.6 (7.7)	24.9 (9.8)	11.0 (4.3)	11.5 (4.5)
165 x 800	Plain Dutch	.051 (.0020)	.036 (.0014)	24.1 (9.5)	30.7 (12.1)	13.6 (5.3)	14.2 (5.6)
80 x 700	Dutch Twill	.102 (.0040)	.076 (.0030)	15.5 (6.1)	19.7 (7.8)	8.7 (3.4)	9.1 (3.6)
50 x 250	Plain Dutch	.127 (.0050)	.114 (.0045)	8.9 (3.5)	11.3 (4.5)	5.0 (2.0)	5.2 (2.1)
850 x 155	Robusta	.030 (.0012)	.102 (.0040)	28.4 (11.2)	36.1 (14.2)	15.9 (6.3)	16.8 (6.6)
200 x 200	Square	.053 (.0021)	.053 (.0021)	9.7 (3.8)	12.3 (4.8)	5.4 (2.1)	5.7 (2.2)

48
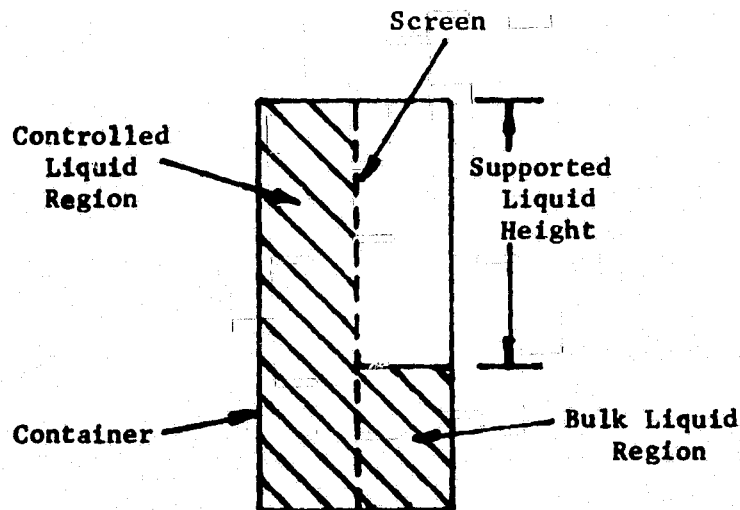
Figure IV-1. Hydrostatic Screen Retention

susceptibility of the screen to breakdown due to a given vibration environment. In order to have low vibration level caused breakdown, the screen had to be long enough for hydrostatic pressures near the bubble point. However, a short screen length was desired from the standpoint of a simple shaker mounting that would permit good transmission of the input vibration. By using Freon 113 to "preload" the finer mesh screens, a vertical screen height of 38 cm (15 in) was adequate. By using the alcohol with the coarser screens the retention capability was improved, allowing the effects of vibration to be better resolved.

3.   Screen Mounting - Six different methods of supporting the screens were selected. The methods, shown with sketches in Figure IV-2, could give the screen total support, virtually no support or various degrees of support in between. All of these methods are proven techniques, based on fabricated prototype and flight surface tension devices.

In the following paragraphs, each of the support methods is described.

a.   Bonded to Perforated Plate - This support method gave the most rigid screen of any of the selected methods. The screen and the backup perforated plate were diffusion bonded together, using a metallic bond that was formed in a furnace. The perforated plate had a high open area (47% open) so that the flow restriction was minimized. The only screen not supported was that over the round holes of the plate (0.95 cm (3/8 in) diameter).

b.   Supported by Perforated Plate - For this support method, the rectangular screen was resistance seam welded to a frame around its edges. The

49

Plate

Resist-
ance
Seam
Weld

Screen

Bent Up
Rib

| Bonded to Perforated Plate | Supported by Perforated Plate | Unsupported | Pleated Screen End View | Internal Rib | External Rib |
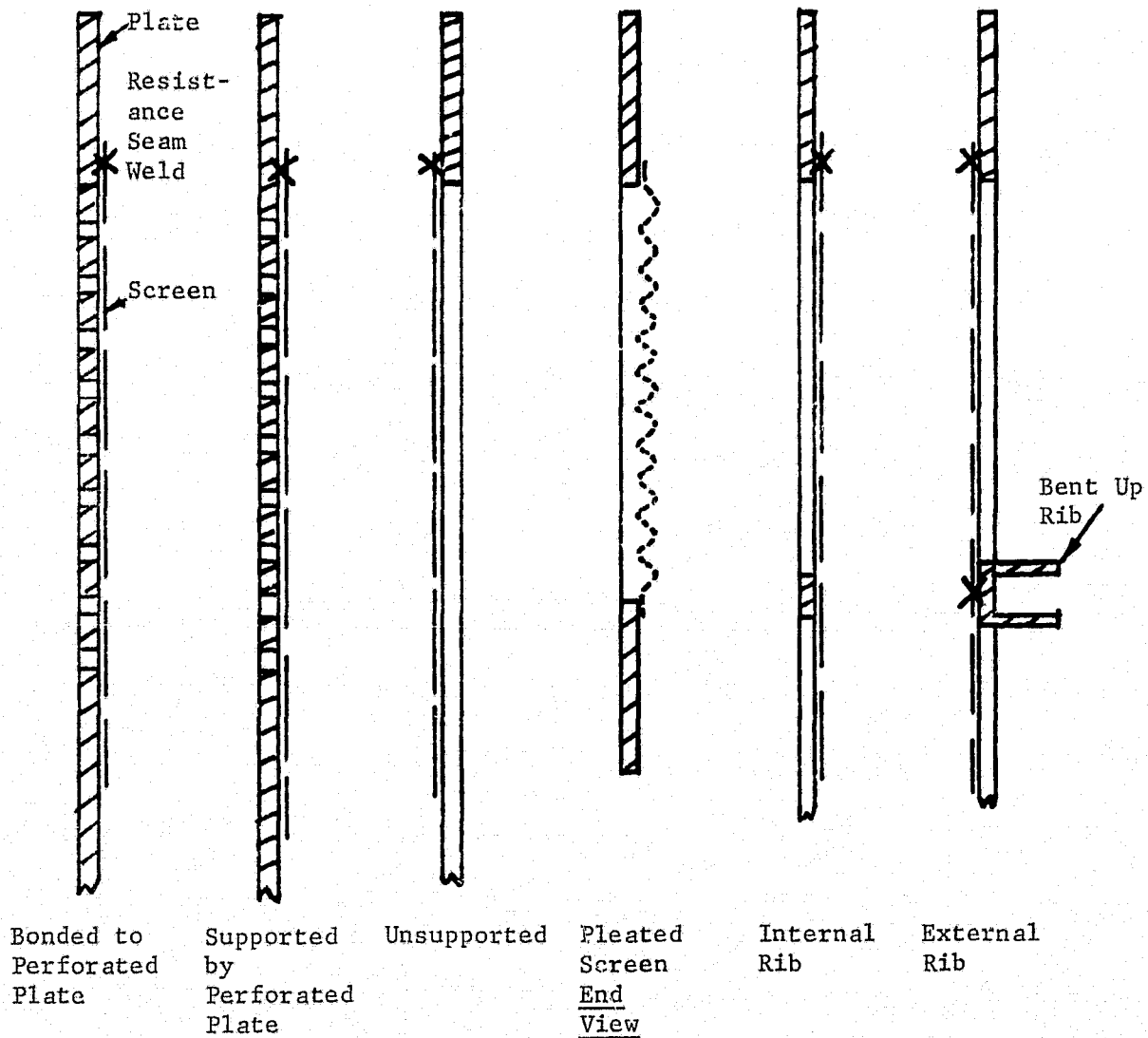
Control Liquid Side on Left
Bulk Region on Right

Figure IV-2 -Screen Mounting Configuration

screen rested on perforated plate within the frame. Normal static pressure differentials reduce the pressure in the controlled liquid region with respect to the ullage, so the screen is forced against the perforated plate. The perforated plate offers no support if the pressure differential is reversed.

c.   Unsupported - This method provides the least support of the screen. The edges of the screen were resistance welded to an open frame.

d.   Pleated Screen - The screen was made somewhat self-supporting by pleating. Following the pleating, the screen was attached to an open frame.

e.   Internal Rib - This method is essentially a modification to the unsupported configuration. Support ribs were added at fixed intervals on the controlled liquid side of the screen. The screen rested on the ribs, but was not joined to them. To prevent any interference with the flow path, the ribs need to be flat in cross section.

f.   External Rib - These ribs were located on the bulk region side of the screen and the screen was seam welded to each rib. Since the rib was outside the flow passage, a "U" shape cross section was permissible.

Other than the 200 x 200 screen, the selected screens have different wire diameters and numbers of wires in the warp and shute directions. For most applications the screen is mounted so that the warp and shute wires run parallel and perpendicular to the support structure, giving two possible orientations of the screen. Since the screen structure is not uniform in every direction (orthotropic), its response could be dependent on orientation. This variable was considered in the testing.

Three special screen specimens were also tested to establish the basic response of screen to vibration. These specimens had simple square openings, rather than any of the above described support methods, to give an easily analyzed screen deflection. Each of the three specimens had a 7.6 cm (3.0 in) square screen opening at the top (Figure IV-3). Specimen 1 had the same screen opening at the bottom, Specimen 2 had the opening at the bottom but no screen, and Specimen 3 had a tube positioned half way through the plate at the bottom.

4.   Configuration - The controlled liquid region could be represented by one or two screen specimens. One element represented a portion of a flow channel of which the other sides are solid and rigid. This also represented a portion of a screen barrier. Two parallel elements represented a portion of a flow channel that allows liquid to enter from either side. The opposite sides of this configuration had solid and rigid walls.

The vibration can act in any direction with respect to the screen. Steady accelerations can also act in any direction and can influence the response of the screen to vibration. Six possible orientations, in which the vibration and one-g were either parallel or perpendicular to the screen, were identified. These orientations are illustrated with respect to the model in Figure IV-4.
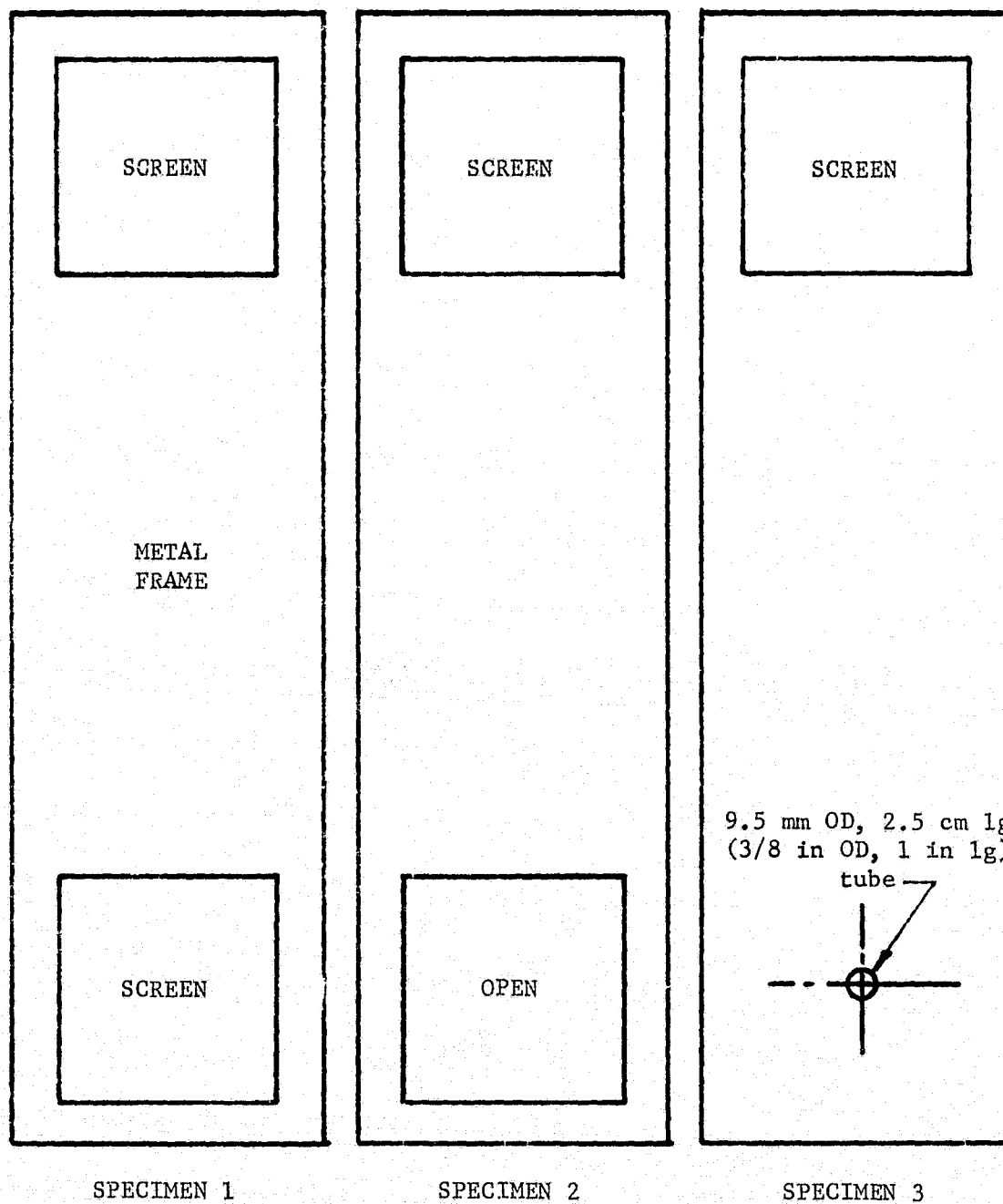
Figure IV-3.   SPECIAL SCREEN SPECIMENS

Figure IV-4. Model and Vibration Orientation

Vertical Vibration

Vertical Vibration

① ②

Horizontal Vibration

Horizontal Model

③ ④

Vertical Model

⑤ ⑥

One-g is Vertical   Axis of Vibration

53
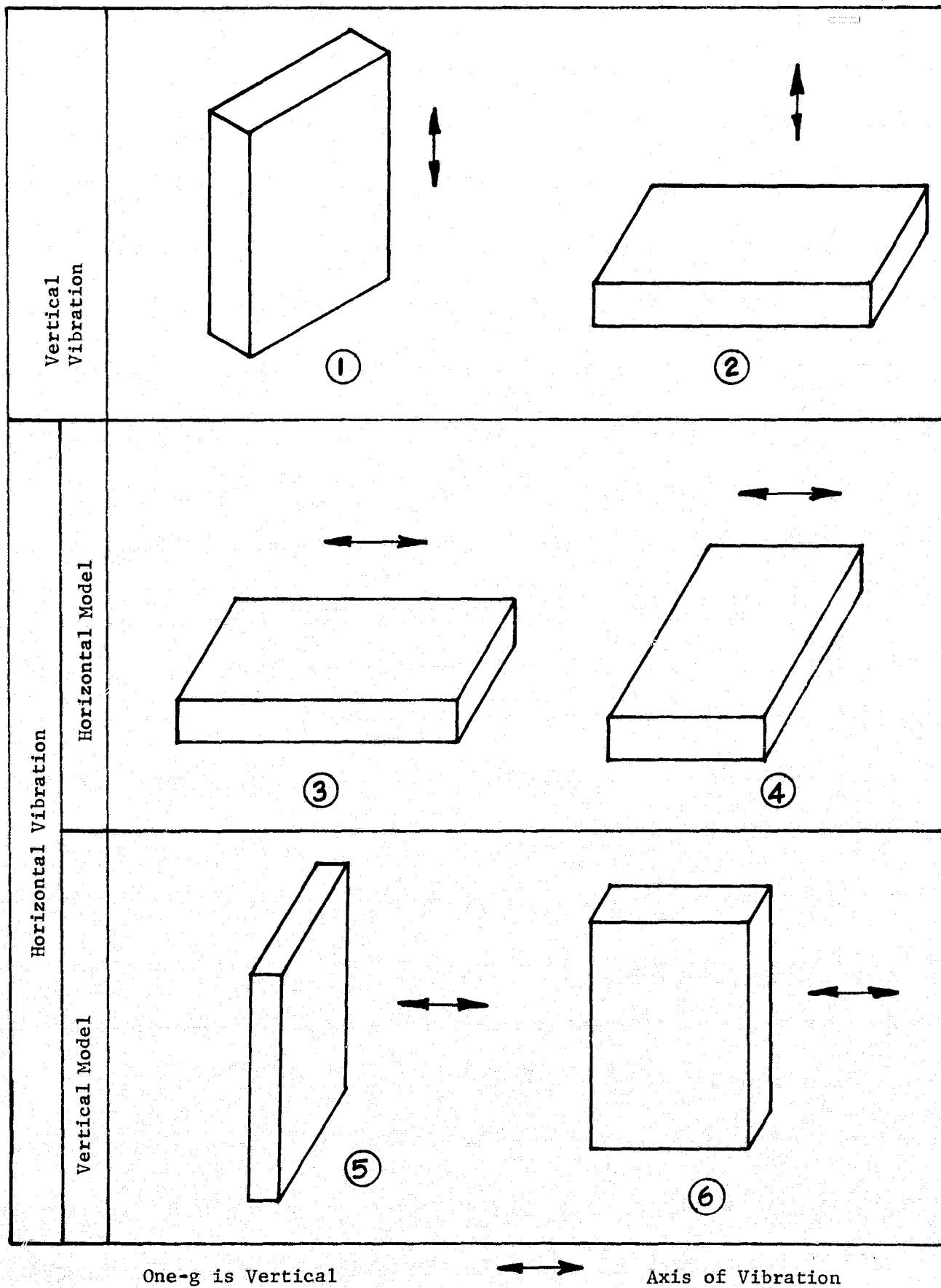
Orientations 2 and 5 were achieved by mounting the model directly to the shaker face plate (the shaker vibration axis is perpendicular to that plate). The shaker axis can be positioned either vertically (Orientation 2) or horizontally (Orientation 5). A thick mounting plate, to which the model was mounted, was bolted perpendicular to the shaker face plate to achieve Orientation 1 (Figure IV-13). For Orientation 6 the same mounting plate was used, but the shaker was positioned horizontally. Orientations 3 and 4 required a slide plate. The slide plate rested on a large block and was bolted perpendicular to the horizontally positioned shaker. Rotating the model 90 degrees on the slide plate changed the orientation from 3 to 4. When the model was vertical, the bulk region liquid level could be varied to change the hydrostatic pressure applied to the screen. When the model was horizontal, the controlled liquid region was above the screen and the bulk liquid was not in contact with the screen. This lack of bulk liquid contact is representative of a barrier that positions the liquid in a tank. It can also represent a portion of a flow channel, far enough from the bulk liquid that liquid flow through the screen does not influence its response to vibration.

5. Applied Vibration - The vibration was in two forms: sinusoidal and random. Sinusoidal vibration was applied at a specific frequency and peak amplitude. The usual method of performing sinusoidal tests is to sweep a range of frequencies, starting at some low value and incrementing at a fixed rate, keeping the amplitude constant. This technique can quickly identify the harmonics and the amplification of the system. Frequencies from 5 to 2000 Hz were covered. For any test configuration, an amplitude sufficient to cause screen breakdown was found, which ranged from 0.3 to 5.0g.

Random vibration was applied based on a spectrum of the power spectral density versus frequency. For a given spectrum, the RMS g-level can be defined. As the survey in Chapter II illustrated, there can be many possible spectra, but they usually ramp up from a low frequency to a constant level and then ramp down at around 1000 Hz. A prime concern was where the system harmonics fall with respect to the power spectrum. The influence of the spectrum was evaluated by using various spectra as discussed in Chapter V.

The shape of the spectrum was held constant while the values of power were increased or decreased, varying the applied RMS g-level. For each configuration and spectrum, the RMS level was varied to find the point of screen breakdown. A range of 0.2 to 3.0g RMS was covered.

B. Test Apparatus

The apparatus used to perform the tests is described in this section. The test system consisted of an electrodynamic shaker, the surface tension device model and the associated plumbing required to operate the model. The surface tension device model was a container in which the screen specimen was mounted.

1. __Test Model__ - The unassembled parts of the surface tension device model are shown in Figure IV-5. The container walls formed the controlled liquid region and the bulk region on opposite sides of the screen specimen. When sandwiched together with the back plate and the window, the model formed a sealed container. The volume between the back plate and the screen was the bulk region of the model, that contained varying amounts of liquid. The volume between the window and the screen was the controlled liquid region, that was completely full of liquid. The window permitted the passage of gas through the screen to be observed.

The wall was fabricated from aluminum stock. The volume formed by the wall was 39.4 cm (15.5 in) long, 8.9 cm (3.5 in) wide, and 2.4 cm (0.95 in) thick. Bolts passed through the window, one of the walls, the screen specimen and were screwed into the other wall to seal the container. A liquid gasket material was used to seal mating surfaces. A thin gasket was formed so the walls rigidly clamped the edges of the screen specimens. The outer, larger holes were for bolting the model to the shaker. The walls were drilled and tapped to accept all the necessary plumbing fittings. This was the configuration used when a single screen element was tested.

When two parallel screen specimens were tested, a spacer was added. The sandwich then consisted of: window - wall - screen specimen - spacer - screen specimen - wall - back plate (Figure IV-6). The spacer had the same profile as the wall but was only 1.3 cm (0.5 in) thick. It was made of sheet plastic so that the controlled liquid region, which was between the screen specimens, could be observed for screen breakdown.

The screen specimens were all fabricated using a common frame that fit the model. Six versions of this frame, for each support method, were made. The frame was made of stainless steel sheet 0.69-mm (0.027-in) thick. The screen opening, within the outer seam welds, for all the specimens was 7.6-cm (3.0-in) wide and 38.1-cm (15.0-in) long.

A resistance seam weld was used to attach the screen to the plate. For each screen mesh a few trial welds were performed to obtain the correct welder settings. Leak-tight seam welds were produced for each of the eight screen meshes. Most of the screens were welded using a 0.13-mm (0.005-in) thick foil strip that was located in top of the screen. This foil strip improves the penetration of the weld for the finer screen meshes. For the screens with larger wires (80 x 700, 50 x 250 and 850 x 155), no foil strip was necessary. There was some warping of the frames due to the welding. If the weld schedule had been optimized, a lower pressure could have been used and the warping could have been eliminated. The warping of the frame added some wrinkles to the screen, but when the specimen was mounted in the model the frame was flattened and these wrinkles were removed.

Front and back views of the various support methods for the screen specimens are shown in Figures IV-7 through IV-11. The screen is supported by the perforated plate in Figure IV-7. The bonded to perforated plate method used the same frame but the screen was diffusion welded to the plate. All perforated plate was the same: 47% open area and 0.95 cm (3/8 in) diameter holes.

55
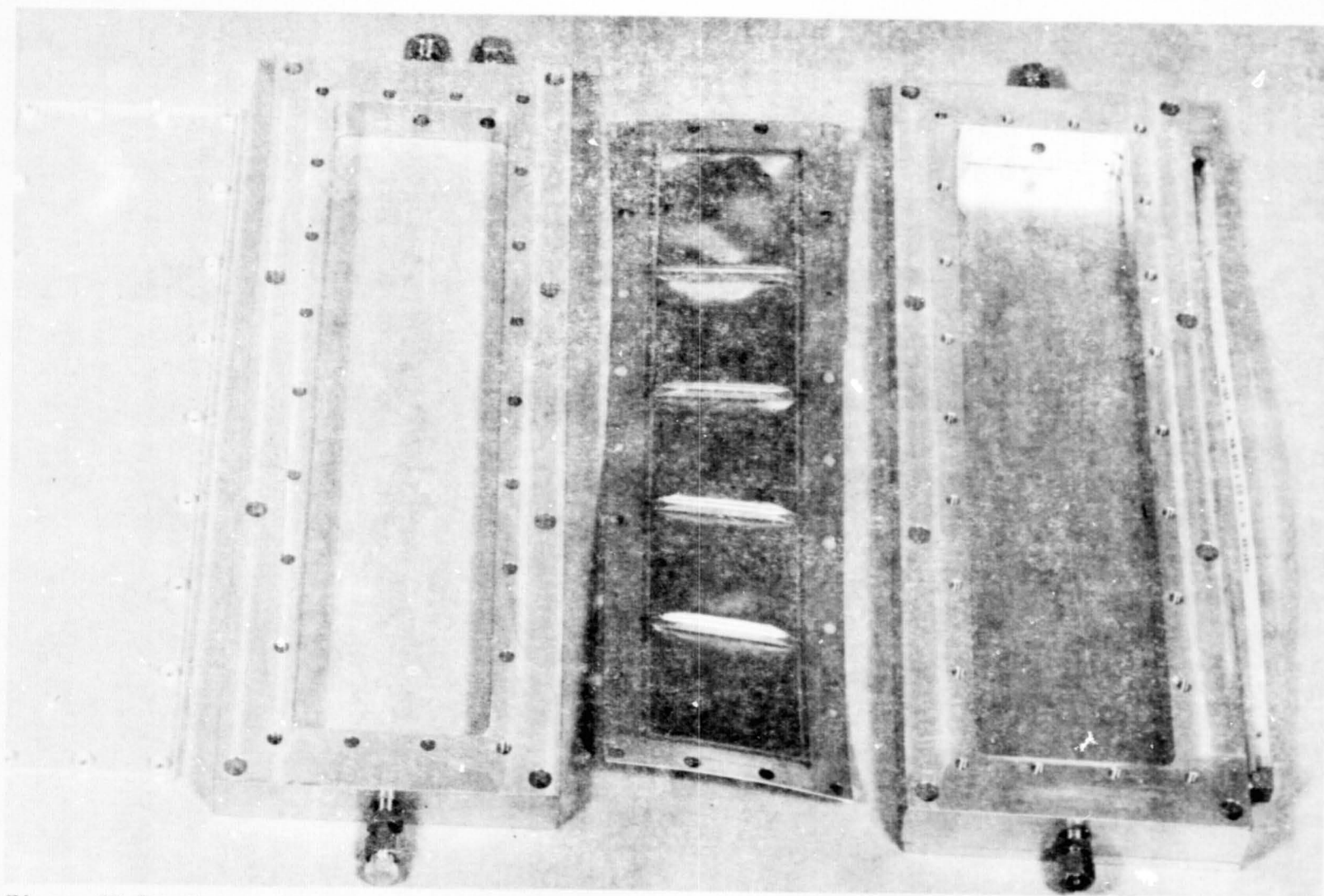
Figure IV-5.   Components of Test Model, Single Element Configuration
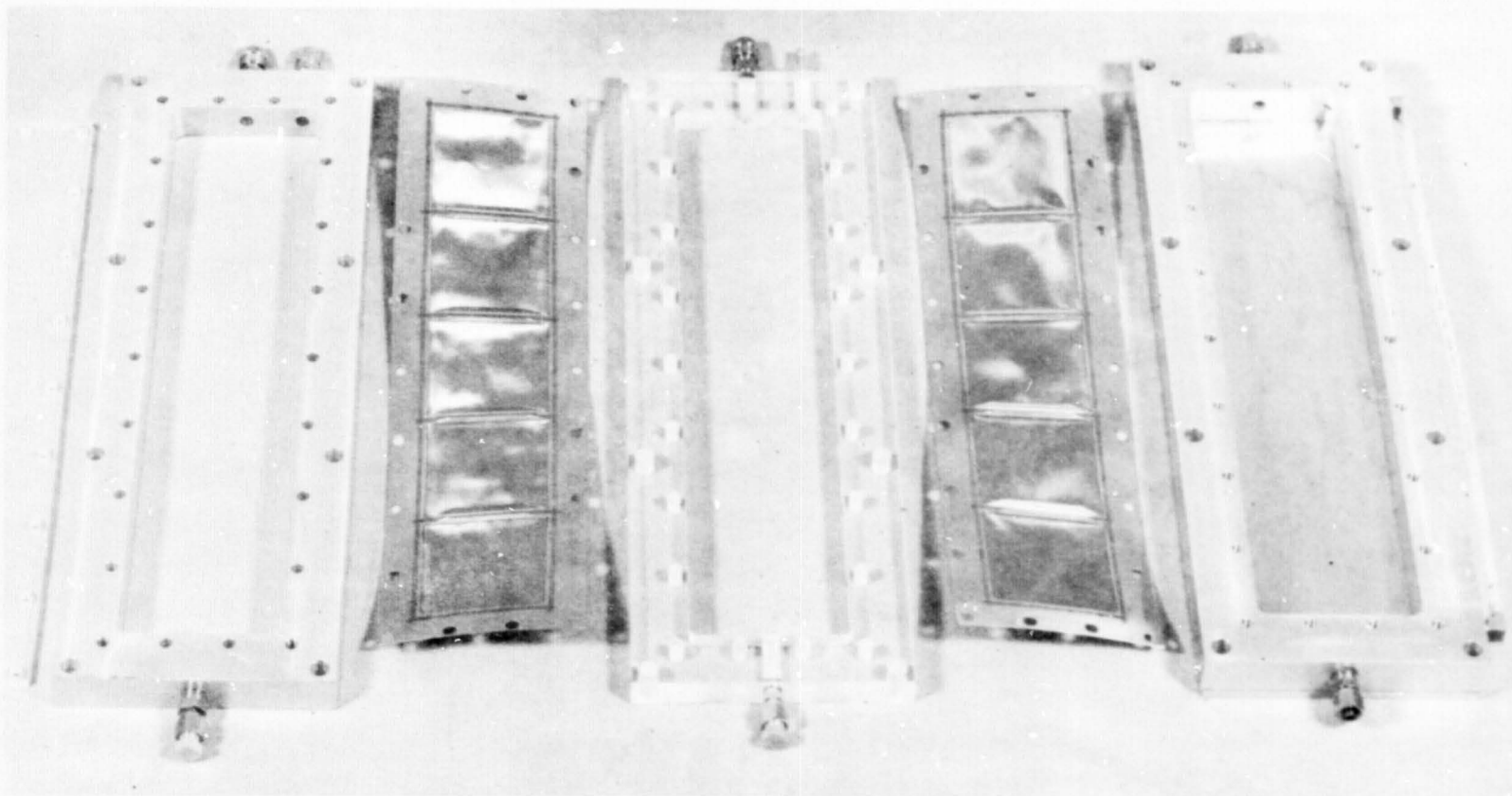
Figure IV-6.   Components of Test Model, Dual Element Configuration

57
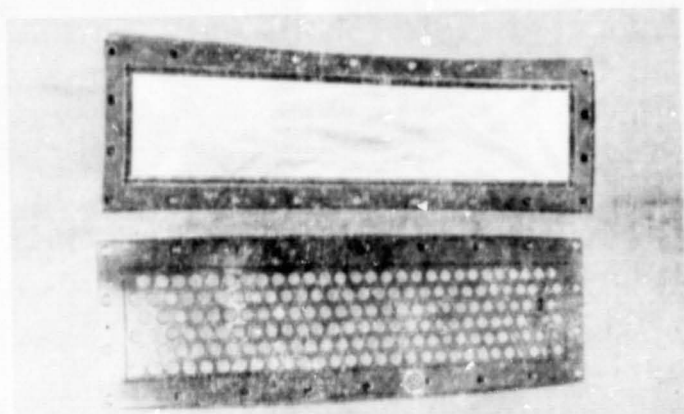
Figure IV-7. Supported by Perforated Plate
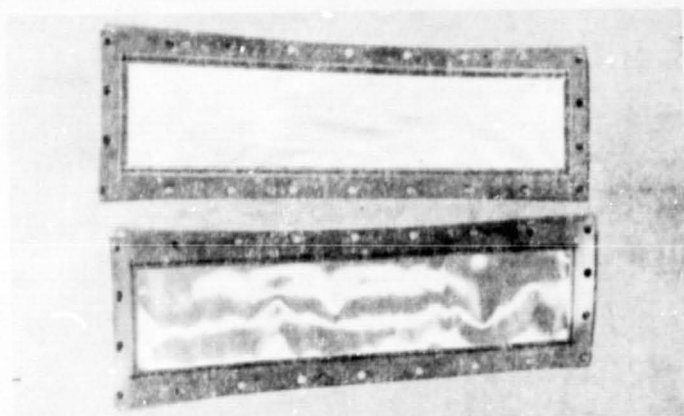
Figure IV-8. Unsupported
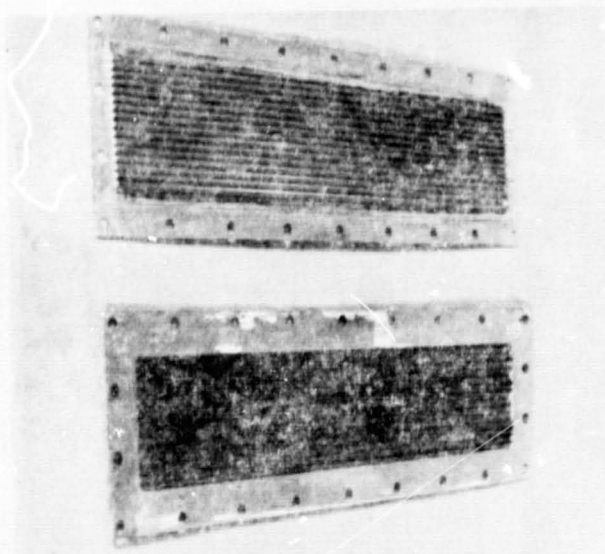
Figure IV-9. Pleated Screen

58
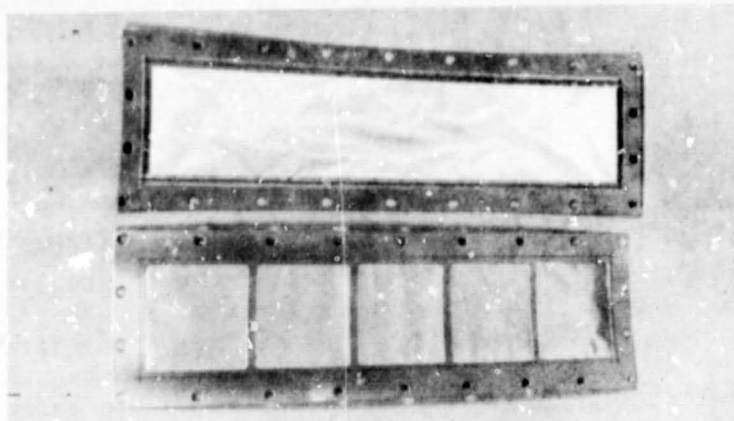
Figure IV-10.   Internal Ribs
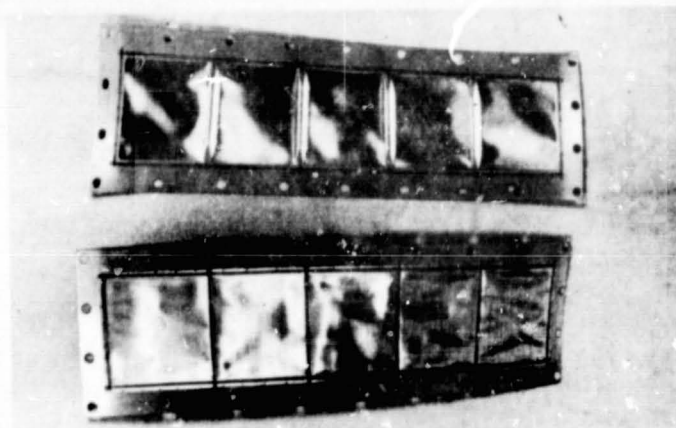
Figure IV-11.   External Rib
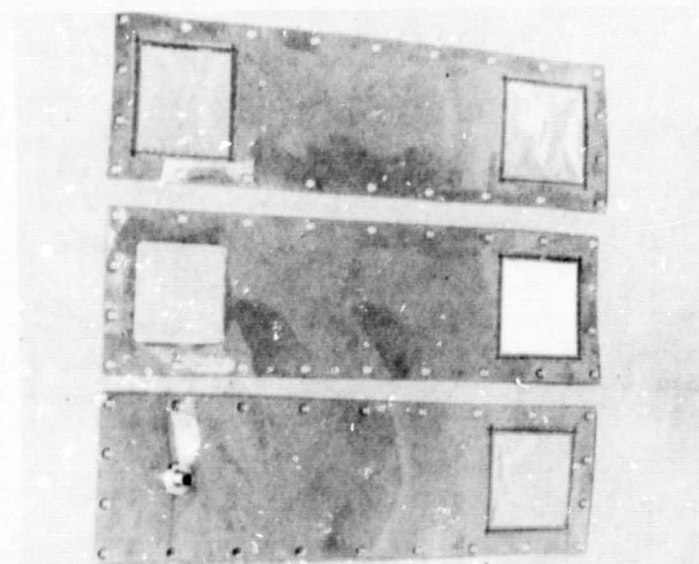
Figure IV-12.   Specimens 1, 2 and 3 (from Left to Right)

The pleated screen specimens, shown in Figure IV-9, were fabricated differently. The pleats ran the longer length of the specimen. A pleat geometry of 6 pleats per inch and a pleat ratio (length of screen before pleating to length after pleating) of 2 was used. After pleating, the screen was soldered to the frame, eliminating the need to crimp the pleats to make the joint.

The three special specimens are shown in Figure IV-12.

The bubble point of each of the screen specimens was measured after they were fabricated using the standard bubble point test method. The screen was oriented horizontally and covered with a thin layer of isopropyl alcohol. The wet screen was then pressurized from below and the differential pressure required to cause the first gas bubbles to pass through the screen was recorded. After the testing was complete the bubble point was rechecked to determine if any screen degradation had occurred.

2. Test System - The test model was directly mounted to the shaker so that the vibration applied to the model was the same as the output of the shaker. The model was either mounted to the face plate of the shaker or to a mounting plate that was perpendicular to the face plate. With these two possible mountings and by orienting the shaker axis either vertical or horizontal, the six different orientations were achieved.

The model is shown mounted in Orientation 1, with the vibration and one-g acceleration vectors parallel to screen surface, in Figure IV-13. A closer view of the model is presented in Figure IV-14.

The necessary plumbing for the non-flow tests is shown in Figure IV-13. A supply tank gravity fed the bulk region of the model and gas was purged from the controlled region through the vent line. A vent port in the window allowed purging of the controlled region when the model was oriented horizontally.

Outflow was simulated by recirculating the test liquid through the model as shown in Figure IV-15.

The shaker used to perform the testing was a Ling Electronics, Inc. Model 249. It has a force output of 133,000N (30,000 lbf) and a frequency range of 5 to 2000 Hz with a sweep rate of 0.09 to 22.9 octaves/minute. The output can be either sine or random with a maximum acceleration of 75 g and a maximum displacement of 2.5 cm (1.0 in) peak-to-peak.

3. Instrumentation - Screen breakdown was the key piece of data acquired during the testing. The passage of gas through the screen was visually detected. In addition to relating the point of breakdown to the applied vibration, the location of the breakdown on the screen and an estimate of the quantity of gas was noted.

The shaker control system provided the basic monitoring of the input frequency and amplitude of the applied vibration. The output of the accelerometer on the shaker that was used to control the shaker operation was used to determine the input vibration level.

61

Model

Supply tank
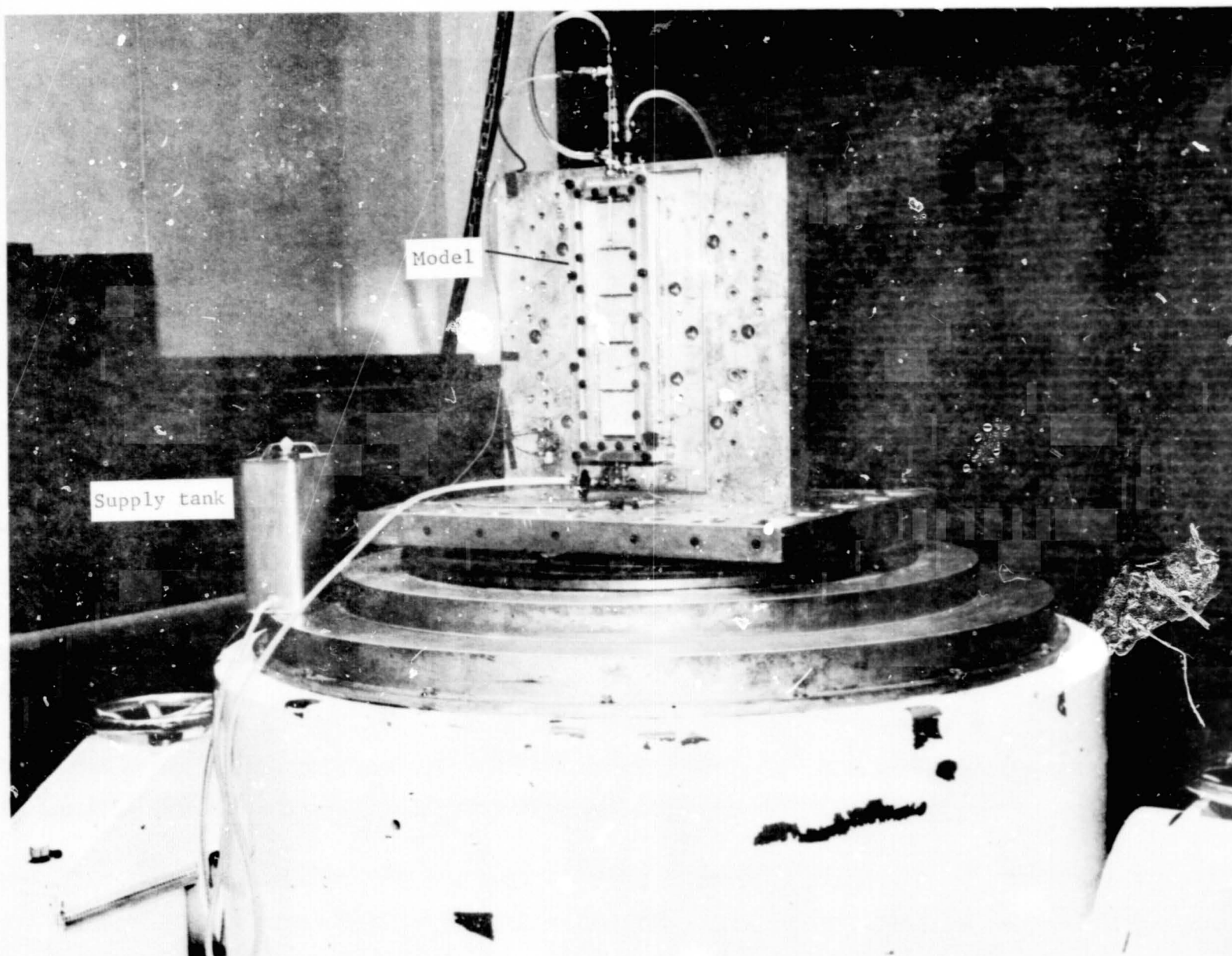
Figure IV-13.   Model Mounted on Shaker
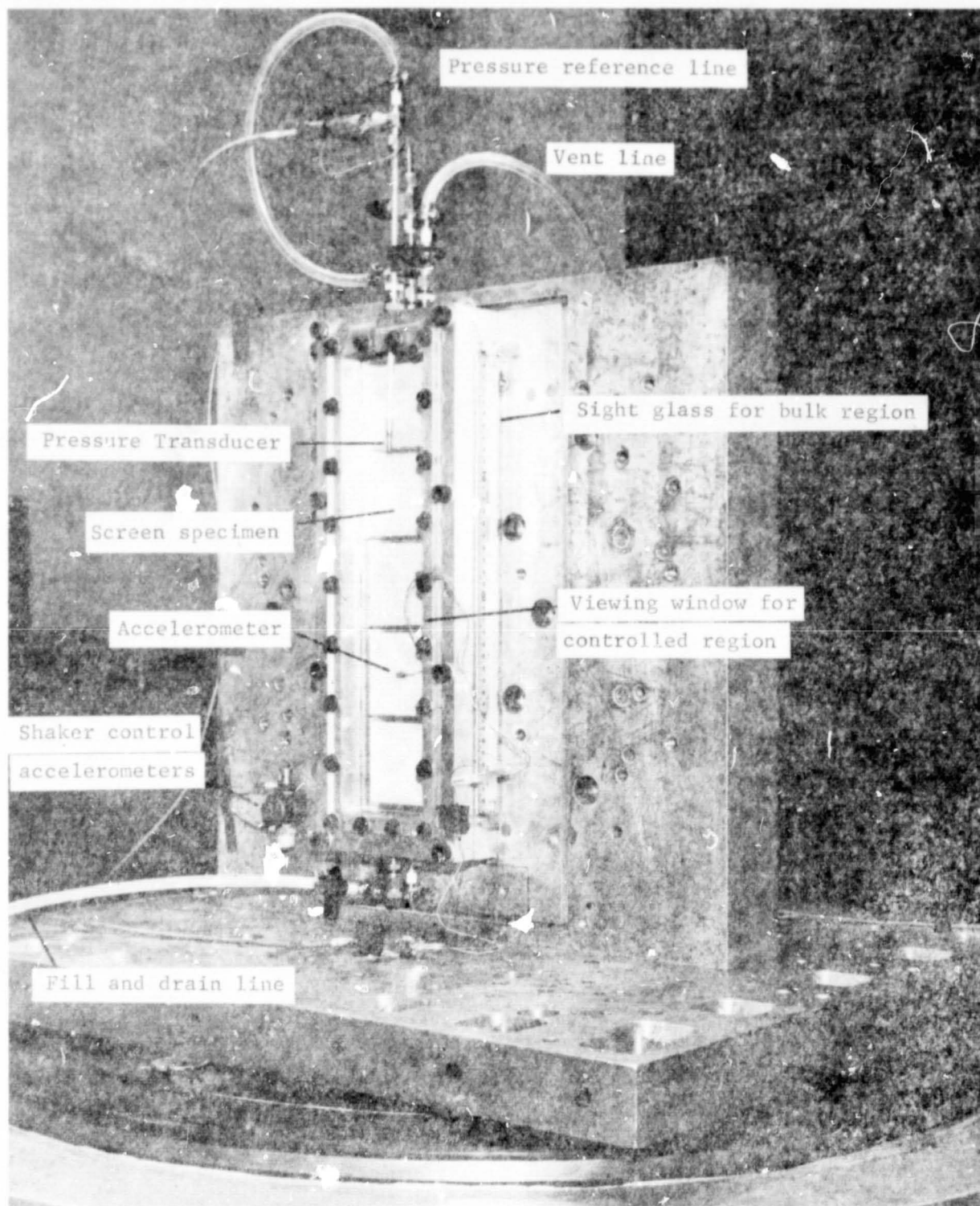
Figure IV-14. Close Up View of Model
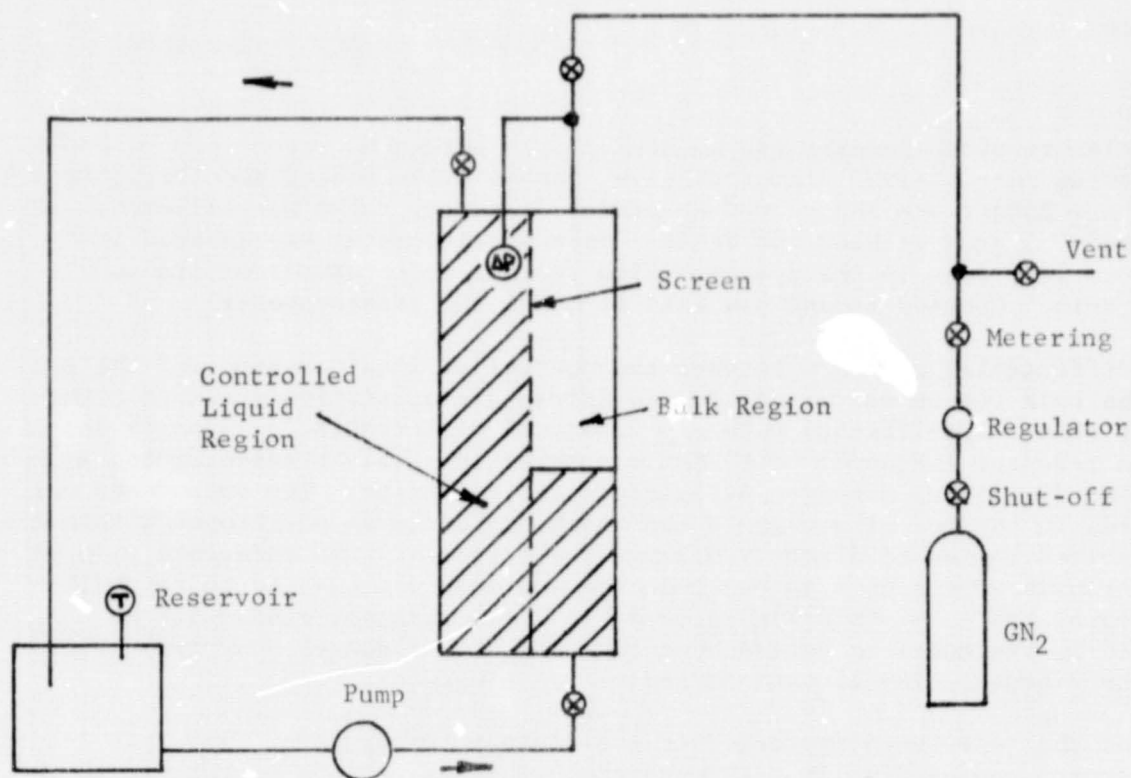
a. Single Element Configuration
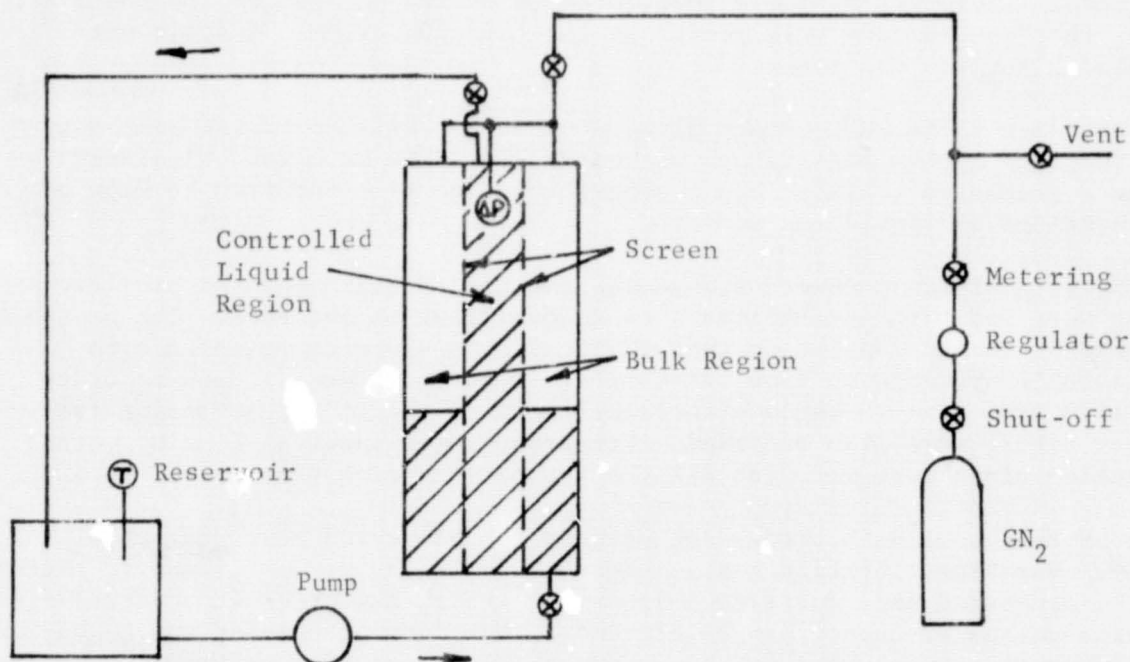
b. Dual Element Configuration

Figure IV-15.   Flow Test Schematic

A miniature accelerometer was mounted on the screen to record its response. An Entran EGA-125-250D piezoresistive, hermetically scaled accelerometer with a $\pm$ 250g range and a 1000 Hz useful frequency range was selected. It weighed 0.5 gram without the leads. This accelerometer was mounted in various locations on the specimen with various orientations of its sensitive axis. Contact cement was used to mount the accelerometer.

The differential pressure between the controlled liquid region and the gas in the bulk region was measured. An Entran piezoresistive pressure transducer (Model EPA-125E-5D) with a $\pm$ 3.5-N/cm^2 differential ($\pm$ 5 psid) range and a resonant frequency of 60 KHz was selected. This transducer has a 3.18-mm (0.125-in) diameter stainless steel diaphragm. The transducer was mounted in the end of a tube so the diaphragm could be positioned within the controlled region to directly measure the pressure. The reference side of the transducer was open to the tube and the tube was coupled to the bulk region of the model (see Figure IV-14). Tests were performed with no liquid in the model to verify that the pressure transducer was insensitive to the vibration levels used during the testing.

All of the tests were performed at the ambient temperature. The test liquid was stored and used at that temperature. The temperature of the liquid in the reservoir was monitored. When required for flow tests or the subcooled liquid tests, the model was pressurized with gaseous nitrogen. A dial-type pressure gage monitored the model pressure.

A sight glass was used to measure the liquid level in the bulk region of the model. This was a simple tube, mounted on the outside of the container wall, that entered the bulk region at the top and bottom. A scale was mounted alongside the tube.

For the flow tests, a constant flow rate, as established by the pump output and the flow system resistance, was used. The flow rate was calculated by using a graduated cylinder and a stopwatch. The time required to flow a given volume of liquid was measured.

The outputs of the pressure transducer and the specimen-mounted accelerometer were fed through amplifiers to an oscillograph recorder. The pressure transducer was AC-coupled so that the static pressure component due to hydrostatic pressure or flow losses was eliminated. When a tape recorder was also used, the shaker monitor accelerometer output and an analog frequency signal were also recorded. Vibration power spectral density versus frequency plots were made for all the random vibration tests.

Some of the usual data processing methods for vibration test data were tried. For sine vibration tests, pressure amplitude versus frequency plots can be generated and, for random vibration tests, the pressure spectral density versus frequency can be plotted. This data processing was found to be unsatisfactory because the pressure is processed as an RMS signal. The key component of the pressure, the positive peak value, was lost in the processing. The best data were the oscillograph records since they showed the actual pressure waveform.

Motion pictures of selected tests were made. A high-speed camera recorded the breakdown of the screen during the test.

C.   Test Program

In this section the screen specimens and the tests that were performed are presented. The general test procedures are outlined.

1.   Test Matrix - A preliminary test matrix was formulated when the tests were planned. This matrix was laid out by selecting the more significant test conditions from the multitude of possibilities indicated in the Approach, discussed previously. As the testing proceeded, the matrix was expanded and modified based on the results of the tests.

One of the first steps in defining the test matrix was to identify the screen specimens. A total of 27 specimens were fabricated and tested. Four specimens were added during the testing to further explore certain vibration effects. The specimens tested are listed in Table IV-3. Specimens of each of the support methods using a single screen mesh (325 x 2300) and specimens of various meshes using a single support method (external rib) were required so that these effects of mesh and support could be compared. The 325 x 2300 was selected because it gave the best resolution of the vibration effects due to its high bubble point. The external rib structure was selected because it was judged to provide the most basic response of the support methods.

The special specimens (1, 2 and 3) were made using the 325 x 2300 screen, again to improve resolution. Two specimen pairs (Specimens 4 and 5, and Specimens 24 and 25) had opposite weave orientations to evaluate that effect. The remainder of the specimens were selected to aid in further investigating the effects of screen mesh and support method.

Table IV-4 is the matrix of the test program, as performed. Each test consisted of a number of individual runs. Sine sweeps over a frequency range with various acceleration amplitudes and ullage heights were performed as part of each test. Sine dwell runs and random vibration runs were also included in many of the tests. A total of 551 vibration runs were performed.

The tests were laid out such that new variables were introduced one at a time. The intention was to perform tests that were identical, except for a single variable, so the effect could be established by a direct comparison of the data.

Tests 1 through 6 were aimed at establishing the basic vibration characteristics, so these tests incorporate a large number of runs (~120 runs). Tests 7 through 13 investigated the effects of weave orientation and model orientation. Tests 14 through 21 considered the influence of the various support methods. Tests 22 through 51 brought the effects of screen mesh and liquid outflow into the investigation. Two element models were tested for tests 52 through 57. Finally, the effect of liquid subcooling was investigated in tests 58 through 65.

65

Table IV-3.   Screen Specimens

	A Bonded to Perf. Plate	B Supported by Perf. Plate	C Un- supported	D Pleated	E Internal Rib	F External Rib
325 x 2300	6	7	1,2,3,4,5*	8	9	10, 27
200 x 1400			20			11
165 x 800 Dutch	18		21			12
165 x 800 Plain		19*	22*		23*	13*
80 x 700				26		14
50 x 250						15
850 x 155			24*, 25			16
200 x 200						17

Note: Screen weave orientated with the warp in the long direction for those
specimens with *, all others have the weave oriented with the warp in
the short direction.

Table IV-4. Test Matrix

Test No.	Screen Specimen	Number of Elements	Test Liquid			Out-Flow	Orientation					
			Isopropyl Alcohol	Freon 113	Freon 11		1	2	3	4	5	6
1	1	1	X			NO	X					
2				X								
3	1	1	X			NO					X	
4	2	1	X			NO	X					
5	3	1	X			NO	X					
6	3A	1	X			NO	X					
7	4	1	X			NO	X					
8	5	1	X			NO	X					
9								X				
10									X			
11										X		
12											X	
13												X
14	6	1	X			NO	X					
15	7A	1	X			NO	X					
16				X			X					
17	7	1	X			NO	X					
18				X			X					
19	8	1	X			NO	X					
20	9	1	X			NO	X					
21	10	1	X			NO	X					
22	1	1	X			YES	X					
23	1	1		X		YES	X					
24	11	1	X			NO	X					
25	11	1	X			YES	X					
26	12	1	X			NO	X					
27		1	X			YES	X					

67

Table IV-4. Test Matrix (continued)

Test No.	Screen Specimen	Number of Elements	Test Liquid Isopropyl Alcohol	Freon 113	Freon 11	Out-Flow	1	2	3	4	5	6
28	13	1	X			NO	X					
29		1	X			YES	X					
30	19	1	X			NO	X					
31		1	X			YES	X					
32	22	1	X			NO	X					
33		1	X			YES	X					
34	18	1	X			NO	X					
35		1	X			YES	X					
36	26	1	X			NO	X					
37	23	1	X			NO	X					
38		1	X			YES	X					
39	21	1	X			NO	X					
40		1	X			YES	X					
41	20	1	X			NO	X					
42		1	X			YES	X					
43	14	1	X			NO					X	
44		1	X			NO	X					
45		1	X			YES	X					
46	15	1	X			NO					X	
47	17	1	X			NO					X	
48		1	X			YES					X	
49	16	1	X			NO	X					
50	24	1	X			NO	X					
51	25	1	X			NO	X					
52	10-27	2	X			NO	X					
53		2	X			YES	X					
54		2	X			NO					X	

Table IV-4. Test Matrix (concluded)

Test No.	Screen Specimen	Number of Elements	Test Liquid Isopropyl Alcohol	Test Liquid Freon 113	Test Liquid Freon 11	Out-Flow	Orientation 1	2	3	4	5	6
55	10-27	2		X		NO	X					
56	22-23	2	X			NO	X					
57		2	X			YES	X					
58	25	1		X		NO	X					
59		1			X	NO	X					
60	15	1		X		NO	X					
61		1			X		X					
62	11	1		X		NO	X					
63		1			X	NO	X					
64	10	1		X		NO	X					
65		1			X	NO	X					

2.   Test Procedure - Prior to each test the initial conditions were established. The controlled liquid side of the model was filled completely with liquid and the vent was closed. The liquid level on the bulk side of the model was set. If it was a flow test, the pump would be started and a steady flow condition was established. The ullage was pressurized to obtain the correct bulk liquid height under flow conditions. Liquid temperature, pressure, ullage height and liquid flow rate were recorded.

Three basic tests were performed: sine vibration sweep, sine vibration dwell and random vibration tests. For a sine sweep test, the amplitude of the vibration was held constant while the frequency was varied. The test always began at 5 Hz, the minimum shaker frequency. The frequency was increased at a constant rate. Most of the sine sweep tests were performed using a sweep rate of 2 octaves per minute, which means that the frequency doubles every 30 seconds. An upper frequency limit of 100 Hz was used most of the time, but 50 Hz and 500 Hz were used depending on how well the harmonics of the system were known. Usually the frequency was swept back down to 5 Hz after reaching the upper limit, to determine if decreasing the frequency changed the response. The pressure differential and the screen acceleration were recorded throughout the test. The occurrence of screen breakdown, the frequency, severity, and location on the screen were recorded. Screen breakdown was usually avoided for the sine sweep tests by using lower accelerations and ullage heights because it made the determination of the harmonic peaks in the pressure data more difficult (see the discussion of the pressure data in Chapter V).

Sine vibration dwell tests held the acceleration level and frequency constant, while the ullage height was varied during the test. These tests best establish the conditions under which screen breakdown would occur. The ullage height at which screen breakdown first began was determined, and transducer output was recorded at that condition.

Random vibration tests were similar to the sine dwell tests. For a fixed random vibration spectrum and overall g RMS level, the ullage height was varied to find the point of screen breakdown. It was found that no useful data was obtained from the transducers during the random vibration test due to the nature of the random excitation.

The specific procedures used during the testing are further discussed along with the test results in Chapter V.

This chapter presents the results of the screen vibration tests. As discussed under the test approach in the previous chapter, the test program was set up to achieve two objectives. It provided the vibration data for all the various screen meshes, support methods, and test conditions that were used in performing the analytical correlation. In addition, the test program was composed so as to permit direct comparison of the same test data to establish vibration effects, independent of the analytical models. The following discussion in Section A presents the results of those comparisons. In Section B the correlation between the data and the predictions of the analytical models is presented.

A.   Discussion of Results

The vibration tests provided a large quantity of data on the general effects of vibration on screen acquisition systems. The initial specimens tested were used to make a detailed study of the pressure differentials produced by vibration. As the test program progressed and various screen specimens were tested, many effects, such as the support method and liquid flow, were evaluated. These results were derived from the measured pressures and accelerations, and by comparing the screen response between the various tests.

1.   Basic Screen Response - The data obtained with the pressure transducer provided information on the basic response of the screen specimens to vibration. This pressure transducer measured the vibration produced pressure differential between the liquid in the controlled region and the gas in the bulk region of the model. Signal conditioning removed all steady pressure differentials (due to liquid flow and hydrostatic pressure) so only the vibration produced pressure differential was recorded.

Specimen 1, the first specimen tested, was used to make a study of the characteristics of the pressure differential due to vibration. This specimen had two 7.6-cm (3.0-in) square openings covered with 325 x 2300 screen and located at the top and bottom of the specimen. Due to its simple structure, the response of Specimen 1 was more basic in nature than the other full length specimens The pressure data obtained from Specimen 1 is smoother and has more distinct trends than the data from the other specimens. At the same time, the response of Specimen 1 is representative of the typical response of the other specimens.

The first part of this discussion concentrates primarily on tests performed with the model mounted with the vibration axis and one-g Earth gravity acting parallel to the length of the screen specimen (Orientation 1). As is discussed later in this chapter, this orientation made the screen the most sensitive to the applied vibration. Isopropyl alcohol was used as the test liquid for these tests since it yields relatively high retention capability and therefore improved the resolution of the vibration effects.

a.   Differential Pressure Waveform - The measured pressure differential due to the vibration had a waveform that varied with the frequency of the applied vibration. How the amplitude of the pressure differential varied will be discussed in the following section, but the basic form of the pressure differential will be considered here.

For most of the screen specimens, the pressure differential had a definite positive bias, where positive is defined to mean that the ullage pressure in the bulk region is greater than the pressure of the liquid in the controlled region. Near the harmonic frequency, large positive peaks developed, but the negative component of the differential pressure did not change significantly. For the full length specimens, some variation of the negative component of the pressure differential was seen.

The specimens that had the screen bonded to perforated plate were the only exception to the above described pressure bias. The pressure differential was symmetrical, with equal amplitude negative and positive pressures, over the full range of frequencies. With the bonded support method, the screen could only displace as much as the perforated plate. None of the other support methods limited the screen displacement to the extent of the bonded specimens.

Since the screen displacement had little involvement in the response of the bonded specimens, the pressure differential was primarily due to only the coupling between the liquid mass and the model vibration. There was nothing to bias the response of the system and the pressure differential due to the vibration was symmetrical. For the other specimens, the displacement of the screen caused the positive bias to the pressure. Negative pressure differentials were relieved by the displacement of the screen.

The development of the pressure waveform with frequency is shown by Figure V-1. This is a typical plot derived from the data for Specimen 1. The frequency has been normalized in making the figure so that only two cycles are illustrated, regardless of the actual frequency of the waveform. The differential pressure is positive upwards. The applied acceleration of the model is shown at the bottom of the figure with positive acceleration being upwards.

At 5 Hz, the pressure differential was sinusoidal in form and was in phase with the applied acceleration. A positive acceleration of the model lowered the pressure of the liquid in the controlled region with respect to the gas in the bulk region, producing a positive pressure differential. The relationship is the same as if the model was given a steady acceleration and the hydrostatic pressure of the controlled liquid was measured.

As the first harmonic was approached, but before any amplification of the pressure had occurred, the positive differential pressure developed some small peaks (Figure V-1a). These peaks developed into two distinct peaks at a slightly higher frequency and some amplification became evident (Figure V-1b). The second of the two peaks gradually receded as the first grew, giving a waveform that was basically a series of positive pulses at the first harmonic (Figure V-1c). At this harmonic, the pressure lagged the applied acceleration by a phase angle of 90 degrees.

72
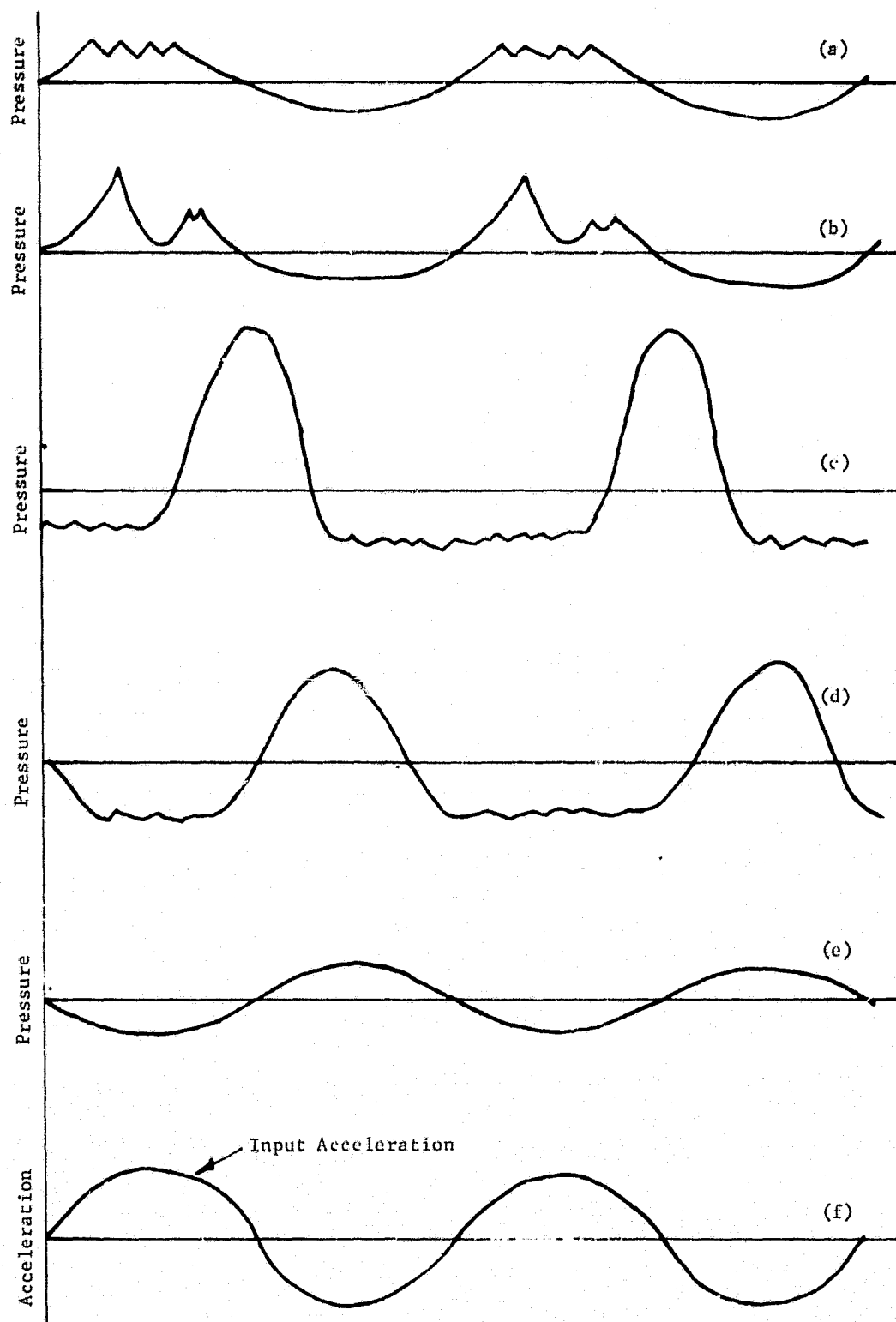
Figure V-1. Pressure Waveforms

73

At the harmonic the combined response of the liquid and the screen, due to the vibration, was a maximum. Based on a comparison of the pressure differential data from the rigid and loose screen specimens, the form of the positive component of the pressure differential was essentially the same. The method of screen support does influence the amplitude of the positive pressure differential, as is discussed later in this chapter. The negative component of the pressure differential, as shown by Figure V-1, is small in comparison to the positive component. Apparently the motion of the screen reduces the amplitude of the negative component of the pressure differential. It is not clear why the screen movement does not influence the positive component of the pressure differential as strongly.

At a frequency above the harmonic the amplitude of the pulses decreased and the phase lag continued to increase (Figure V-1d). Then at some higher frequency the waveform was again sinusoidal and the amplitude was small. The pressure now lagged the applied acceleration by a phase angle of 180 degrees (Figure V-1e). The phase lag of the pressure described above is typical of the phasing of the input and output of a classical spring-mass system. This transition in the waveform of the pressure with frequency could be observed in the test data for most of the specimens. The most distinct characteristic was the growth of one pulse as the other recedes.

Screen breakdown significantly altered the form of the measured differential pressure. If the breakdown was not significant, the pressure oscillations due to the vibration developed a lower frequency component. Differential pressure transients in excess of the screen bubble point were observed. If excessive screen breakdown occurred, the pressure measurement became very erratic. Sine sweep tests, in which no breakdown occurred, provided the best data regarding the peak differential pressures and the harmonic frequencies. Sine dwell data were acquired just as breakdown occurred so that valid differential pressure data could be obtained.

This response was partly due to the direct interaction of the bubbles produced by the screen breakdown with the pressure transducer. Bubbles passing by or hitting the transducer will produce transients. The gas that accumulated within the controlled region oscillated with the applied vibration, adding to the measured differential pressure.

h. Differential Pressure Variation with Frequency - A typical plot of the variation of the differential pressure with frequency for Specimen 1 is shown in Figure V-2. The pressure differential plotted is the positive zero-to-peak pressure. The positive pressure differentials act so as to cause screen breakdown (see discussion of screen breakdown in this chapter).

At frequencies near 5 Hz (the minimum shaker operating frequency), the differential pressure was directly responding to the applied acceleration, since the test model did not provide any amplification of the input vibration. The differential pressure rapidly increases, achieving a maximum value at the harmonic frequency. At frequencies above the harmonic the differential pressure decreases, approaching zero. The model also has second and higher harmonic modes. Usually the first mode produces the maximum pressure differential and the higher modes are less significant, but a few exceptions were noted during the testing.
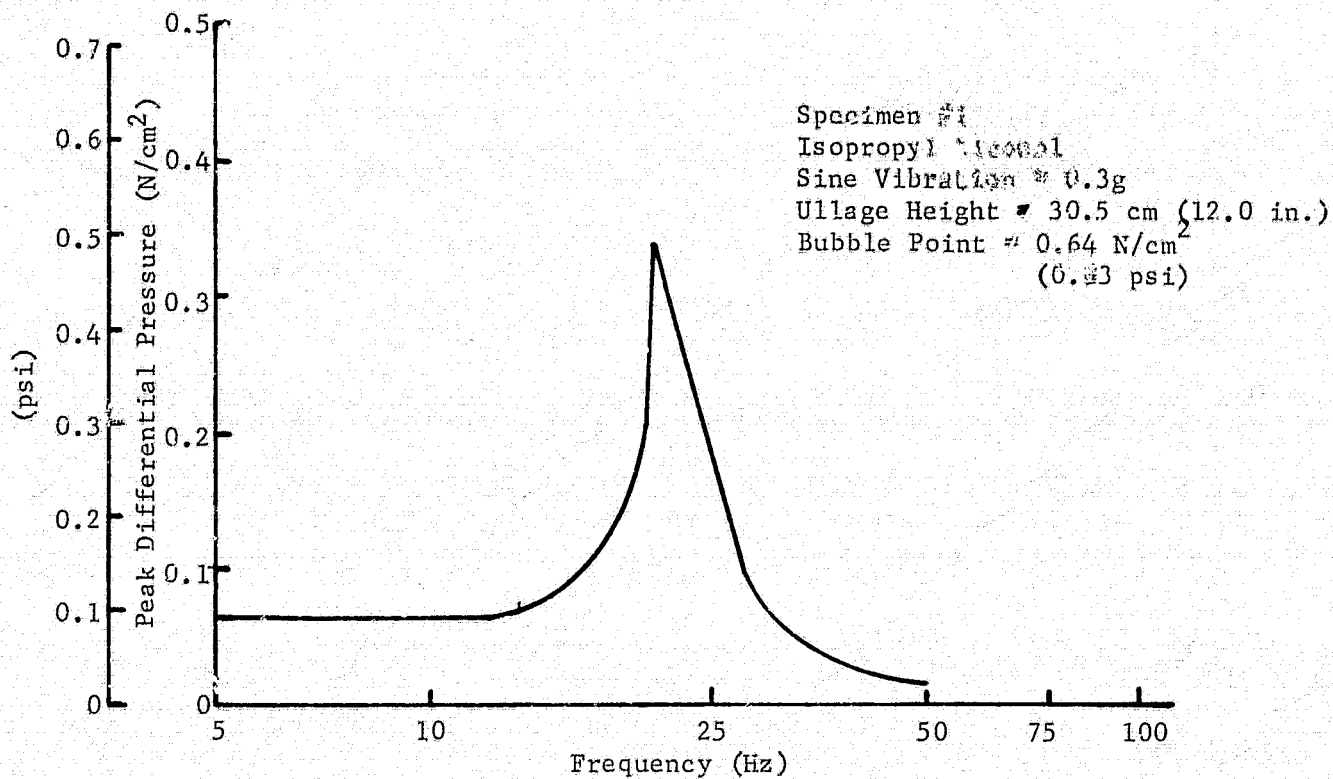
Figure V-2. Variation of Differential Pressure with Frequency

Specimen 1 had the most basic response of the specimens, giving a well defined first mode response. The full length specimens and the various support methods gave the screen many degrees of freedom. Depending on the amplitude and frequency of the applied vibration and the ullage height, the relative significance of the modes changed. In many tests, the first mode was not distinct. The differential pressure would gradually rise, remain at some higher level over a range of frequencies and then begin to decrease. Sometimes there would be a small peak in the differential pressure at a low frequency, followed by a distinct differential pressure rise more typical of the first mode.

When many of the coarser screens were tested, it was found that the maximum differential pressure occurred at 5 Hz and then decreased as frequency was increased. This appears to indicate that the first mode frequency was less than 5 Hz. These specimens had to be tested at small ullage heights, due to the low retention capability, and the large liquid mass in the model tends to decrease the harmonic frequency.

c. Differential Pressure Variation with Position - The location of the pressure transducer could be varied along the length of the model, but was always centered with respect to the model width. With the model mounted in Orientation 1 (refer to Figure IV-4 for the model orientations), the maximum pressure differential due to vibration was found to be at the top of the model. Figure V-3 is a plot of the pressure field measured for Specimen 4, a full length unsupported 325 x 2300 screen. The amount of liquid mass being vibrated was the maximum at the top of the model, producing the maximum differential pressure due to the vibration.

In Orientations 5 and 6, the same response with transducer position was recorded. The maximum differential pressure was measured at the top of the model. In all three of these orientations the model was vertical so the result is consistent. For Orientations 2 and 4 no significant differences in differential pressure with transducer position were measured, which would be as expected due to the orientation of the vibration. When the model was mounted in Orientation 3, interference between the pressure transducer tube and the shaker permitted the pressures to only be measured at the center of the model.

d. Softening Spring Effect - When the sine sweep tests were performed they were started at 5 Hz, the frequency was increased to a selected value and then was decreased back to 5 Hz. At low acceleration levels, the differential pressures measured when sweeping up and down were the same. Figure V-2 is an example where the differential pressure was the same regardless of whether the frequency was increasing or decreasing.

When sine sweep tests were performed, using Specimen 1 and applying accelerations of 0.75g or greater, the hysteresis effect shown in Figure V-4 was observed. As frequency was increased, one path on the pressure versus frequency plot was followed (indicated by arrows), and when frequency was decreased, another path was followed. Above and below the harmonic the path was the same regardless of whether frequency was increased or de-
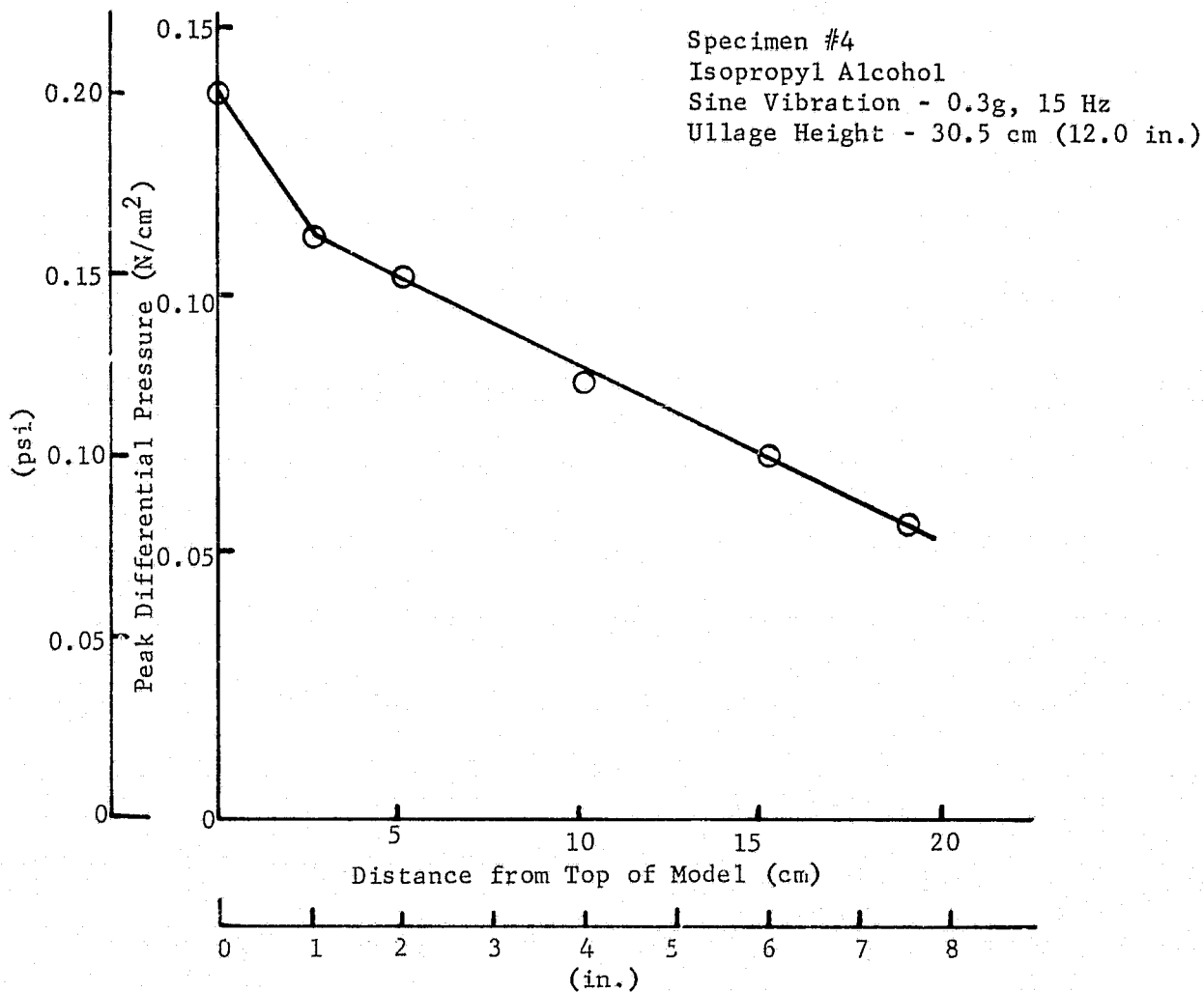
Figure V-3. Variation of Pressure with Position in Liquid
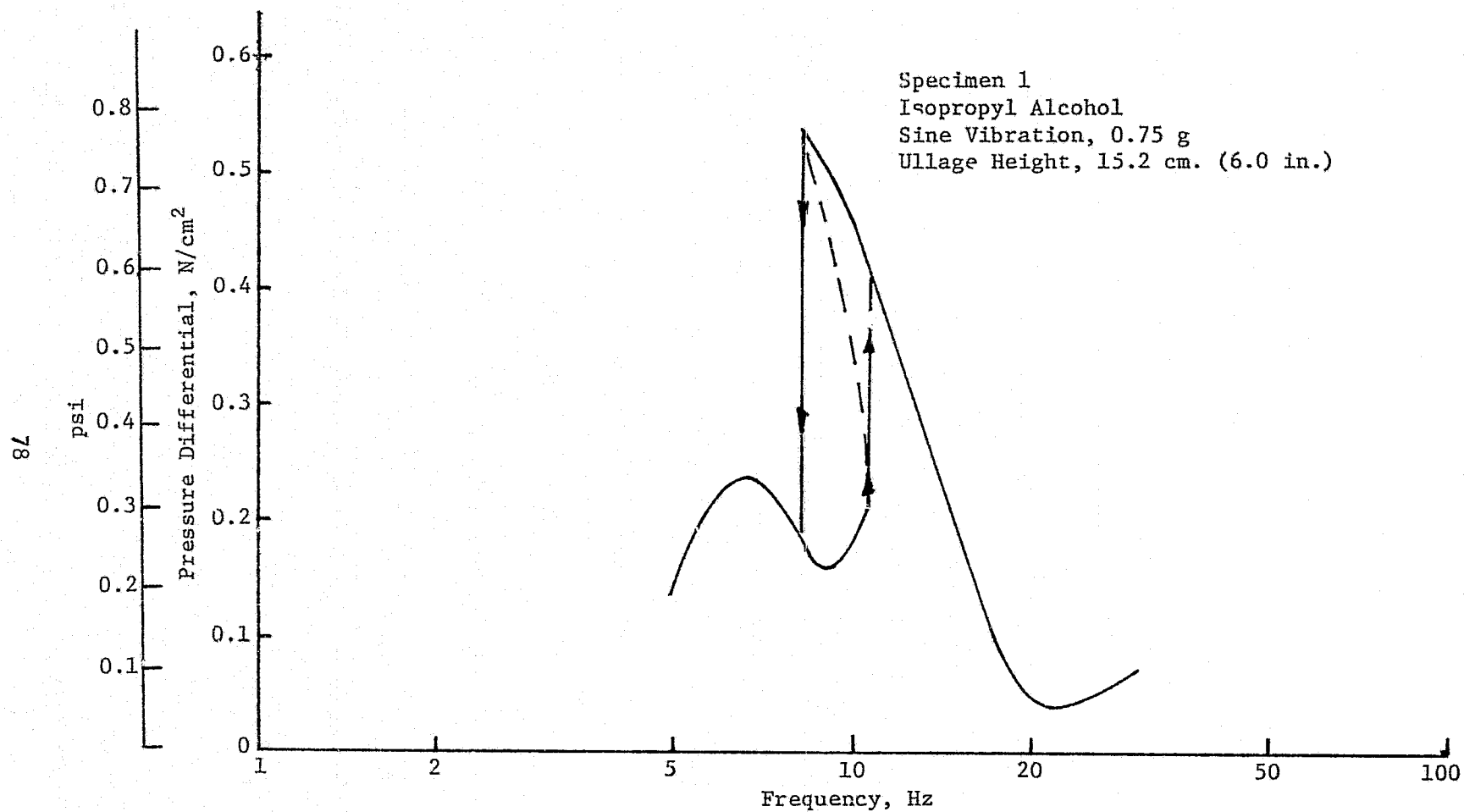
Figure V-4.   Screen Response to Sinusoidal Vibration

creased. The actual form of the curve just below the harmonic is indicated by the dashed curve. Since the curve is double valued over a range of frequencies the differential pressure jumps from a low to high value as the frequency increases or vice versa, giving the observed hysteresis. The response curve is similar in form to the one shown in Figure V-2, except that it leans over towards lower frequencies.

This hysteresis effect caused the peak differential pressure at the harmonic to be greater when the frequency was being decreased. This effect was directly observed when screen breakdown occurred during the sine sweep. For example, if the screen breakdown was slight and took place over only a small frequency range ($\sim$ 5 Hz) as the frequency was increased, then as frequency was decreased breakdown began, became excessive and continued over a wider frequency range.

This type of response is typical of a "softening spring," that is, a spring that becomes less stiff as it is displaced. An actual metal spring usually has the opposite characteristic, it becomes harder as it is displaced. The same would be expected of a screen membrane: displacing the screen would make it stiffer. Another mechanism must be involved to cause the softening effect. This mechanism must be the gas/liquid interface within the screen pores.

The interface within the screen has the form of a gas bubble at each pore. While these gas bubbles are attached to a surface, their response is similar to a free gas bubble. The response of a single gas bubble to a sinusoidally varying pressure field has been analyzed and it has been found that it has the softening spring characteristic (Ref. V-1). The gas/liquid interface must contribute to the stiffness of the screen. The bubbles at each pore are small, having a diameter that is on the order of the pore diameter, but there are many pores per unit area. For Specimen 1, the contribution of the interface was enough to overwhelm any hardening spring effect from the screen wires and give the softening spring response. The harmonics of the gas bubbles are not involved, they have a very high harmonic frequency (order of 10^5 Hz), it is only their stiffness characteristic that influences the response.

Specimens 1 and 2 were the only specimens that exhibited this distinct softening spring effect. These two specimens had the effect of the vibration concentrated on a single screen window, while it was distributed over the full length of the other specimens. Also, the high retention capability of the 325 x 2300 screen used in these specimens permitted larger accelerations and ullage heights that could not be used with the coarser screens. These factors made the softening spring effect more obvious. For the other specimens, the effect was not sufficient to produce a measurable difference in the frequency of the harmonic due to increasing and decreasing frequency.

e.   Ullage Effects - The pressure transducer measured the differential pressure between the bulk ullage and the liquid in the controlled region. An evaluation was performed to determine the contribution of the ullage region to the differential pressure. Three sine sweep tests, with varied

accelerations and ullage heights, were selected for this evaluation. Tests
in which the pressures were significant, but no screen breakdown occurred
(which would produce erratic pressures) were selected. After performing
the test with the transducer properly connected, the test was repeated with
the reference side of the transducer disconnected from the ullage side and
left open to atmospheric pressure. Two conditions were considered, the
bulk side sealed (the normal condition) and the bulk side open to the
atmosphere.

For each pair of tests, the measured pressure differential was the same re-
gardless of whether the reference line was connected or disconnected. The
fact that the transducer was AC coupled eliminated the static pressure dif-
ferences that would normally be observed when the reference line was dis-
connected. These results indicate that the effect of the vibration is to
vary the pressure of the liquid in the controlled region. The ullage pres-
sure, even with the relatively small volume of the model, remains constant
and does not contribute to the pressure differential due to vibration.

2.   Screen Breakdown - Most of the tests that were performed had the ob-
jective of causing screen breakdown so that the contribution due to vibra-
tion could be established. For the sine dwell and the random vibration
tests the vibration environment was held constant and the hydrostatic pres-
sure was increased, by draining liquid from the bulk region, until screen
breakdown occurred. In many of the sine sweep tests, screen breakdown
occurred at a specific value of frequency.

a.   Manner of Screen Breakdown - The degree of screen breakdown, the rate
at which gas passes through the screen, can cover a wide range. For the
purpose of this discussion, breakdown can be classified as slight, signifi-
cant and excessive. Slight breakdown is defined as the initial onset of
breakdown, when very small bubbles penetrated the screen and continued
breakdown was necessary before any real accumulation of gas bubbles could
be observed. The amount of breakdown is small enough to be neglected.
This type of breakdown occurred when the total pressure differential was
close to the screen bubble point and a few pores were made to breakdown.
The cause of slight breakdown could be localized screen vibration effects,
periodic components of the random vibration that make the differential pres-
sure exceed the bubble point, a few pores that are somewhat larger than ad-
jacent pores, or some similar effect.

Significant breakdown is due to readily observable bubbles being detached
from the screen and resulted in a definite accumulation of gas in the con-
trolled region. This type of breakdown is similar to the first breakdown
of a screen when a conventional bubble point test is performed. Over a
small area of the screen, the total pressure differential slightly exceeds
the bubble point of the screen.

Excessive breakdown results when a large quantity of gas abruptly passes
through an area of the screen and begins to fill the controlled region.
To produce this condition, the total pressure differential acting over an
area of screen much exceeds the bubble point of the screen. These are only
qualitative definitions and the boundaries separating them are not well
defined.

80

This range of screen breakdown rates was best demonstrated by the random vibration tests. As the hydrostatic pressure was increased a distinct transition from slight to significant to excessive breakdown could always be observed. This transition could not be observed during the sine tests and in many cases the first indication was excessive breakdown. With sine vibration, breakdown was usually associated with a system harmonic, that involved a rapid change in amplification with either frequency or ullage height. With random vibration, a range of frequencies are being excited so a more gradual approach to the point of screen breakdown was possible.

When slight breakdown began, the bubbles were difficult to see. Their size is estimated to be on the order of 0.2 mm (0.01 in) diameter. After the breakdown had continued for about one minute, coalescence of the bubbles would result in the collection of gas bubbles on the order of 5 mm (0.2 in) diameter. For the random vibration tests, performed with 325 x 2300 screen (isopropyl alcohol, Orientation 1), there was a significant span in ullage height between the first indication of slight breakdown and excessive breakdown. Spans between slight and significant breakdown ranged from 2 cm (0.8 in) to 10 cm (4 in), which corresponds to between 2 and 12 percent of the screen bubble point. From slight to excessive breakdown, spans as much as 15 cm (6 in) were measured (18% of the bubble point).

Slight breakdown during the sine vibration tests was more of a short duration, transient breakdown. The very small bubbles observed during the random vibration test were not observed during the sine vibration tests. The span in ullage height between slight and excessive breakdown for a sine dwell test was small, on the order of 2 cm (0.8 in).

It was also possible in a sine dwell test to have breakdown begin at some ullage height and then as the ullage height was further increased, breakdown can cease. The results shown in Figure V-5 are an example of this phenomena. There was a harmonic peak in the effect of the vibration that is a function of liquid mass, which was varied by the ullage height. The sum of the hydrostatic pressure differential plus the pressure differential due to vibration shows that the total pressure differential exceeded the bubble point at ullage heights of 23 cm (9 in) and 38 cm (15 in), where screen breakdown was observed.

Under all conditions of screen breakdown, the breakdown would continue as long as the condition that caused breakdown was sustained. Once the vibration conditions had been changed to sufficiently reduce the pressure differential acting on the screen, breakdown ceased. When breakdown stopped, the screens always regained their retention capability and under even the most excessive breakdown conditions, some liquid height was still being retained by the screen. There was no catastrophic breakdown of the screens, where all retention capability was lost. This type of response, as it applies to liquids with various amounts of subcooling, is discussed later in this chapter.

b.   Localized Effects - It was found that the manner in which the screen was supported influenced where the screen broke down. Consider the basic case where the model was in Orientation 1 (vibration and one-g parallel to
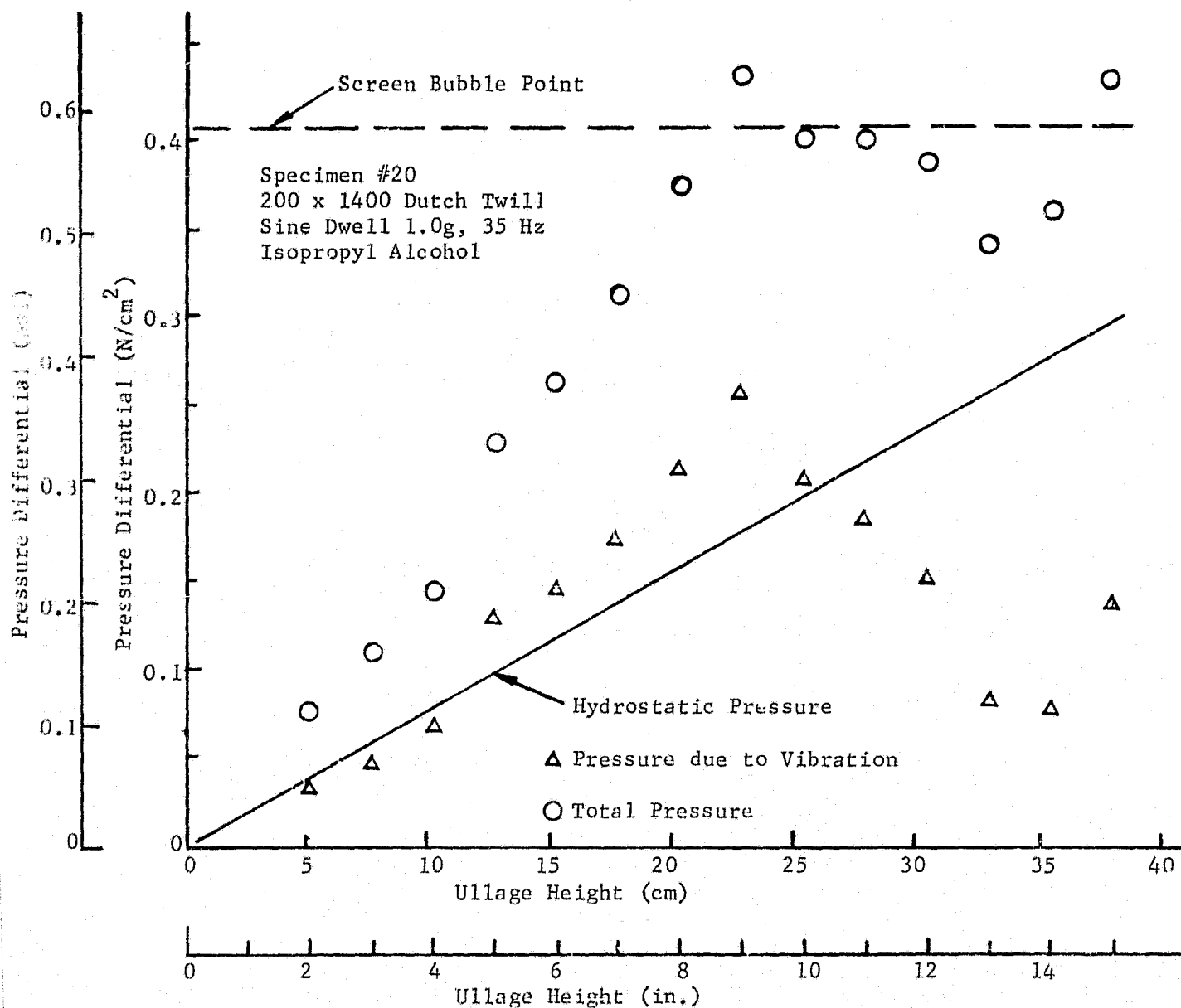
Figure V-5.   Effect of Liquid Height on Screen Response

the longer length of the screen). The pressure differential across the screen due to hydrostatic pressure differential was the maximum at the top pores of the screen. The measured pressure differential due to the vibration was also a maximum at the top of the screen. Therefore, screen breakdown would be expected to first occur at the top of the screen. The screen breakdown observed during the tests did usually occur at the top of the screen for this orientation. For the more rigidly supported screen specimens, such as the ones that had the screen bonded to a perforated plate and the ones that had pleated screen, screen breakdown always occurred at the top of the screen. However, for the more loosely supported screens, screen breakdown was observed at various locations on the portion of the screen that was exposed to the ullage. When breakdown first occurred at locations other than the top of the screen, it was very localized. Only small patches of screen, about 1 cm (0.4 in) in diameter or less break down. The breakdown would be classified as slight. The occurrence and location of the breakdown was a function of frequency and ullage height. As either factor was varied, breakdown would occur and cease at various locations on the screen. It was also observed that the finer mesh screens, that are thinner and lighter, are more likely to break down at locations other than the top of the screen.

The combination of the loose support method and the thin screen material permitted portions of the screen to flutter, independent of the net oscillation of a screen panel. Small wrinkles were present in the screen material as a result of the fabrication process. Typical fabrication methods do not include any means of holding the screen taut, so these wrinkles are inherent in the non-rigid support methods. These wrinkles could be observed to flutter under various vibration conditions and the wrinkles were the positions where the localized screen breakdown did occur. Apparently, the rapid movement of the screen due to this localized flutter, produced a fluctuation in the liquid pressure in the vicinity of the flutter. This localized pressure oscillation, added to the bulk pressure oscillation from the screen panel vibration, was sufficient to cause the localized screen breakdown, even though the hydrostatic pressure differential was less than it was at the top of the screen.

The pressure transducer could only measure the bulk effect of the screen vibration. While the transducer could be moved up and down within the controlled region of the model, the diaphragm was always 1.2 cm (0.48 in) away from the screen. At that distance the pressure oscillations due to the flutter could not be measured.

Some measurements made using Specimen 4 (unsupported 325 x 2300 screen) illustrate this effect very well. For a sine dwell at 1.0g and 20 Hz, screen breakdown was first observed at a point 10 cm (4 in) down from the top of the screen, in the center of its width, when the ullage height was 20 cm (7.9 in). With the pressure transducer positioned at the top of the screen, a pressure differential due to vibration of 0.43 N/cm^2 (0.62 psi) was measured. Added to the hydrostatic pressure differential, the total pressure differential at the top pores of the screen was 0.58 N/cm^2 (0.84 psi), which is close to the bubble point of 0.62 N/cm^2 (0.90 psi). When the pressure transducer was positioned opposite the point of screen

breakdown, a pressure differential due to the vibration of only 0.25 N/cm^2 (0.36 psi) was measured. Since the hydrost ....ssure differential was also less at that position, the total pressure differential was 0.32 N/cm^2 (0.47 psi), which is only half the bubble point. The localized flutter must be creating the additional pressure differential to cause screen breakdown. The above described conditions are typical of many similar measurements that were made. The pressure differential acting on the screen at the top of the model (Orientation 1) is usually near to the bubble point (about 20% less) when localized breakdown occurs elsewhere.

c.   Contribution of Vibration to Screen Breakdown - The primary purpose of the sine dwell tests was to determine how the measured pressure differential due to vibration contributed to the breakdown of the screens. Conditions were produced at which the screen began to break down and the pressure differential due to the vibration was measured. This measured pressure differential due to vibration was then added to the hydrostatic pressure differential, calculated from the ullage height and the liquid density, and the sum was compared to the bubble point of the screen.

These sine dwell tests were performed on all the screen meshes, using a range of vibration accelerations and frequencies. The analysis of this data shows that screen breakdown can be predicted based on the sum of the vibration and hydrostatic pressure differentials. The pressure differential due to vibration that causes screen breakdown is the positive peak of the time varying pressure differential. A positive pressure differential lowers the pressure of the liquid in the controlled region with respect to the ullage.

For the finer mesh screens that were rigidly supported and the coarser screen meshes, the sine dwell data repeatedly demonstrated that the sum of the measured pressure differential due to vibration and the calculated hydrostatic pressure differential, equalled the bubble point when screen breakdown was occurring. For those cases where localized screen flutter was adding to the vibration produced pressure differential, the pressure transducer was not measuring the local effects. It can only be presumed that if the true pressure differential due to the vibration was known, the sum of the pressure differentials would yield the bubble point when screen breakdown occurred. As previously discussed, the bulk vibration effect that was measured gave a total pressure differential that could be about 20% less than the bubble point.

This result established that the frequency of the pressure oscillations due to the vibration was low enough to allow the screen to respond to the peak pressure differential of the oscillations. Sine dwell tests at frequencies up to 50 Hz were performed to determine if the pressure oscillation frequency influenced the effect of the vibration. Around a 50 Hz frequency and above, the pressure differential due to vibration was usually so small that it was difficult to resolve it from the hydrostatic pressure differential needed to produce screen breakdown. The significant effects of sine vibration occurred in the range of 10 to 20 Hz, where the first harmonics for the specimens tested fall. At these low frequencies the screen does not have the accumulator effect that is considered by the Bubble Growth Model discussed in Chapter III.

3.   Effect of Weave Orientation - Most of the screens used in acquisition devices have a different number and configuration of their wires in the warp and shute directions. The only exception is the square weave screens that have an identical warp and shute configuration. The differences in screen geometry can influence the structural properties of the screen in opposite directions. Since the response of a screen to vibration involves the deflection of the screen, which is a function of the structural properties, it might be expected that the orientation of the screen weave within the screen specimen could influence the screen response.

Four of the screen specimens were specifically intended to investigate the effects of screen weave orientation. Each of these screen specimens had the "unsupported" structural configuration. The screen was only supported at the seam weld around the edges, leaving the 7.6 cm (3.0 in) by 38.1 cm (15.0 in) center span unsupported. Two specimens were made for each of the screen weaves considered, one with the warp wires running in the short direction and the other with the warp wires running in the long direction. This configuration should produce the most significant difference in response between two specimens of the same weave, within the geometric constraints of the test model. The narrow dimension could have been reduced, but the deflection of the screen would have been too limited to provide adequate screen response.

The stiffness of the screens in the warp and shute directions was estimated to determine which screens would most show the effects of weave orientation. This was done by calculating an average thickness of the screen in the warp and shute directions, based on the volume of the wires per unit length. If it is assumed that the stiffness of the screen in one direction is independent of the loading in the other direction, then the stiffness is given by the product of the modulus of elasticity and the average thickness. Tensile test data for some of the screens used here is available (Ref. V-2) that shows that there is a reduction in the stiffness due to the bending of the slightly curved wires. The shute wires are usually more curved than the warp wires and the reduction is most pronounced in that direction. When measured values for the effective stiffness were not available, a reduction factor was estimated.

Presented in Table V-1 are the estimated stiffness values. These stiffness values indicate that there is little difference in the screen stiffness between the warp and shute directions. One exception is the 850 x 155 screen. Due to the unusual Robusta weave, this screen was predicted to have a factor of 8 difference in stiffness between the warp and shute directions.

Based on this evaluation, two screen meshes were selected to establish if an effect of weave orientation exists. One set of samples was made of the 850 x 155 screen, since it was predicted to be the most sensitive to orientation. The other set was made of 325 x 2300, which was predicted to have a stiffness independent of orientation. The high bubble point of

Table V-1. Predicted Screen Stiffness

Screen Mesh (wires per inch)	Weave	Wire Diameter mm (in.)		Actual Stiffness N/cm (lbf/in.)		Effective Stiffness N/cm (lbf/in.)	
		Warp	Chute	Warp	Shute	Warp	Shute
325 x 2300	Dutch Twill	0.038 (0.0015)	0.025 (0.0010)	27,800 (15,900)	80,900 (46,200)	19,400 (11,100)	20,300 (11,600)
200 x 1400	Dutch Twill	0.071 (0.0028)	0.041 (0.0016)	60,400 (34,500)	133,000 (76,000)	49,600 (28,300)	33,300 (19,000)
165 x 800	Dutch Twill	0.071 (0.0028)	0.051 (0.0020)	49,700 (28,400)	123,000 (70,400)	33,800 (19,300)	29,600 (16,900)
165 x 800	Plain Dutch	0.051 (0.0020)	0.036 (0.0014)	25,400 (14,500)	60,400 (34,500)	17,300 (9,900)	14,500 (8,300)
80 x 700	Dutch Twill	0.102 (0.0040)	0.076 (0.0030)	49,200 (28,100)	243,000 (139,000)	39,400 (22,500)	60,900 (34,800)
50 x 250	Plain Dutch	0.127 (0.0050)	0.114 (0.0045)	48,200 (27,500)	194,000 (111,000)	33,800 (19,300)	48,700 (27,800)
850 x 155	Robusta	0.030 (0.0012)	0.102 (0.0040)	47,100 (26,900)	95,400 (54,500)	8,060 (4,600)	66,900 (38,200)
200 x 200	Square	0.053 (0.0021)	0.053 (0.0021)	34,000 (19,400)	34,000 (19,400)	10,500 (6,000)	10,500 (6,000)

the 325 x 2300 aids in data resolution, so as to better indicate any effect of orientation. Orientation 1 (vibration and one-g parallel to the long axis of specimen), which is the most sensitive axis and isopropyl alcohol, which also aids in resolution, were used in performing these tests.

Identical sine sweep tests were performed on both of the samples of a given mesh. For the two 850 x 155 specimens (specimens 24 and 25) 0.5g with a 15.2 cm (6.0 in) and 20.3 cm (8.0 in) ullage height, and 0.75 g with a 15.2 cm (6.0 in) ullage height were used. The two 325 x 2300 specimens (specimens 4 and 5) were tested with identical 0.3g, 30.5 cm (12.0 in) ullage height and 1.0g, 20.3 cm (8.0 in) ullage height sine sweeps. The frequency, amplitude and form of the measured pressure differential at the first harmonic of the system were used to perform the comparison.

In all cases the observed results, occurrence and amount of screen break-down, if any, were the same for all the pairs of tests. For the 850 x 155 screen, both specimens had a first harmonic that occurred at the same frequency (within 1 Hz) and the peak pressure differentials were essentially the same (within 0.03 N/cm^2 (0.05 psi)). The first harmonics for the pair of 325 x 2300 screen were also alike. While the peaks were the same, some minor differences in the way the pressure varied with frequency were noted. These differences are attributed to the localized effects that were discussed earlier in this section. The "unsupported" screen support method, while being of the needed length and width to indicate weave orientation effects, introduces localized effects that are difficult to control. Typical fabrication methods were used in making the specimens, so there was no way to accurately duplicate the screen tautness between the two specimens in the pair.

It is concluded from these tests that the effect of weave orientation is negligible. If there were any significant differences there would have been a noticeable change in the frequency and amplitude of the first harmonic. If there were differences, they were of the same order of magnitude as the localized effects caused by the differences in screen tautness between the specimen pairs.

This result is consistent with data gathered under a prior study (Ref. V-3). Various screen specimens were pressurized as a membrane and the deflection with pressure was measured. It was found that the screen behaved as an isotropic medium (uniform in all directions) and could be modeled as such.

4. Effect of Model Orientation - Some of the specimens were tested in varied orientations. Specimen 5 (unsupported 325 x 2300 screen) was used to perform an investigation of the effect of the orientation of the screen surface with respect to both the vibration and one-g. Six possible model orientations, shown in Figure IV-4 were considered (the screen specimen is parallel to the largest face of the model).

In each orientation sine sweeps and dwells with various accelerations were performed. The ullage height could be varied when the model was tested in

87

Orientations 1. 5 and 6. In Orientations 2, 3 and 4 the liquid in the controlled region was supported above the screen and the liquid in the bulk region was drained away, completely exposing that side of the screen to gas.

The tests established that the effect of the vibration is directly proportional to the length of the liquid column being supported by the screen, parallel to the direction of the vibration. The model had a similar response and was most sensitive to vibration in Orientations 1 and 3. Orientation 3 made the model the most sensitive since the vibration always acted over the full 38 cm (15 in) length of the screen specimen. In Orientation 1 the sensitivity of the screen was varied by changing the ullage height, which varied the height of the liquid column on which the vibration acts and changed the hydrostatic pressure differential acting on the screen. Accelerations as low as 0.5g readily produced screen breakdown in these two orientations.

Orientations 2 and 5 made the model the least sensitive to vibration. Accelerations greater than 2g were needed to cause breakdown of the screen. In Orientation 5 the thickness of the controlled region (2.4 cm (0.95 in)) plus a contribution of the liquid column in the bulk region, was the liquid column on which the vibration acted. The vibration only acted over the thickness of the controlled region in Orientation 2, making the model least sensitive in that orientation.

Orientations 4 and 6 were intermediate in sensitivity. The liquid column was determined by the width of the model for Orientation 4 and a contribution due to the bulk liquid column was added for Orientation 6.

The liquid column upon which the vibration can be defined to act in each orientation can be estimated by evaluating the pressure differential due to vibration at low frequencies. At the minimum test frequency of 5 Hz, the screen and the structure did not appreciably amplify the pressure differential due to the vibration. This pressure differential can be calculated based on a purely ρgh hydrostatic relationship where the acceleration is the zero-to-peak amplitude of the sine vibration and the h is the above discussed column height. These calculations indicated that the liquid column height for Orientations 2, 3 and 4, where there was no bulk liquid height, was close to the dimension of the controlled liquid mass parallel to the direction of the vibration. The presence of bulk liquid on one side of the screen made the column height approximately equal to the ullage height, based on the data for Orientation 1. For Orientations 4 and 5, the contribution of the bulk liquid was not as distinct.

Based on this evaluation of the effect of model orientation, Orientation 1 was selected as the primary orientation for the remainder of the testing. This orientation was the critical condition for the effect of vibration on the model. Orientation 3, which was the most sensitive to vibration, can be considered to be only a special case of Orientation 1. Since the ullage height could be varied in Orientation 1, the test conditions could be controlled to establish the point of screen breakdown for a given input

acceleration. Most of the testing was performed using Orientation 1. When some of the coarser mesh screens were tested, Orientation 5 was also used. In Orientation 5 the ullage height could still be varied, but the model was much less sensitive to the vibration. This was desired due to the low retention capability of the coarse screens.

When the dual element model with the 325 x 2300 Dutch twill screen was tested, Orientations 1 and 5 were used. On a relative basis, the response was similar to that with a single screen element. This comparison established that the orientation effects investigated with the single element model were not unique to that configuration.

5. Effect of Screen Support Method - The screen of each specimen was supported by one of six methods. These support methods are typical of standard screen fabrication methods used in current development and flight acquisition systems. The six methods were:

(1) Bonded to Perforated Plate - by a diffusion welding process the screen was bonded to a perforated plate.

(2) Supported by Perforated Plate - the screen rested on perforated plate, with the screen facing the bulk liquid side of the model.

(3) Unsupported - the screen was attached to an open frame around its periphery.

(4) Pleated - the screen was pleated prior to attaching it to an open frame.

(5) Internal Rib - the screen rested on ribs that were located on the controlled liquid side of the screen.

(6) External Rib - the screen was attached to ribs located on the bulk side of the screen.

The details of the fabrication of the specimens were presented in Chapter IV. These support methods gave a wide range of variation to the rigidity of the screen support.

Six screen specimens (Specimens 5 through 10) were made using each of the support methods, but with the same screen mesh, to perform a relative evaluation of the support methods. The 325 x 2300 Dutch twill screen and isopropyl alcohol as a test liquid were selected to give a large retention capability and therefore improve the resolution of the effects of the vibration. Orientation 1 was used for all the tests. The controlled region was completely filled with liquid, random vibration was applied to the model and the bulk region was drained until screen breakdown was detected. The ullage height at which slight, significant and excessive screen breakdown (see the screen breakdown discussion) occurred was identified for various vibration levels. The point of significant breakdown was used in this comparison since it was the most well defined breakdown condition.

89

C-2

A random vibration spectrum with a constant power spectral density over a range of frequencies was selected for these tests (Figure V-6).
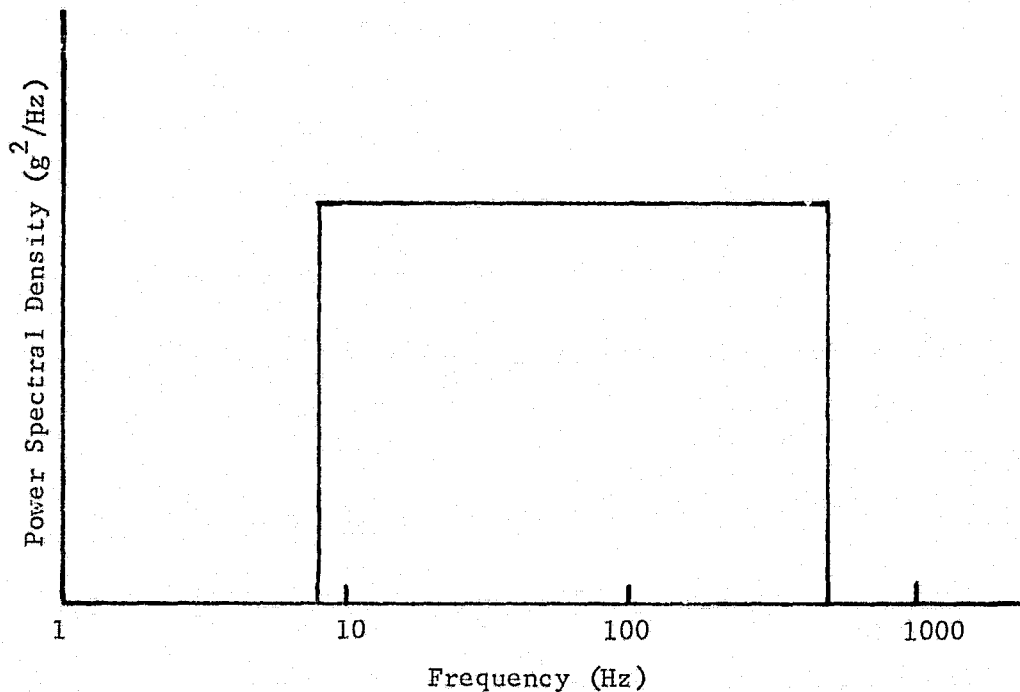
Figure V-6. Random Vibration Spectrum

The spectral density of this spectrum can be shifted either up or down to change the applied overall gRMS level. Such a spectrum adequately excited the lower frequencies where the harmonics of the model lay. A lower limit of 8 Hz for the frequency range extended the spectrum below the harmonic frequencies. By setting an upper frequency limit of 500 Hz, the resolution of the spectrum at the low frequency end was improved. This is due to the logarithmic frequency increments of the filters used to form the spectrum. The resolution of the logarithmic increments to the spectral density, provided with this spectrum, also fit the total test system sensitivity. It was also found that this spectrum could be accurately reproduced each time a test was performed.

The objective of these tests was to establish a constant set of conditions under which each support method could be evaluated. For each support method the same range of gRMS levels were applied and the liquid retention

height for each level was established. In effect, these tests simulated various surface tension devices in the same spacecraft, with a given vibration environment, and the available retention capability of the screen was established.

The results of these comparative tests are shown in Figure V-7. The power spectral density defines the level of the vibration and the ullage height is the point at which the screen breakdown became significant.

The general trend in the curves indicates that as the ullage height increases, the screen was more sensitive to vibration. This is consistent with the previous discussion of the effects of model orientation. Increasing the ullage height, increased the liquid column on which the vibration acted and produced greater pressure differentials due to vibration.

The curves show that there was a definite effect due to the screen support method. The two extremes caused a difference in retention capability that amounted to around 15 cm (6 in) in ullage height. All six curves are similar in form. The curve for the external rib support method has more curvature than the others, causing it to be the only one that crosses another. There is an unusual bend in the curve for the pleated support method.

The curves converge at small values of ullage height. This is to be expected because the influence of the support method will become less as the amount of screen exposed is less. The support method lost its influence when the screen was submerged in the liquid. For the same reasons the trends of the curves are most varied at large ullage heights, when the effect of the support method was most pronounced. If all the curves are extrapolated in the region of small values of ullage height, they almost intersect at a point on the zero ullage height axis. If this truly did happen, it would imply for this model that the screen would always break down if the spectral density was greater than about 0.1 g^2/Hz.

The pleated support method made the screen the least sensitive to the vibration environment. The bonded to perforated plate support method was next in sensitivity. These are the two methods that most rigidly support the screen. The external rib support method or the supported by perforated plate support method make the screen the most sensitive to vibration, depending on the range of the ullage height.

It is hypothesized that the support method influences the sensitivity of the screen to vibration in two ways. One factor is the bulk displacement of the screen that occurs when the entire screen panel or the individual windows of the specimen displace in response to the vibration. The other factor is the localized displacement of only a small area of the screen. This localized displacement occurs due to any looseness of the screen, which is inherent in the typical fabrication methods that were used. When localized displacement did occur it could be observed and did lead to screen breakdown in those same areas (see Screen Breakdown discussion).

POWER SPECTRAL DENSITY (g²/Hz)

$1X10^{-1}$

$5X10^{-2}$

$1X10^{-2}$

$5X10^{-3}$

$1X10^{-3}$

UNSUPPORTED

BONDED TO
PERF. PLATE

PLEATED

EXTERNAL
RIB

INTERNAL
RIB

RANDOM VIBRATION
ISOPROPYL ALCOHOL
ORIENTATION 1

SUPPORTED BY
PERF. PLATE

2   4   6   8   10   12   14

ULLAGE HEIGHT (INCHES)

5   10   15   20   25   30   35

(CENTIMETERS)
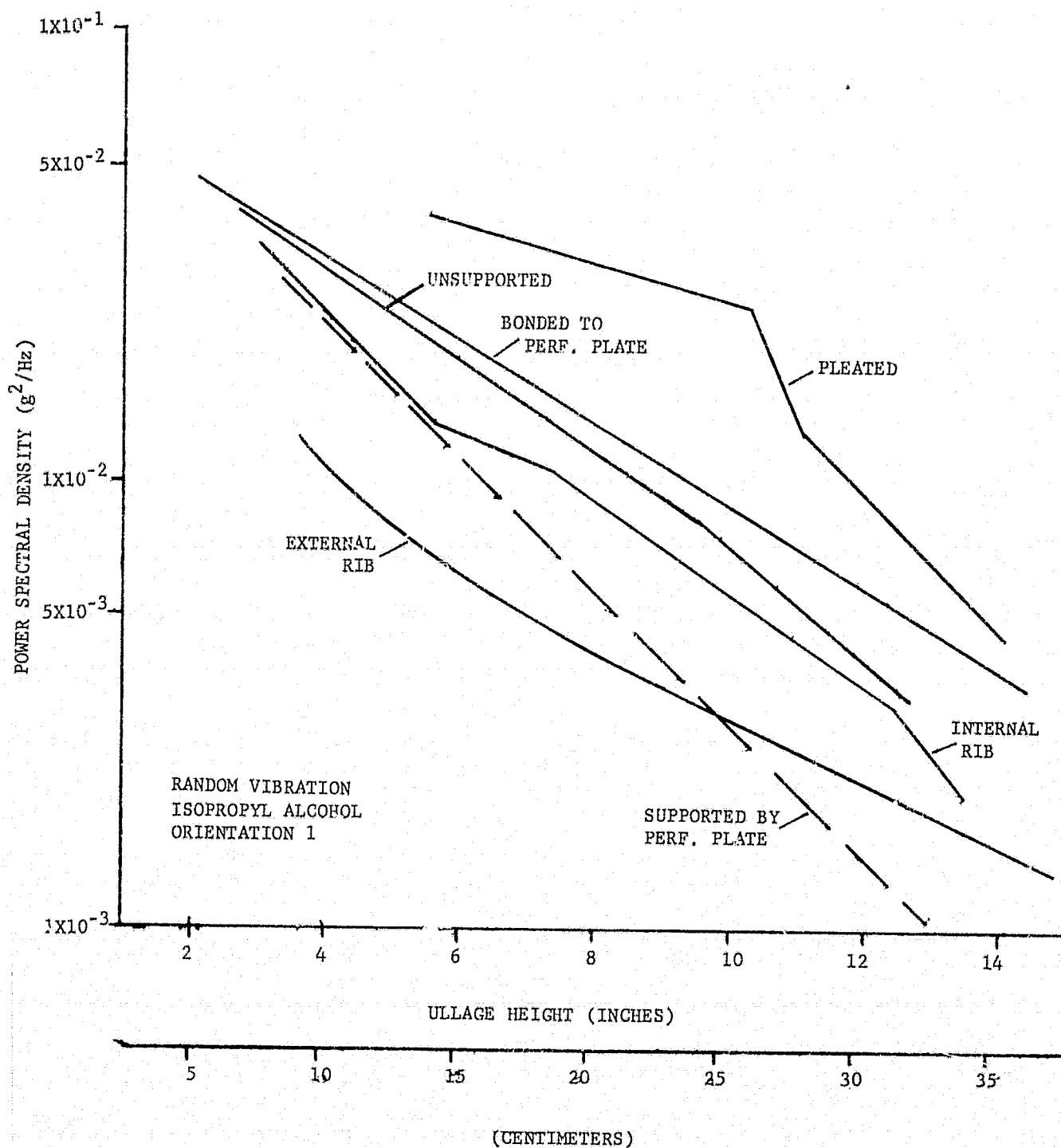
Figure V-7. Influence of Screen Support Method
on Response to Vibration

92

Bulk displacement of the screen permits the controlled liquid volume to change with very little hinderance, thereby relieving the pressure differentials that could be created by the vibration. Displacement of the screen toward the controlled liquid side of the model acts to relieve a lowering of the pressure in that region which is tending to cause screen breakdown. However, the localized displacement produces pressure gradients in the area of the oscillation that add to the pressure differential produced by the bulk displacement, increasing the total pressure differential acting on the screen.

This hypothesis is applied to the test results as described in the following paragraphs. The specimen with the pleated support method had the pleats running the long direction of the specimen. This pleat configuration allowed considerable bulk deflection of the screen. Approximately 0.7 cm (0.3 in) of displacement of the screen at its center occurred during the bubble point test. The displacement was constrained more by the flexibility of the screen pleats than by the stiffness of the screen material. The pleat geometry rigidly constrained the screen with respect to localized displacement and no localized screen breakdown was observed. This combination of bulk flexibility and localized rigidity made the pleated specimen least sensitive to the vibration. As the ullage height varied, there must have been a change in the mode of the bulk displacement which would account for the slope changes in the curve for this specimen. If the pleats of the specimen ran in the opposite direction (the width of the specimen) the bulk displacement would be much less. It would be expected that its response would be similar to that of the bonded specimen.

The bonded specimen also has local screen rigidity. The small unsupported span of 0.95 cm (0.38 in) eliminates the local screen displacement effects. No localized screen breakdown was observed with this specimen. Bulk displacement of this screen was limited by the perforated plate. This lack of bulk displacement increased the sensitivity of the screen to vibration. However, the lack of localized displacement made this specimen less sensitive to vibration than the remaining specimens.

The unsupported specimen had considerable bulk displacement, but there was some localized displacement. The two effects balanced out to make it somewhat more sensitive than the bonded specimen.

The internal ribs limited the bulk displacement of the screen as it deflected toward the controlled liquid side of the model, increasing the sensitivity in comparison to the unsupported specimen. When the screen was supported by perforated plate, no displacement toward the controlled region was possible making this specimen more sensitive than the internal rib specimen.

The external ribs limited the bulk displacement in both directions because the screen was attached to the ribs. The added seam welds across the ribs introduced more wrinkles, which are the cause of the localized displacement. Localized screen breakdown was the most pronounced with this support method. As the ullage height increased, the bulk displacement of the external rib specimen improved since more panels were exposed. In comparison,

93

the bulk displacement of the screen supported by perforated plate, in the direction of the controlled liquid region (the critical direction), could not change the ullage height. These effects explain why the curves for the external rib and the supported by perforated plate specimens cross.

At small ullage heights the bulk effect was essentially the same for all specimens since most of the screen is submerged. Localized displacement was somewhat independent of ullage height, especially in the case of the external rib specimen. For these reasons, the external rib specimen was much more sensitive to vibration in comparison to the other specimens at low ullage heights.

Sine sweep tests were also performed on each of the six above discussed specimens. These tests aid in substantiating the above conclusions derived from the random vibration tests. By comparing the results of sine sweeps at various accelerations and ullage heights a relative ranking of the sensitivity of the specimens can be established. The occurrence of screen breakdown or the peak pressure amplitude are the data used to make the comparison.

The pleated and bonded specimens were again shown to be least sensitive, but there were not enough tests to clearly define the relative ranking of the other four specimens. It was noted that Specimen 1 would be ranked as more sensitive to vibration than the external rib specimen. Specimen 1 was supported similar to the external rib method, except that Specimen 1 had only two windows at top and bottom, instead of five. Specimen 1 would have less bulk displacement making it more sensitive to vibration.

During the sine sweep tests the specimen with the screen supported by perforated plate was tested in two different ways. First, the screen was installed in the model as intended with the perforated plate on the controlled region side of the model. Then the same tests were repeated with the specimen reversed so the perforated plate was facing the bulk side of the model. Under identical test conditions the pressure differential amplitudes were found to be about fifty percent greater when the perforated plate was facing the controlled region of the model. When bulk displacement into the controlled region was permitted (perforated plate on bulk side) the screen was less sensitive to vibration.

A similar substantiation was achieved with the sine sweep data for the other screen meshes. The 325 x 2300 screen mesh was the only mesh for which all the support methods were tested. This was done so that the above described comparisons could be made. To verify the effect of the support method, only a few selected support methods were used for the samples of the other screen meshes. As a minimum, an external rib specimen was fabricated for each screen mesh.

Two 200 x 1400 specimens were tested: one that was unsupported (Specimen 20) and one with external ribs (Specimen 11). From the four sine sweeps that could be directly compared, little difference in their response was

measured. In one test the pressure differential peaks were greater for one specimen, but the opposite was true for another test. The occurrence and degree of screen breakdown was the same for all four tests. Due to the way that external rib specimen was fabricated the localized effects must have been much less, making the two specimens similar in response. Since the 200 x 1400 screen has thicker wires than the 325 x 2300 screen, it was stiffer and would be less susceptible to the localized effects.

Three 165 x 800 Dutch twill screen specimens were tested: bonded to perforated plate (Specimen 18), unsupported (Specimen 21) and external rib (Specimen 12). The data were limited, but the same ranking obtained from the 325 x 2300 tests was indicated.

Four 165 x 800 plain Dutch screen specimens were tested: supported by perforated plate (Specimen 19), unsupported (Specimen 22), internal rib (Specimen 23) and external rib (Specimen 13). The two specimens with ribs were similar in response, both being more sensitive to vibration than the others. Based on the measured pressure differentials the unsupported specimen was more sensitive to vibration than the supported by perforated plate specimen. However, the wide variation in bubble point for these 165 x 800 plain Dutch specimens (17%) made their comparison difficult.

A pleated 80 x 700 screen specimen (Specimen 26) was tested in addition to an external rib specimen (Specimen 14). Their sensitivity was essentially the same. The pleated specimen had a lower bubble point due to the screen pleating operation. This screen mesh, and some of the other coarse screens, did not display the harmonics that were present with the finer screens. The peak pressure differential amplitude occurred at 5 Hz and decreased as the frequency increased during the sine sweep. This type of response is a function more of the liquid mass than the support structure. The low bubble point required that low acceleration values (0.5g) and low ullage heights ($<$13 cm (5 in)) be used, further reducing the structural contribution. In addition, the stiffness of the coarse screens eliminated any localized screen oscillation effects.

Three 850 x 155 screen specimens were tested. Two were unsupported with opposite weave orientations (Specimens 24 and 25) and the third was an external rib (Specimen 16). In four like tests the external rib specimen was definitely more sensitive to vibration than the others. As previously discussed, weave orientation did not influence the response.

It can be concluded that the support method does influence the response of the screen to vibration. A structural support method that allows bulk displacement of the screen, makes the screen less sensitive to vibration. Displacement into the controlled region acts to relieve the pressure differential due to the vibration. This approach conflicts with the need to limit deflection into the controlled region so that the channel flow area is not constricted. Localized displacement of the screen increases its sensitivity to vibration. Certain support methods induce localized displacement due to screen wrinkling that is inherent in the fabrication process. The coarser mesh screens are less likely to exhibit this localized displacement because of their greater stiffness.

95

6.   Effect of Screen Mesh - The bubble point of a screen determines the capacity of a screen to maintain its retention capability in a vibration environment. Another factor is the structural stiffness of the screen material which influences the dynamic response of the screen to vibration. Eight different screen meshes were evaluated in the course of the testing. The various meshes, listed in order of decreasing bubble point, were:

325 x 2300	Dutch twill
200 x 1400	Dutch twill
850 x 155	Robusta
165 x 800	Plain Dutch
165 x 800	Dutch twill
80 x 700	Dutch twill
50 x 250	Plain Dutch
200 x 200	Square

These screens are representative of the full span of available fine-mesh screens. Most of the above screens are or soon will be used in flight qualified surface tension devices.

A set of eight screen specimens, all using a common support method, were fabricated and tested. The external rib support method was used since it was judged to provide a representative, but basic in nature, response. Specimens using the "unsupported" support method for five of the screen meshes were also tested, permitting further comparison.

It was found that the finer mesh screens were more likely to exhibit local-ized screen breakdown (see Screen Breakdown discussion). Localized screen oscillation and breakdown did not occur with the 50 x 250 and 80 x 700 screens, both of which have relatively large wire diameters and are stiff. Localized effects were most prevalent with the very fine 325 x 2300 screen and it was noticed to some degree in the other meshes.

The 200 x 200 screen also displayed localized effects, but this was due to its open and flimsy structure. It could also be observed that the impact of sloshing liquid on the bulk side caused gas penetration with this screen.

When significant or excessive screen breakdown occurred with the 200 x 1400 screen it had a characteristic difference from the other screens. Break-down would produce lines of bubbles, aligned with the shute wires of the screen. This effect was not observed during the bubble point test.

It is difficult to draw very many conclusions regarding the effects of screen mesh from a direct comparison of the data. Depending on the reten-tion capability of the screen, different acceleration and ullage heights had to be used. These data were primarily intended for the analytical model development.

One direct comparison that was performed was to compare the peak differen-tial pressures and the occurrence of breakdown for all the external rib specimens. Most of the specimens were tested in Orientation 1 and isopropyl

alcohol was used as the test liquid. The 50 x 250 and 200 x 200 screens were only tested in Orientation 5 due to their low retention capability.

The relative ranking of the screen specimens, based on their sensitivity to vibration is the same as their rank based on bubble point. One exception could be the 325 x 2300 screen, but there was not sufficient data to be sure. In one pair of tests (1.0g sine sweep with 20.3-cm (8.0-in) ullage height) there was excessive breakdown with the 325 x 2300 screen, but only slight breakdown with the 200 x 1400 screen. In two other pairs of tests, the 325 x 2300 and 200 x 1400 screens had no breakdown in one case and significant breakdown in another case. The 325 x 2300 screen had a bubble point that is 50% greater than the 200 x 1400 screen, but the data indicate that they were approximately equal in their sensitivity to vibration or the 200 x 1400 may be less sensitive (based on the one data point). This may be due primarily to the influence of the localized effects on the response of the 325 x 2300 specimen. The external rib support method was found to make the screen more sensitive to vibration because the localized effects were most pronounced with this support method (see discussion of the effect of support method). The 200 x 1400 screen, being somewhat stiffer, was not as strongly influenced by the external rib support method.

A similar comparison was performed using data from the various mesh unsupported specimens. Again, the ranking of their vibration sensitivity was consistent with their retention capability, except for the 325 x 2300 screen. These results indicate that the 325 x 2300 screen was more sensitive to vibration than the 200 x 1400 screen. For one set of like conditions, the screen breakdown was more severe with the 325 x 2300 screen. For another set of like conditions the peak differential pressure amplitude, with no screen breakdown, was about twice as great with the 325 x 2300 screen.

7. Effect of Liquid Flow - Many of the screen specimens were tested under the combined conditions of vibration and outflow. The approach was to first perform a sine sweep test of the specimen with no flow and then to repeat the test with outflow. Outflow was simulated using a flow loop that was described in Chapter IV (see Figure IV-15). Basically, liquid was pumped from a reservoir into the model and then returned to the reservoir. This flow loop made the bulk region of the model equivalent to an infinite reservoir of liquid. The ullage region was pressurized, balancing the pressures so that a selected value of ullage height could be maintained during the test. The flow conditions remained constant during the test so the only variable was the frequency of the sine vibration.

Flow tests were performed with isopropyl alcohol and Freon 113, using Orientations 1 and 5, and using the single and double element models. All of the tests were sine sweeps since effects of the flow on the harmonics of the system were desired. A single flow rate of 20 ml/sec (1.2 in^3/sec) was used for all the tests. This flow rate was adequate to produce an effect on the vibration response without causing significant flow losses within the model. By using this approach, the flow losses did not complicate the interpretation of the test results.

97

Some selected flow tests are shown in Table V-2. All of these tests were performed using Orientation 1 and with isopropyl alcohol as the test liquid. The effect on the screen response is shown in this table by comparing the frequency and amplitude of the first harmonic with both flow and no flow.

In general, it was found that the effect of the flow was to increase the frequency at which the first harmonic occurred, which resulted in the peak differential pressure either remaining the same or decreasing. There are a few exceptions to the above conclusions which will be discussed later. The shift in the frequency ranged from only 1 Hz (the dual element model test with Specimens 10 and 27) to one test with Specimen 1 where it changed by almost a factor of 3. The shift in frequency appears to be a function of the screen flow area, with the frequency shift being greater for a small area. For the test with the dual element model (Specimens 10 and 27) the screen flow area was 271 cm^2 (42 in^2) and a small frequency shift resulted. Specimen 1 had only a 58 cm^2 (9.0 in^2) screen flow area, which gave the largest frequency shift. The other data points also fit this trend.

When the outflow caused a decrease in the peak differential pressure, the non-flow case was the worst case test condition. For example, during the first test listed in the table, slight screen breakdown occurred when the non-flow test was performed. Under flow conditions liquid was expelled from the top of the model so the flow losses added to the hydrostatic pressure, making the screen more susceptible to breakdown. However, the pressure differential due to vibration was reduced by the flow such that no screen breakdown occurred during the flow test.

Tests were performed using Specimen 1 to determine if the flow path through the model influenced the response of the screen to vibration. For an actual surface tension device in a tank, liquid in the bulk region flows through the screen and out of the tank through the device. In the model this was simulated by flowing liquid into the bulk region at the bottom of the model and expelling from the top of the controlled region. In the other case, the model simulates a portion of a surface tension device in which the flow is just passing through the controlled region. The flow entered the controlled region at the bottom and left at the top. Some ullage height was maintained in the bulk region to control the hydrostatic pressure differential acting on the screen.

The first two tests listed in Table V-2 show the results of this comparison. With identical vibration conditions, the flow path did alter the response to vibration. When the flow enters the bulk side and must pass through the screen, the response was as described above. When the flow entered the controlled region and did not pass through the screen, the response was different. The frequency of the harmonic was slightly reduced (1 Hz) and the peak differential pressure increased somewhat.

There are three exceptions listed in Table V-2 to the above conclusions regarding the effect of flow. One is the test with Specimen 11, a 200 x 1400 screen, in which no change in either frequency or pressure differential between the non-flow and flow condition was detected. Compared to the

Table V-2. Effect of Flow on Screen Response

Specimen Number	Screen Mesh	Sine Acceleration g	Ullage Height cm (in.)	Inlet Side of Model	First Mode Response			
					No Flow		Flow	
					Freq. Hz	Differential Pressure N/cm^2 (psi)	Freq. Hz	Differential Pressure N/cm^2 (psi)
1	325x2300	0.5	20.3(8.0)	Bulk	14	0.36(0.52)	25	0.17(0.25)
	325x2300	0.5	20.3(8.0)	Controlled	14	0.36(0.52)	13	0.41(0.60)
	325x2300	1.0	10.2(4.0)	Bulk	7.5	0.41(0.60)	21	0.16(0.23)
11	200x1400	0.5	20.3(8.0)		18	0.17(0.25)	18	0.17(0.25)
20	200x1400	0.5	30.5(12.0)		16	0.24(0.35)	20	0.17(0.25)
	200x1400	1.0	20.3(8.0)		13	0.31(0.45)	14	0.29(0.42)
12	165x800 Dutch	0.5	15.2(6.0)		42	0.21(0.30)	56	0.14(0.20)
21	165x800 Dutch	0.5	15.2(6.0)		39	0.13(0.19)	41	0.13(0.19)
13	165x800 Plain	0.5	15.2(6.0)		13	0.13(0.19)	15	0.13(0.19)
22	165x800 Plain	0.5	20.3(8.0)		18	0.15(0.22)	21	0.09(0.13)
23	165x800 Plain	0.5	20.3(8.0)		17	0.17(0.25)	20	0.17(0.25)
14	80x700	0.5	12.7(5.0)		5	0.06(0.09)	5	0.06(0.09)
10,27	325x2300	1.0	20.3(8.0)		7.5	0.59(0.85)	8.5	0.47(0.68)
22,23	165x800 Plain	0.5	20.3(8.0)	Bulk	6	0.15(0.22)	6	0.15(0.22)

results with Specimen 20, another 200 x 1400 screen, this result would be expected. The effect on frequency was small with the greater 1.0g acceleration and the same ullage height and flow area. With the greater ullage height and much smaller flow area, the frequency shift was still only 4 Hz for the other 0.5g test.

The other two exceptions are the results with Specimen 4 and the dual element tests with Specimens 22 and 23. In these two cases the system did not have a true harmonic frequency. The pressure differential was a maximum near the minimum shaker frequency of 5 Hz and decreased at higher frequencies. Flow did not change this condition, either in frequency or amplitude. With this type of response the flow condition will be the worst case. The effect of vibration remains constant, but the flow losses will increase the pressure differential acting on the screen.

To summarize, this evaluation indicates that the effect of liquid flow is to either not change the effect of vibration or to reduce the effect. A reduction in the vibration effect is accompanied by an increase in the harmonic frequency, that is a function of the flow area through the screen. If the pressure differential due to vibration was known under static conditions, a conservative approach would be to use the same differential for the flow condition, but also consider the flow losses. No explanation for the mechanisms of the flow effects can be given.

8. <u>Effect of Dual Screen Elements</u> - Two basic model configurations were tested. The previous discussion in this chapter has considered the single element model, with a bulk region and a controlled region separated by the screen specimen. The other model configuration used two screen specimens to form the controlled liquid region. This configuration simulated a channel of a surface tension device having screen panels on opposite sides.

There were three regions to the dual element model: a controlled region in the center and a bulk region on each side of the controlled region. The two bulk regions were externally coupled so they had the same pressure and ullage height (a complete description of the dual element model was presented in Chapter IV). The tests with the dual element model were performed in the same manner as the single element tests.

Some of the dual element data has already been discussed in this chapter. It was found that the effect of model orientation on the sensitivity of the model to vibration was the same for the dual element model as it was for the single element model. The effects of flow on the response to vibration were also similar.

The response measured during the single element tests could be compared with the results of the dual element tests. Specimen 10 was tested as a single element and then Specimens 10 and 27 were tested as dual elements. Both Specimens 10 and 27 were 325 x 2300 screen and were supported using the external rib method. The ribs of the two specimens were aligned so that they were staggered. The ribs of one were positioned so that they were located between the ribs of the other specimen.

The comparison of four common sine sweep tests between the single and dual element models shows that the dual element was less sensitive to the same vibration environment. Comparing the occurrence of screen breakdown showed that either breakdown occurred with the single element while it did not with the dual elements or breakdown was more severe with the single element model.

This direct comparison may not be valid because there was a difference in the liquid mass in the controlled regions of the two configurations. For the single element model, the thickness of the controlled region was 2.4 cm (0.95 in). The length and width of the controlled region for the dual element model was the same, but it was only 1.3 cm (0.50 in) thick. It would be expected that the pressure differential due to vibration would decrease as the mass being vibrated is decreased. Based on the conclusions for the effect of the support method, the increase in screen area, due to two screen specimens instead of one, would permit more bulk deflection and also reduce the sensitivity to the vibration. The contributions of each of these aspects in reducing the vibration sensitivity in the dual element configuration cannot be established by a direct comparison.

A similar comparison can be attempted, considering the other screen mesh that was tested in the dual element configuration. Specimens 22 and 23, both 165 x 800 plain Dutch screen, were tested individually and then were tested in the dual element model. They have different support methods, unsupported for Specimen 22 and internal rib for Specimen 23. A comparison, based on the occurrence of screen breakdown, of five common sine sweep tests does not indicate any pronounced difference between the single and dual element results. There was a definite decrease in the harmonic frequency, going from about 15 to 20 Hz as a single element to 6 Hz in the double element configuration.

9.   Effect of Liquid Subcooling - The effect of liquid subcooling on the response of the screen to vibration was evaluated by performing identical tests with two different test liquids. The two liquids used were Freon 113 and Freon 11. They both have similar densities and surface tensions (see Table IV-1), but their saturation curves are quite different (Figure V-8). At $20^{\circ}C$ ($68^{\circ}F$) Freon 113 has a vapor pressure of 3.7 N/cm^2 absolute (5.3 psia) while for Freon 11 it is 8.8 N/cm^2 absolute (12.8 psia). With a local atmospheric pressure of about 8.3 N/cm^2 absolute (12.0 psia), Freon 11 is boiling at room temperature. In terms of subcooling, at a temperature of $20^{\circ}C$ ($68^{\circ}F$) and with the model pressurized to 3.4 N/cm^2 gage (5.0 psig) the Freon 11 would be $8.3^{\circ}C$ ($15^{\circ}F$) subcooled and the Freon 113 would be $32^{\circ}C$ ($58^{\circ}F$) subcooled. The results for these liquids could also be compared with the results from the isopropyl alcohol tests, which would be $70^{\circ}C$ ($126^{\circ}F$) subcooled under the same conditions. However, the different density and surface tension of the alcohol does not permit the direct comparison possible with the Freons.

Under conditions in which no screen breakdown occurred, no difference in the response would be expected between the two test liquids. As long as there is an adequate reservoir of liquid on one side of the screen (provided by the controlled region in this case), the retention capability of
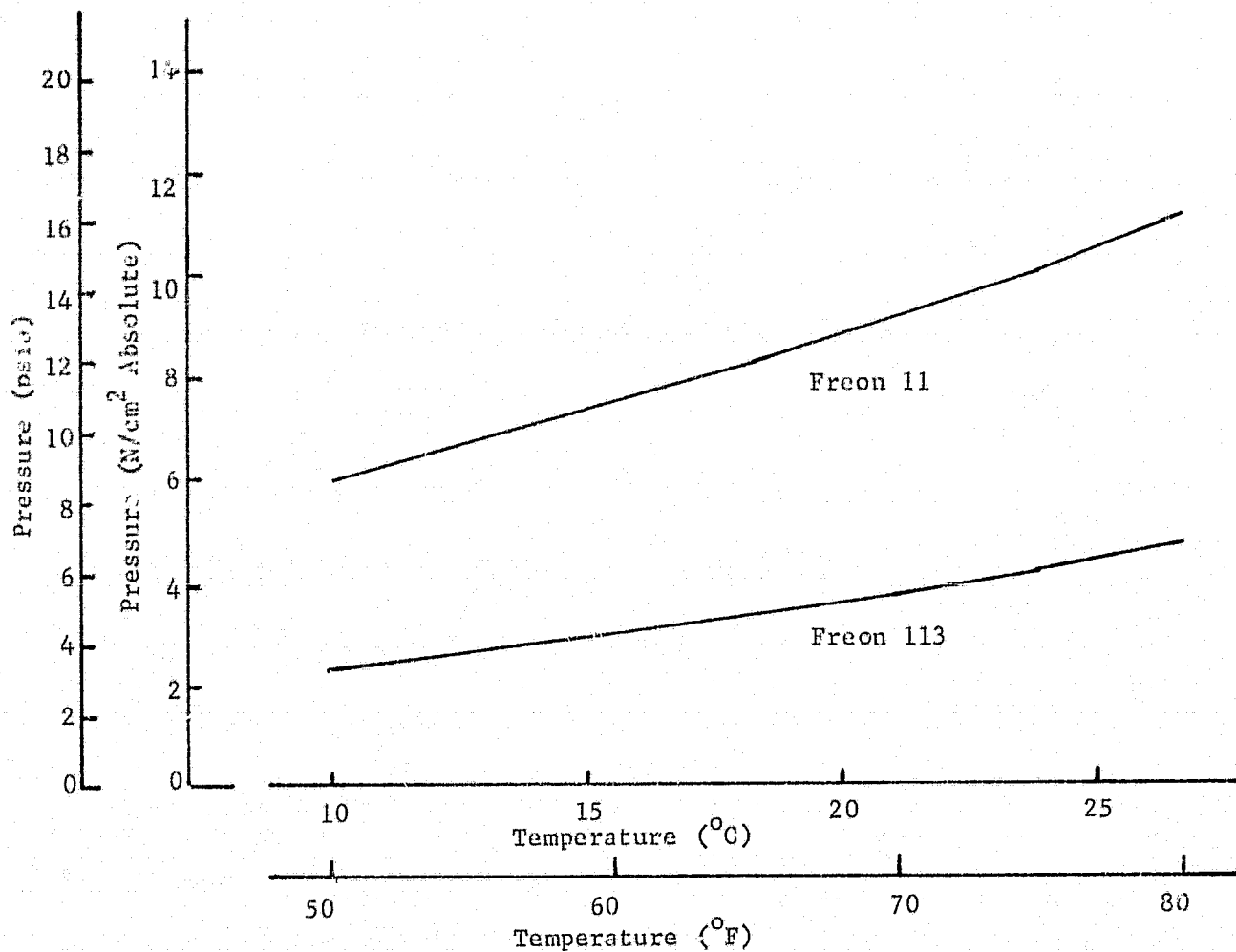
Figure V-8. Saturation Curves for Freon 11 and Freon 113 (Ref. V-4)

the screen is not influenced until very high heat fluxes are applied and the liquid is at saturation (Ref. V-5). However, in the case where a wetted screen is exposed to gas on both sides, its retention capability is highly dependent on the pressurant saturation and thermodynamic effects (Ref. V-6). The objective of these tests was to evaluate the response of the screen when breakdown occurred due to vibration, to determine if the amount of subcooling had an effect.

The approach was to find sine sweep test conditions, first using the Freon 113, that cause excessive screen breakdown resulting in the exposure of the controlled liquid side of the screen to gas. Since the screen was being exposed to gas during the test and continued to be vibrated, the test was primarily evaluating the effects of vibration on its retention capability and not screen dryout due to thermodynamic effects. Up to five sine sweep tests producing the conditions described above were identified. Then the tests were repeated using the Freon 11 as the test liquid.

Four screen specimens were used in this evaluation: Specimen 10, 325 x 2300; Specimen 11, 200 x 1400; Specimen 25, 850 x 155; and Specimen 15, 50 x 250. All of these tests were performed using model Orientation 1. The model was pressurized to 3.4 N/cm^2 gage (5.0 psig) and the room temperature was used to establish the saturation condition. The sine sweep started at 5 Hz and when the frequency reached 100 Hz the shaker was shut off and the liquid levels in the bulk and controlled region were monitored for about one minute to determine if the screen still had any retention capability. Screen breakdown usually commenced at or near 5 Hz and had ceased by 100 Hz.

With only a few exceptions, there was no difference in the screen response between the Freon 113 and Freon 11 tests, regardless of acceleration level, ullage height and screen mesh. The volume of gas that passed through the screen as it broke down was approximately the same for both test liquids. At the end of the test the screen was still supporting some hydrostatic pressure differential, as indicated by the difference in liquid levels between the bulk and controlled regions.

The exceptions occurred during the tests of the 50 x 250 screen, which was the most susceptible to dryout of the screens tested. At the end of the test the liquid levels were equal in two out of three of the Freon 113 tests. For the same conditions but using Freon 11, which would be more likely to cause screen dryout, the screen still had some retention capability at the end of the test.

These results indicate that the amount of liquid subcooling did not effect the screen response to vibration. If there was an effect there would have been a significant difference in the response with the Freon 11 test liquid. The unusual results with the 50 x 250 screen are due to the minimal wicking capability of this screen rather than the subcooling of the liquid.

10. Miscellaneous Effects - A few other factors regarding the response of the screen to vibration which were derived from the test data are noted in this section.

a.   Screen Acceleration - In all the tests a miniature accelerometer was mounted somewhere on the screen specimen. Various mounting locations and orientations of the accelerometer's axis were used.

In the early tests with Specimen 1, the accelerometer was mounted on the frame of the specimen and its axis was parallel with the vibration axis. In this mounting the accelerometer output was the same as that of the shaker control and monitor accelerometers. This arrangement permitted the pressure response to be compared with the input acceleration. As previously discussed, the phasing between the pressure and acceleration, as influenced by the harmonics, was established with these measurements.

The accelerometer was then mounted in the center of the 7.6 cm (3.0 in) screen panel of Specimen 1, with the accelerometer axis perpendicular to the screen. Comparisons of the pressure data showed that the small accelerometer did not change the response of the screen. It was also found that the accelerometer could be glued to the screen and removed without causing any screen damage or bubble point degradation. In all the subsequent tests the accelerometer was mounted on the screen.

There was no requirement for the accelerometer to provide data to perform the data correlation. The pressure differential due to the vibration was the primary measurement and the screen acceleration was just supporting data.

The accelerometer showed that there was a definite relationship between the screen acceleration and the pressure differential due to vibration. At the harmonic frequency indicated by the pressure there was a peak in the acceleration. However, the maximum acceleration was not always at the frequency of the maximum pressure differential. Large screen accelerations occurred at higher frequencies, accompanied by only a small or no increase in the pressure differential. This indicates that the screen can respond at high frequencies, but the liquid does not, and the liquid response produces the pressure differential.

The accelerometer, due to its small size, also indicated the localized screen oscillation effects. In some cases accelerations that were in excess of 30 times the input were measured by the accelerometer. The localized motion of the screen was rotating the accelerometer in addition to translating it, giving the unreasonably large outputs. For this reason, the data from the accelerometer were not a true indication of the screen response.

b.   Screen Structural Integrity - The vibration tests provided a qualitative assessment of the capability of screen structures to withstand vibration. A surface tension device must be structurally designed to withstand the vibration loads applied throughout its operational life. The structural effects of vibration were determined by rechecking the bubble point of all the screens, using the standard bubble point test method, after the testing was complete.

Only one of the screen specimens showed any degradation in bubble point. The pleated 325 x 2300 screen (Specimen 8) had a bubble point of 61.5 cm (24.2 in) of water before the testing and 32.3 cm (12.7 in) of water (using isopropyl alcohol at 20°C (68°F) after the testing, a very significant change. The pleating operation by itself caused some degradation of the screen bubble point, about 3.8 cm (1.5 in) of water. The pleats had a fairly sharp bend radius and screen breakdown during the bubble point test occurred at the bends of the pleats. The pleats ran the long direction of the specimen, giving the entire screen considerable flexibility. As the screen flexed, both in the vibration tests and due to handling, bending of the screen occurred at the bends in the pleats which increased the pore size at that location.

This specimen was subjected to considerable vibration. Ten sine sweeps were performed at accelerations of 0.5g, 1.0g and 2.0g, with half of them being at the 2.0g level. The sine sweeps were from 5 Hz to 100 Hz and back to 5 Hz at 2 octaves per minute, which subjected the screen to about 4.5 minutes of vibration each time it was performed. Sine dwells at 2.0g were performed. Finally, the random vibration tests applied levels between 0.2g RMS and 4.4g RMS over a period estimated to be about 1.5 hours. When the random vibration tests were performed the vibration was continuously applied. After draining to find the point of screen breakdown, the model was refilled and the acceleration level was increased without stopping the shaker.

By avoiding long pleat spans and using larger bend radii, the pleated screen would not be as likely to be degraded by the vibration. Regardless, the effects of vibration on the structural integrity of pleated screen is more of a concern, due to the sharp radius bends, than it is with flat screen.

Specimen 1, which had only two 7.6 cm (3.0 in) square screen openings, experienced the most vibration. One of the screen windows was usually submerged in liquid, so the other was subjected to the full effect of the vibration. With the full length specimens, the effect of the vibration was distributed over the exposed length of the screen. Many days of testing were performed on Specimen 1 because it was used to establish the basic effects of vibration. No record was kept of the actual amount of vibration time Specimen 1 experienced, but it is estimated to be about 20 hours. Sine vibration up to 5.0g and random vibration up to 3.0g RMS was applied. No degradation of this specimen was measured.

All of the screen, with the exception of the 50 x 250, was used "as received" and the only operations performed on it being the attachment of the screen to the frame. The available 50 x 250 screen that was used had been annealed.

B. Data Correlation

In this section the specific results obtained through the correlation of the test data with the predictions of the analytical models are presented. Two models are considered: the hydrostatic model, developed under prior studies, and the structural dynamics model developed as part of this study.

1.   Hydrostatic Model - Prior to the beginning of this program the state-of-the-art for vibration modeling was what is referred to as the hydrostatic model. A complete description of the prior work related to the effects of vibration can be found in the Introduction. The hydrostatic model is described as part of the Chapter III, Vibration Effects Analysis.

The hydrostatic model is primarily applicable to predicting the effects of random vibration. The prior correlations were based on random vibration data. A similar correlation was performed using the random vibration data collected in this study.

The first series of random vibration tests was aimed at evaluating the influence of the vibration spectrum. The hydrostatic model does not consider either the harmonic frequencies of the system or the frequency of the applied vibration. These tests were performed to determine the validity of this approach.

As presented in Chapter II, Survey of Vibrational Effects, random vibration is specified by the power spectral density as a function of frequency. An overall g RMS level can be derived from any given spectrum. The three spectra shown in Figure V-9 were used to perform this evaluation. The first spectrum (Figure V-9a) has a constant power spectral density over a wide range of frequency, 4 to 2000 Hz. The second spectrum (Figure V-9b) applied a constant spectral density at the higher frequencies from 100 to 2000 Hz, with no input at the lower frequencies. The third spectrum (Figure V-9c) has a constant spectral density at low frequencies (4 to 100 Hz) and no input at higher frequencies. In reality, the portions of the latter two spectra that were intended to have no input, did have a low power input due to shaker harmonics and noise. While these contributions cannot be ignored, their influence on this evaluation were minimal.

The constant spectral density of each of these spectra can be adjusted so that a selected value of the overall vibration input, expressed in g RMS, can be obtained. The shape of the spectrum remains constant and only the spectral density level is shifted. In the hydrostatic model, the g RMS value is used to describe the applied random vibration.

The 100 Hz division between the low and high frequency spectra was selected based on the known range for the first harmonic of the screen specimens tested. The harmonic was always less than 100 Hz, so the low frequency spectrum applied vibration at the resonant frequency, while the high frequency spectrum did not.

Screen Specimen 1 (two 7.6 cm (3.0 in) square, 325 x 2300 Dutch twill screen windows) was subjected to these random vibration environments. It was positioned in Orientation 1 (vibration and one-g parallel to the long length of the specimen) and isopropyl alcohol was used as the test liquid. The tests were performed by applying one spectrum, with a selected power spectral density and while maintaining that vibration environment, increasing the exposed screen height until screen breakdown was detected. The same test was repeated for various values of the spectral density and for each of the spectra.

Power
Spectral
Density

Frequency, Hz

a. Flat Spectrum

Power
Spectral
Density
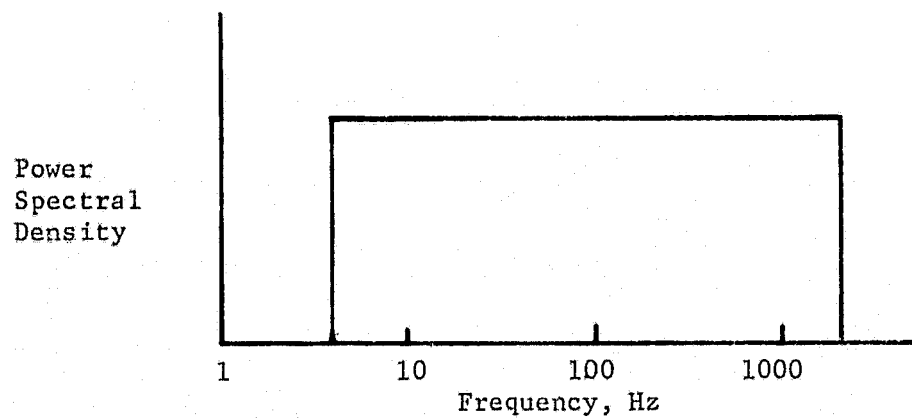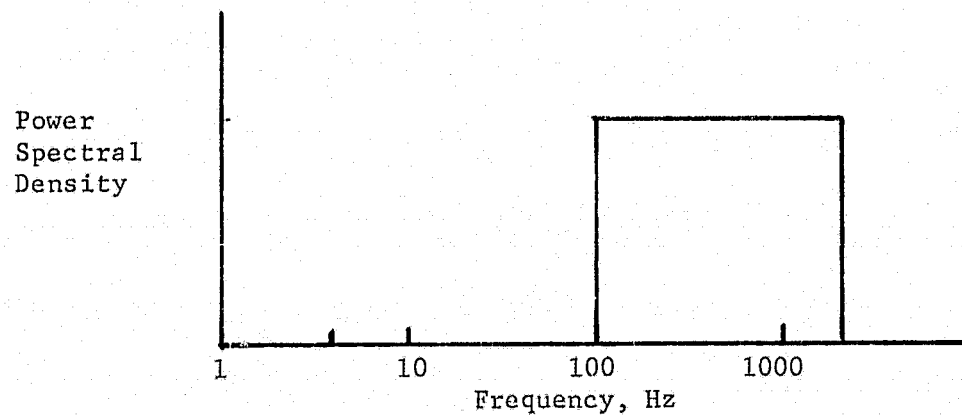
Frequency, Hz

b. High Frequency Spectrum

Power
Spectral
Density
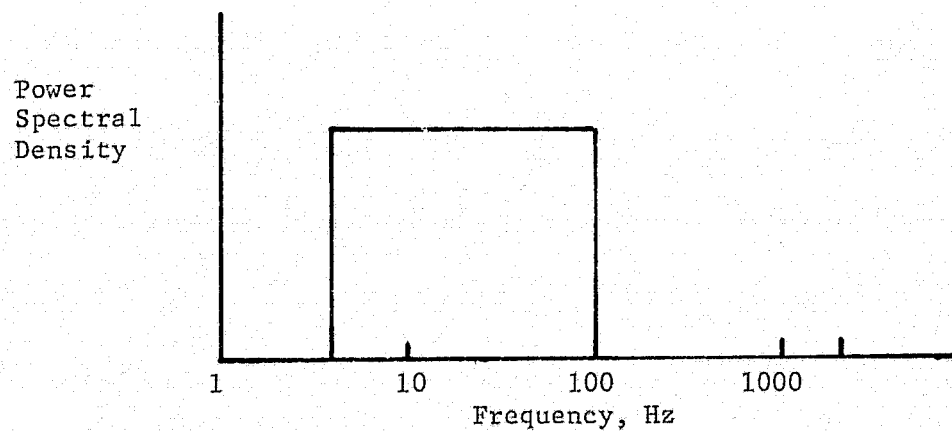
Frequency, Hz

c. Low Frequency Spectrum

Figure V-9.   Random Vibration Spectra

107

The effect on the screen retention capability is shown in Figure V-10. Each of the data points represents the ullage height at which significant screen breakdown was observed for the applied vibration, as defined by the overall g RMS. The point at which slight, significant and excessive screen breakdown began was noted for each test (see discussion of screen breakdown in the first section of this chapter). The amount of gas penetrating the screen during the slight breakdown was negligible. Significant breakdown was the most distinct condition, permitting better definition of the ullage height.

The results as presented in Figure V-10, show a definite effect of the frequency content of the spectrum. When the vibration energy was concentrated near the harmonic frequency of the specimen, the screen was the most sensitive to the random vibration. For a given value of g RMS there was a large difference in the ullage height at which screen breakdown occurred. From these results it is obvious that frequency must be considered in addition to g RMS in predicting the effects of random vibration.

In performing a correlation of this data the hydrostatic model predicts the contribution due to vibration based on the applied g RMS acceleration and the ullage height:

$$\Delta P_v = \rho g_{rms} h_s.$$

For the test conditions, the sum of the hydrostatic pressure differential at the top of the screen, due to the bulk liquid level, and the contribution due to vibration should equal the screen bubble point at the point of screen breakdown, as follows:

$$\Delta P_c = \Delta P_v + \Delta P_s.$$

For the lower g RMS levels (1.2 and 1.5 g RMS) and the 4 to 2000 Hz spectrum the hydrostatic model predicted the effect of the vibration accurately ($\pm$ 5%). For the higher g RMS levels the hydrostatic model predicted an effect due to vibration (ΔP_v) that was approximately one-half the measured effect. For the 100-2000 Hz spectrum the predicted effect was twice the measured and for the 4 to 100 Hz spectrum it was one-third.

One way to consider frequency in evaluating the effects of random vibration is to consider only the power spectral density at the harmonic frequency of the screen specimen. When the results shown in Figure V-10 are plotted as a function of the spectral density a more consistent result is obtained. The same data points now fall on one curve (Figure V-11). In the case of the 100 to 2000 Hz spectrum, the spectral density due to the inherent system noise, at the harmonic frequency of the specimen ($\sim$ 10 Hz), was used. This factor, plus some uncertainty in defining the point of significant screen breakdown, cause some scatter in the data points. The results in Figure V-11 can only be applied, as they stand, to this specific set of test conditions (screen specimen, model orientation and test liquid).
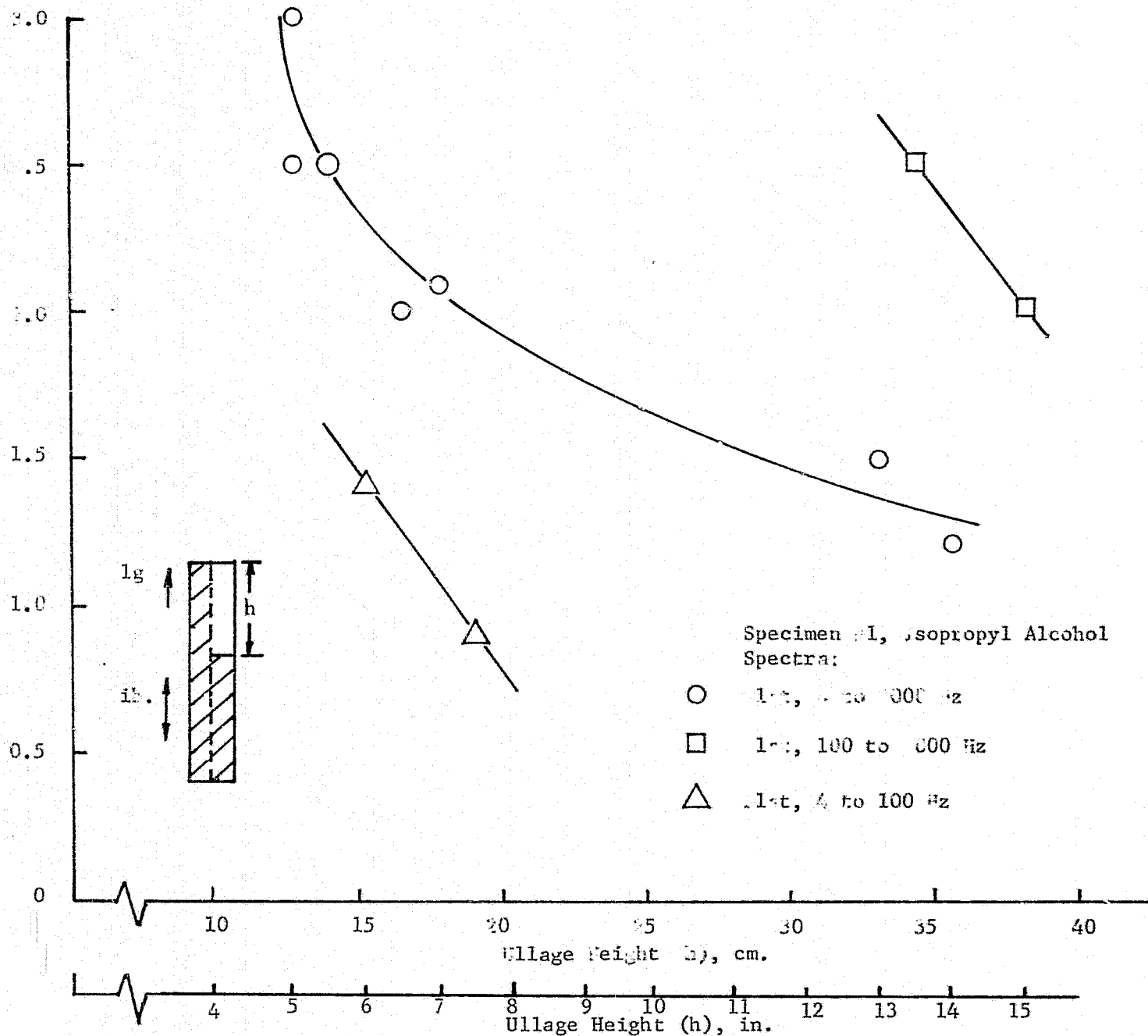
Figure V-10. Influence of Random Vibration Spectrum
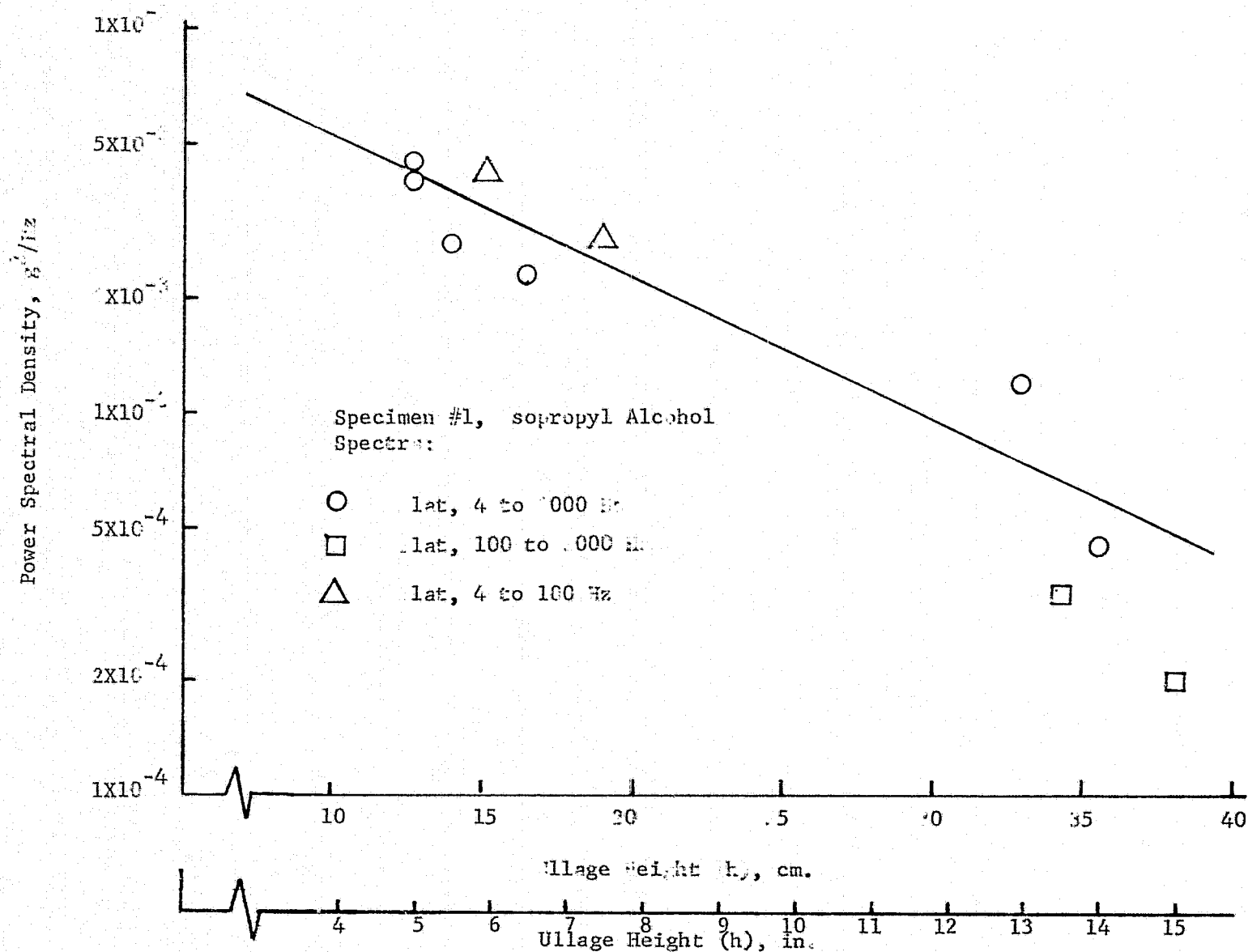
Figure V-11-Influence of Random Vibration Based on Spectral Density

A large quantity of random vibration data was collected for screen specimens 5, 6, 7, 8, 9 and 10 (these tests are also discussed under the effect of screen support method). Each of these screen specimens was made with 325 x 2300 Dutch twill screen, but each was supported in a different manner. A vibration spectrum with a constant power spectral density between 8 and 500 Hz was used for these tests. Such a spectrum covers the range of possible screen specimen harmonic frequencies, provides good low frequency resolution and resolution of spectral density increments, and can be accurately reproduced throughout a series of tests. Again, model Orientation 1 was used and isopropyl alcohol was the test liquid. The various stages of screen breakdown were noted, but only the point of significant breakdown is considered in the correlation.

A somewhat different approach to using the hydrostatic model was used in correlating this random vibration data. The hydrostatic model was defined to include a coefficient, as follows:

$$\Delta P_v = K\rho g_{rms} h_s.$$

Within the coefficient K are all the influences of the specific screen geometry and the applied vibration spectrum. After the value of K has been established, the effect of the vibration can be predicted.

The test data in the form of the coefficient K versus the g RMS level is plotted in Figure V-12. This graph shows that the method of supporting the screen significantly influences the value of the coefficient K. The data for Specimen 6 (screen bonded to perforated plate) falls the closest to a value of K equal to 1 (giving the traditional form of the hydrostatic model), especially when the acceleration is less than 2.5 g RMS. At 4.5 g RMS the value of K must be 2.5 to predict the effect of vibration for this screen. The values of K for Specimens 5, 8 and 9 fall within 25% of K equal to one, below 2.5 g RMS, but the variation becomes wider at higher accelerations. Over the full range of the test accelerations, the value of K for Specimen 8 falls closest to one. Specimens 7 and 10 had the largest values for K.

The data appear to indicate a convergence toward K equal to one as the acceleration approaches zero. Specimen 7 is the only exception, but perhaps could be discounted based on the erratic nature of the data for this specimen. This would indicate that the influence of the support method on the value of K vanishes at low random vibration levels which is typical of actual spacecraft vibration environments. However, this conclusion is only valid for the particular spectrum used in the test, as shown by the previous discussion of the effects of the vibration spectrum.

It is also interesting to note that the relative order of the curves for the specimens follows the same order as their sensitivity to vibration, as discussed in the first part of this chapter. The more sensitive the screen specimen is to vibration, the larger the value of K.
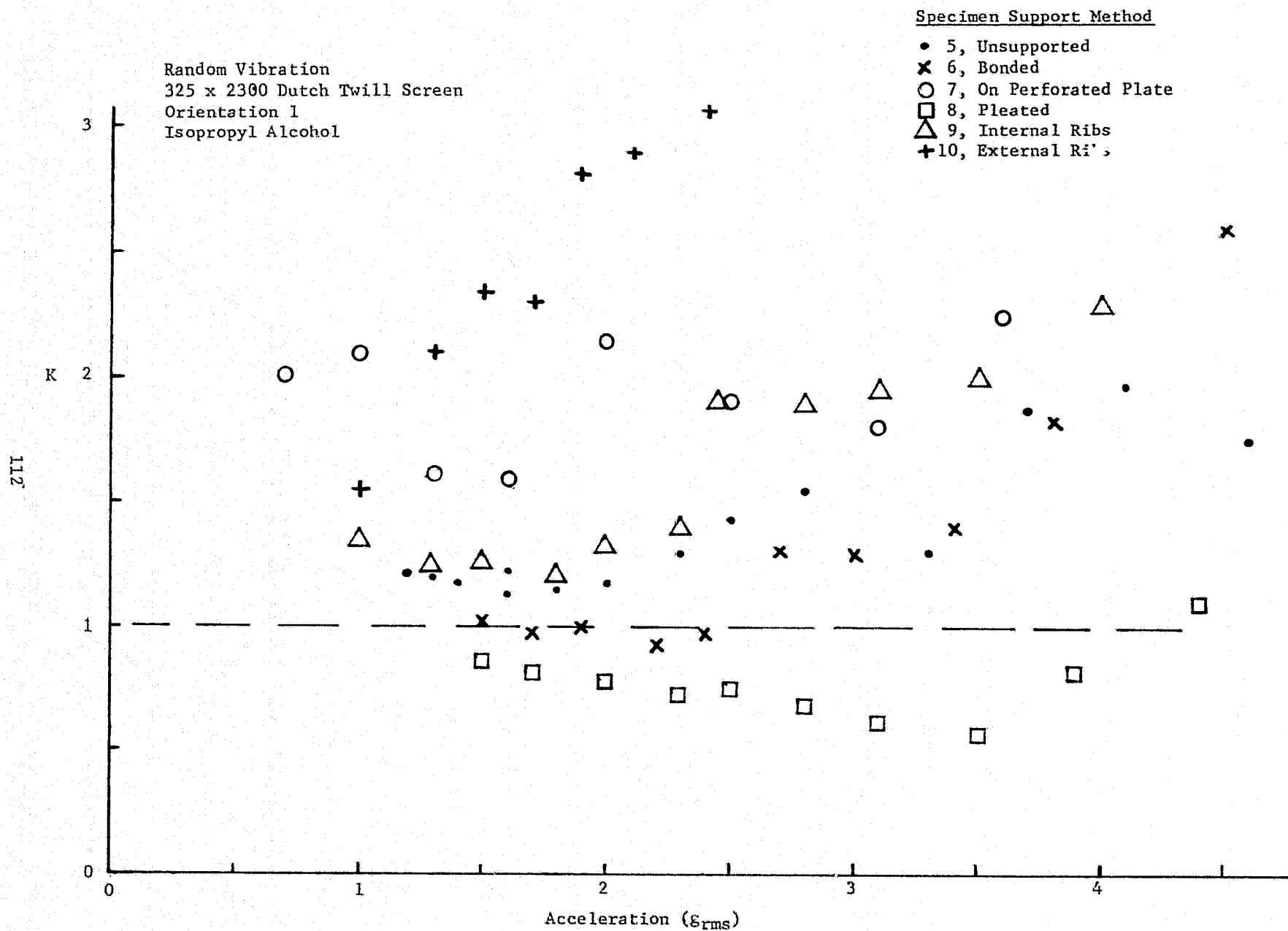
Figure V-12. Correlation with Hydrostatic Model

Specimen 1 is most similar to Specimen 10. Specimen 10 has five windows while Specimen 1 has only two of the same size. The results from the tests with Specimen 1 (4 to 2000 Hz constant spectral density spectrum) are similar to the results for Specimen 10 (8 to 500 Hz constant spectral density spectrum) shown in Figure V-12. For both specimens the value of K was close to one at low accelerations and became larger at larger accelerations.

The hydrostatic model was also applied to the sine vibration tests. As discussed in the first part of this chapter, under the effect of model orientation, the pressure due to vibration at low frequencies (near 5 Hz) could be predicted with the hydrostatic model. In this application the acceleration was the zero-to-peak amplitude of the sine vibration, the height was the length of exposed screen parallel to the vibration axis, and the value of K was one. To predict the pressure due to vibration at higher frequencies the amplification must be known. At the system harmonic, pressures of up to five times the low frequency value were measured.

Based on these tests and the prior vibration studies, it can be concluded that the hydrostatic model has some merit. The effect of vibration on the screen retention is hydrostatic in nature. The effect of frequency, due to the random vibration spectrum or sine vibration, has a significant effect on the ability of the hydrostatic model to predict the vibration effect. All of the screen specimens had harmonic frequencies and the amount of vibration energy applied to the specimen at that harmonic frequency was the primary factor influencing its response. This effect was clearly demonstrated by the tests using various spectra.

The hydrostatic model can be used to make estimates of the effect of vibration if the above discussed factors concerning the screen support method and the vibration spectrum are given consideration. The hydrostatic model also serves as a method of presenting and interpolating random vibration data acquired for a specific screen acquisition device and vibration environment.

2.   Structural Dynamics Model - As pointed out previously (Chapter III), the purpose of the tests performed on the initial three screen configurations was to establish the range of applicability of the single degree-of-freedom flow model and, for this controlled set of test specimens, to establish a measure of mass, stiffness and damping characteristics. It was anticipated that this information would then be extended to the more complex screen configurations (Specimens 4 through 27) and thus the model, if indeed valid for the control specimens, would be refined and extended to the more complex cases and, ultimately, used to predict the peak response pressure differential due to a vibration input for arbitrary screen acquisition system configurations.

The following discussion summarizes selected test results for several configurations. In general, three types of tests (sine sweep, sine dwell and random) were performed. As the intent of the structural dynamics model is to predict the peak vibration pressure differential (assumed to occur at the fundamental mode frequency), the sine dwell data have only limited

113

applicability. Further examination of the random response data indicated that they are difficult to interpret with respect to establishing the pressure differential of the fundamental resonance point.

Specimen 1 consisted of two approximately 7.6 cm (3.0 in) square screen covered openings with a 30.5 cm (12.0 in) distance between centers. Specimen 2 was identical except the submerged screen was removed. Specimen 3 reduced the size of the flow area to a 0.95 cm (0.375 in) diameter tube. All specimens used 325 x 2300 screen. A majority of these tests were conducted with Orientation 1 and isopropanol as the test fluid.

Table V-3 summarizes the results for Specimen 1; Table V-4 summarizes for Specimen 2. The intent of these specimens was to establish preliminary estimates of fluid mass, screen stiffness and system damping characteristics; this was the justification for use of the small screen window(s) and the incorporation of a well defined fluid path. The intent of Specimen 3 was to lend additional insight into these results by providing a known variation in the system mass. This is in view of the fact that the previous development of fluid effective mass was based on the assumption of uniform flow throughout the section AB (see Chapter III, Section B). However, it seems unlikely that truly uniform flow can be achieved due to boundary effects and the possible nonuniformity of screen motion and this implies that the actual system kinetic energy might be different than previously indicated. The intent of Specimen 3 was then to provide a manner by which we might assess this possible discrepancy, i.e., create a known "artificial mass" by restricting the flow between the controlled bulk regions as shown in the sketch. Here the system kinetic energy, with the additional energy due to the orifice flow (and assuming no outflow) is

$$T = \frac{\rho}{2} \left\{ \iiint_{Vol} \dot{q}_1{}^2 \, dV + \iiint_{Vol} \dot{q}_3{}^2 \, dV \right\}$$

where the second integration is over the volume of the tube. The integration yields

$$T = \frac{\rho}{2} \left(ABL \, \dot{q}_1{}^2 + A_o \lambda_o \, \dot{q}_3{}^2 \right)$$

q_3

orifice
area = A_o

bulk liquid level

length = λ_o

114
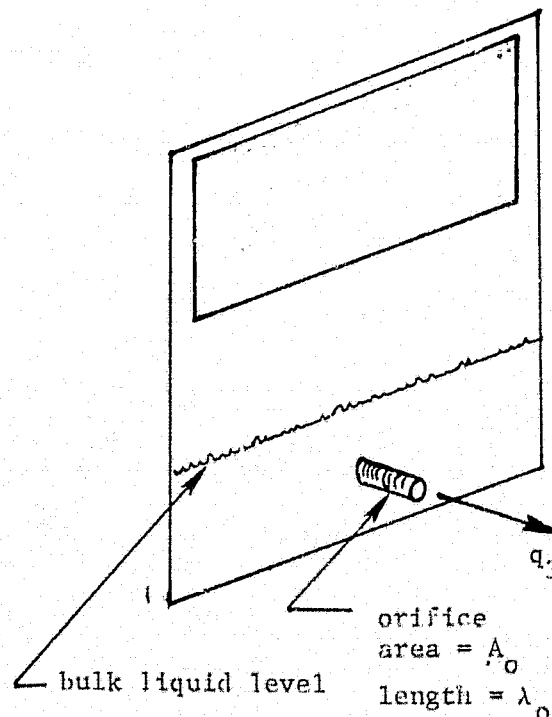
Table V-3. Summary of Test Results, Specimen 1

Date	Conditions and Observations
2/2/77	Sine dwells at 10-40 Hz, input = 1.5g, initial head = 12.7 cm(5 in) drain until breakdown random at 0.9-3.0g rms sweep 5-20-5 Hz, input = 1.5g, head = 12.7 cm (5 in) ΔP_V = 0.55 N/cm^2(0.80 psi) at 8.0-8.5 Hz (upswp) ΔP_V = 0.55 N/cm^2(0.80 psi) at 8.0-8.5 Hz (dnswp)
2/23/77	Sweep 5-30-5 Hz, input = 0.75g, head = 15.2 cm (6 in) ΔP_V = 0.45 N/cm^2(0.65 psi) at 10.8 Hz (upswp - no break) ΔP_V = 0.55 N/cm^2(0.80 psi) at 8.6 Hz (dnswp - no break) sweep 5-30-5 Hz, input = 0.75g, head = 22.6 cm (9 in) ΔP_V = 0.59 N/cm^2(0.85 psi) at 13.0 Hz (upswp) ΔP_V = 0.52 N/cm^2(0.75 psi) at 12.0 Hz (dnswp - prior to break) sweep 5-30-5 Hz, input = 1.0g, head = 15.2 cm (6 in) ΔP_V = 0.52 N/cm^2(0.75 psi) at 10.0 Hz (upswp) ΔP_V = 0.52 N/cm^2(0.75 psi) at 10.0 Hz (dnswp - prior to break)
2/24/77	Sine dwells at 20-25 Hz, input = 5.0g, initial head = 30.5-38.1 cm (12-15 in), orientation #5 sweep 5-30-5 Hz, input = 3.0, 5.0g, orientation #5
3/4/77	Sine dwells at 15 Hz, input = 0.5g, various initial heads sweep 5-50-5 Hz, input = 0.3g, head = 30.5 cm (12 in) ΔP_V = 0.31 N/cm^2(0.45 psi) at 21.0 Hz (upswp - prior to break) ΔP_V = 0.34 N/cm^2(0.50 psi) at 21.0 Hz (dnswp - prior to break)
3/10/77	Sweep 5-500-5 Hz, input = 0.3g, head = 30.5 cm (12 in) ΔP_V = 0.41 N/cm^2(0.60 psi) at 32.0 Hz ΔP_V = 0.31 N/cm^2(0.45 psi) at 21.0 Hz sweep 5-500-5 Hz, input = 0.5g, head = 20.3 cm (8 in) ΔP_V = 0.41 N/cm^2(0.60 psi) at 15.0 Hz (dnswp - prior to break) sweep 5-500-5 Hz, input = 1.0g, head = 10.2 cm (4 in) ΔP_V = 0.52 N/cm^2(0.75 psi) at 10.0 Hz (upswp) ΔP_V = 0.41 N/cm^2(0.60 psi) at 10.5 Hz (dnswp)

Date	Conditions and Observations
4/21/77	Sweep 5-500-5 Hz, input = 0.5g, head = 20.3 cm (8 in) $\Delta P_V = 0.38$ N/cm^2(0.55 psi) at 14.0 Hz (upswp) sweep 5-500-5 Hz, input = 0.5g, head = 20.3 cm (8 in) flow at approx. 20 ml/sec with inlet on bulk side $\Delta P_V = 0.21$ N/cm^2(0.30 psi) at 25.0 Hz (upswp) $\Delta P_V = 0.21$ N/cm^2(0.30 psi) at 25.0 Hz (dnswp) sweep 5-100-5 Hz, input = 1.0g, head = 10.2 cm (4 in) $\Delta P_V = 0.49$ N/cm^2(0.70 psi) at 7.0 Hz (upswp) $\Delta P_V = 0.45$ N/cm^2(0.65 psi) at 8.0 Hz (dnswp) sweep 5-100-5 Hz, input = 1.0g, head = 10.2 cm (4 in) flow at approx. 20 ml/sec with inlet on bulk side $\Delta P_V = 0.17$ N/cm^2(0.24 psi) at 21.0 Hz (upswp) $\Delta P_V = 0.17$ N/cm^2(0.25 psi) at 22.0 Hz (dnswp) sweep 5-100-5 Hz, input = 0.5g, head = 10.2 cm (4 in) Freon 113 $\Delta P_V = 0.24$ N/cm^2(0.35 psi) at approx. 8.0 Hz

Note: Orientation #1 unless noted
      Isopropanol unless noted
      No flow unless noted

Table V-4. Summary of Test Results, Specimen 2

Date	Conditions and Observations
2/23/77	Sweep, input = 0.75g, head = 15.2 cm (6 in.) ΔP_V = 0.41 N/cm^2 (0.60 psi) at 5.7 Hz (upswp) sweep, input = 0.75g, head = 22.7 cm (9 in.) ΔP_V = 0.49 N/cm^2 (0.70 psi) at 7.3 Hz (upswp) sweep, input = 1.0g, head = 15.2 cm (6 in.) ΔP_V = 0.49 N/cm^2 (0.70 psi) at 5.7 Hz (upswp) sweep, input = 1.5g, head = 13.1 cm (5 in.) ΔP_V = 0.55 N/cm^2 (0.8 psi) at 5.3 Hz (upswp) sweep, input = 1.5g, head = 7.5 cm (3 in.) ΔP_V = 0.41 N/cm^2 (0.6 psi) at 5.2 Hz (dnswp) sine dwells at 6-30 Hz, input = 1.5g

head		dwell freq.	ΔP_V	
cm	in.	Hz	N/cm^2	psi
13.1	5.0	10	0.34	0.49
15.2	6.0	15	0.22	0.32
21.5	8.5	20	0.28	0.40
27.8	11.0	30	0.14	0.20
13.8	5.5	10	0.42	0.61
10.2	4.0	8	0.52	0.75
8.7	3.5	6	0.58	0.83

Note: Orientation #1 unless noted
       Isopropanol unless noted
       No flow unless noted

which, with the continuity expression

$$AB \; \dot{q}_1 = A_o \; \dot{q}_3$$

becomes

$$T = \frac{\rho}{2} \; AB \left[L + \frac{\lambda_o \; AB}{A_o} \right] \; \dot{q}_1{}^2 \; .$$

Application of Lagrange's equation to the above yields

$$\frac{d}{dt} \left(\frac{\partial T}{\partial \dot{q}_1} \right) = \rho AB \left[L + \frac{\lambda_o \; AB}{A_o} \right] \ddot{q}_1 = \overline{M}_{eff} \; \ddot{q}_1$$

and

$$\overline{M}_{eff} = \rho AB \left[L + \frac{\lambda_o \; AB}{A_o} \right] = M_{eff} + \Delta M_{eff}$$

where the value of ΔM_{eff} can, hopefully, be controlled by judicious selection of the orifice tube length and cross-sectional area.

Unfortunately, the test results for Specimen 3 are inconclusive as to whether the desired objective (increased fluid mass with corresponding reduced natural frequency) was, in fact, accomplished. Examination of the data indicates that the apparent primary response lies in the 40-50 Hz range which would seem to imply that the effect of adding the orifice was to reduce the effective mass. However, this may be totally misleading. The expected natural frequency range for Specimens 1 and 2 is approximately 8-15 Hz and, if the predicted mass variation was in fact achieved for Specimen 3, it well may be that the resultant natural frequency lies below 5 Hz, the threshold value of the excitation equipment. This inconsistency has not been resolved and further analysis and/or controlled tests appear to be justified.

In an attempt to better understand the results of Specimens 1 and 2, consider the peak vibrational pressure differential as a function of static head as shown in Figure V-13 where the variation in the observed fundamental response frequency is also indicated. It is observed that increasing the static head, h_s, leads to an increase in the observed fundamental frequency. This is thought to occur through a combination, as yet undetermined, of two effects; increasing the static head decreases the effective flow length and increases the static pressure differential at the screen. Reduced effective flow length implies reduced effective fluid mass and increased pressure (static) differential applies a tension to the screen thus increasing its effective stiffness. The net result is the observed increase in the response frequency. Note also that for fixed static head, the observed vibrational
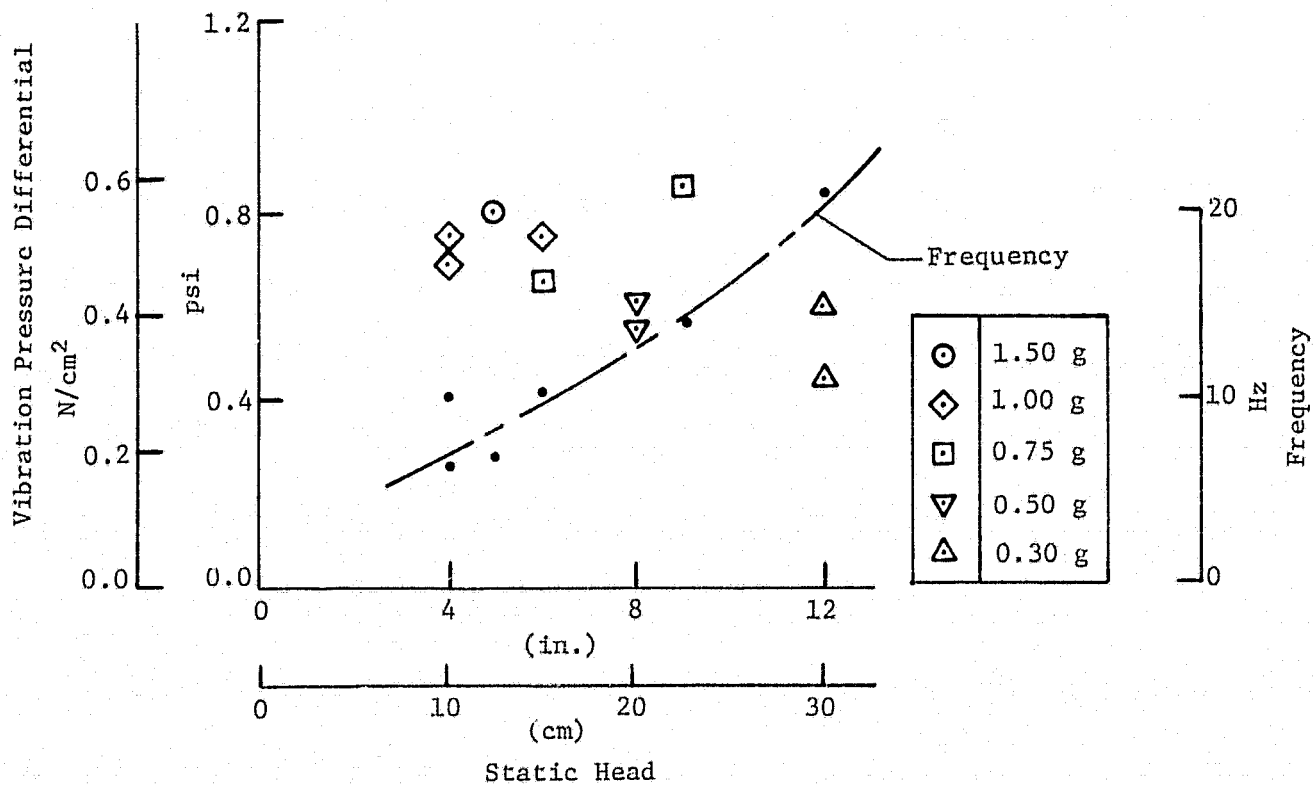
Figure V-13a.   Test Results, Specimen 1
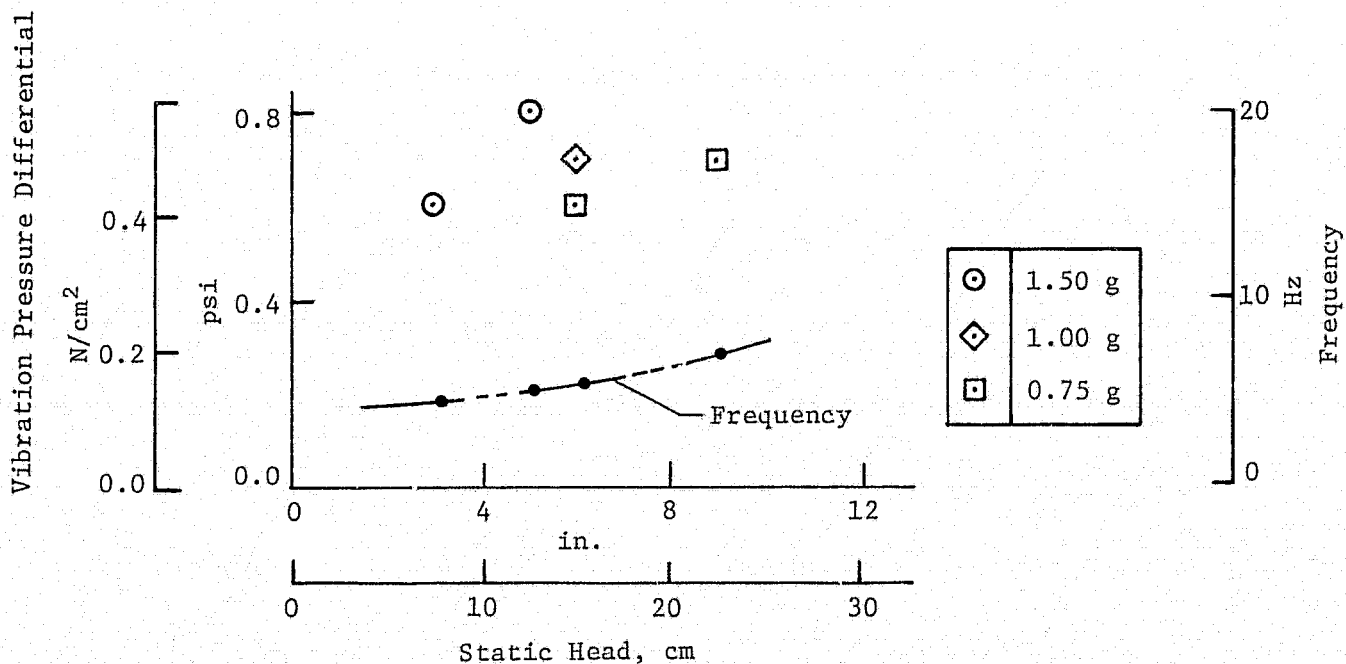
Figure V-13b.   Test Results, Specimen 2

119

pressure differential increases with increasing input vibration level as would be predicted from the analysis presented previously.

Another interesting view of the test results for Specimens 1 and 2 can be constructed by returning to the analysis of Chapter III slightly modified to account for geometric characteristics of the particular test specimens. The total pressure differential can be expressed as

$$\Delta P_t = \Delta P_s + \Delta P_v$$

with $\Delta P_s = \rho g\, h_s$

and $\Delta P_v = \dfrac{\rho g\, QC_x\, h^2\, \ddot{X}}{L}$
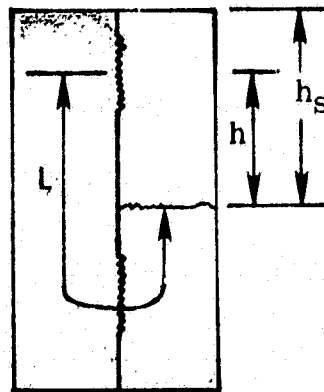
for acceleration in the vertical direction, X.

If we now say $\tilde{h} = h/h_s$, the above expression for pressure differential due to vibration becomes

$$\Delta P_v = \frac{\rho g\, QC_x\, \tilde{h}^2\, h_s^2\, \ddot{X}}{L}.$$

and it follows that the dynamic amplification can be expressed as

$$QC_x = \frac{\Delta P_v\, L}{\rho g\, \tilde{h}^2\, h_s^2\, \ddot{X}} \sim \frac{\Delta P_v\, L}{\rho g\, h_s^2\, \ddot{X}}$$

for $h_s = h$. The results of this equation are depicted in Figure V-14 which indicates that some degree of correlation exists between the two test specimens with (perhaps) Specimen 2 exhibiting slightly higher damping characteristics. This would seem to indicate that the square fluid passageway, permitting lateral fluid motion, acts as a damping device and that, for Specimen 1, no flow passes through the screen mesh. It would have been interesting also to show results for Specimen 3 at this point but, as mentioned previously, those results are not available. The figure indicates that a prediction of vibrational pressure differential is available for these two specimens but the extension to more complicated specimens is not yet evident.
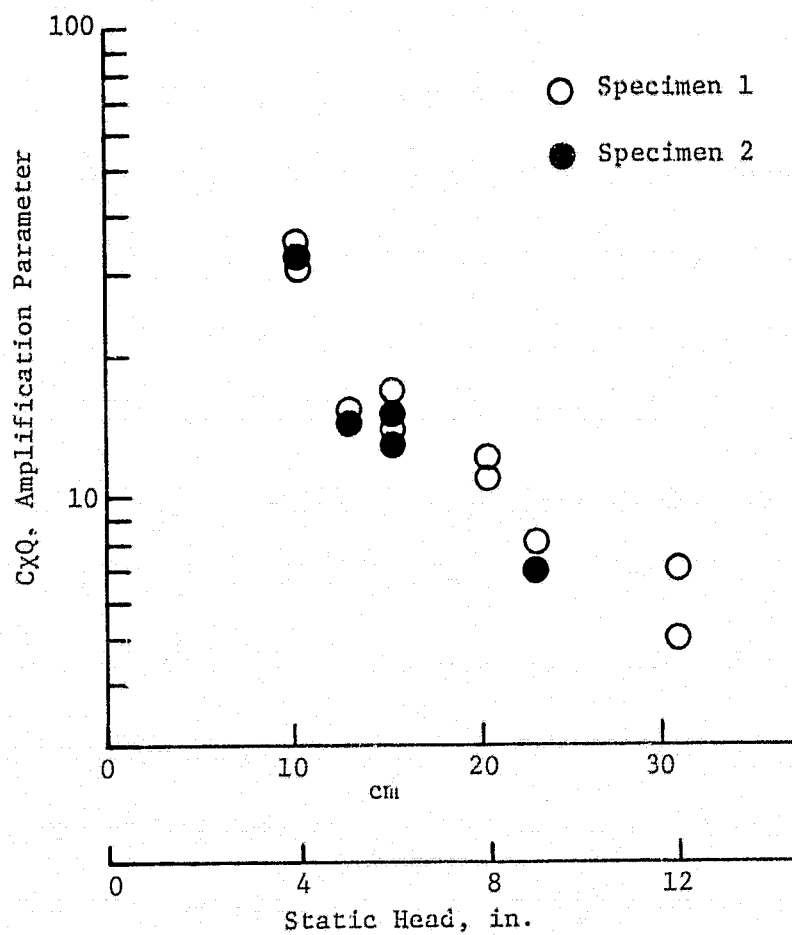
Figure V-14. Amplification Parameter, Specimen 1 and 2

In an effort to extend the previous results, test data for other screen specimens were tabulated and examined in some detail. This examination was made difficult by the fact that the amount of available test data are limited; there being only one or two pieces of data for some screen configurations. Further, the limited range of parameter values makes a graphical representation difficult. This is illustrated by examination of the data resulting from tests on several of the external rib configurations (Table V-5) where the peak vibrational pressure differential and observed fundamental frequency are tabulated for various static heads and input vibration levels. It is clearly evident that additional data are required before development of a fully test validated analytical model can be accomplished.

Table V-5. Test Results, External Rib Configurations

Specimen	Screen	Input (g's)	Head (in)	(cm)	Freq. (Hz)	Peak Pressure (lb/in^2)	(N/cm^2)
10	325x2300	0.5	8.0	20.3	17	0.20	0.14
11	200x1400	0.5	8.0	20.3	18	0.22	0.15
		0.5	8.0	20.3	18	0.22*	0.15
		0.5	12.0	30.4	21	0.32	0.22
		1.0	8.0	20.3	15	0.35	0.24
		1.0	6.0	15.2	14	0.25	0.17
12	165x800	0.5	6.0	15.2	42	0.30	0.21
	(Dutch)	0.5	6.0	15.2	56	0.30*	0.21
13	165x800	0.5	6.0	15.2	13	0.20	0.14
	(Plain)	0.5	6.0	15.2	15	0.25*	0.17

Note: Orientation 1
      Isopropanol test fluid
      * indicates flow test

VI. CONCLUSIONS AND RECOMMENDATIONS

This study has investigated the basic phenomena of the effects of vibration on the liquid retention capability of fine-mesh screens. The problem of the response of a screen to vibration was analytically evaluated in detail. A test program considering a large number of variables that influence screen response was conducted. Data were acquired and analyzed from 551 individual vibration tests.

The pressure differential due to the vibration was measured during the tests. These data give a basic understanding of the amplitude, waveform and characteristics of the vibrational pressure. The key factor in the screen response is the amplification of the vibrational pressure due to harmonics of the screen-liquid system. It was found that the retention capability is influenced by the positive peak pressure (lowering the liquid pressure with respect to the gas on the other side of the screen) due to the vibration. These pressure data also displayed the non-linear characteristics of the screen specimens. Loosely supported screens relieved the negative vibrational pressure, so the pressure was positively biased. A "softening spring" stiffness was noted, indicating that the response of the screen is influenced by the gas/liquid interface at the screen pores. Another non-linear effect was the localized screen breakdown due to the oscillation of small portions of a screen panel. These results establish that the vibrational response of a typical surface tension device is a highly non-linear, multi-degree of freedom problem.

It was found that the effect of the surface tension device orientation with respect to the vibration axis was proportional to the length of the liquid column, supported by the screen, parallel to the vibration axis. The orientation of the screen weave had no noticeable effect.

The screen support method significantly affects the screen response. Bulk displacement of the screen, primarily when the screen can deflect into the controlled liquid region, reduces the sensitivity of the screen to vibration. A support method that allows or enhances the localized oscillation of the screen, increases the sensitivity of the screen to vibration. The finer mesh screens are more susceptible to the localized oscillation, increasing their relative vibration sensitivity.

Liquid flow and dual screen elements can influence the harmonics and the response to vibration, in general decreasing the sensitivity in comparison to the single element, static case.

Prediction of the effects of vibration was most successful using the hydro-static model that was developed in prior studies. This model can predict the effects of sine vibration at frequencies below the first harmonic of the system (~ 5 Hz for the test model used here). Near the harmonics, the amplification would have to be known. The model predicts the effects of random vibration for rigid screen specimens and specific vibration spectra. The shape of the random spectrum and the screen support method definitely

123

influence the screen response, but are not directly considered by the hydrostatic model. It appears that successful use of the hydrostatic model will require that test data for a representative model, using the actual spectrum, be acquired. It would primarily serve as a means of scaling, based on the vibration level and liquid properties.

Limited verification of the structural dynamics model, developed under this program, was achieved. It was based on the premise that the effect of vibration is hydrostatic in nature, which was verified by the results of the hydrostatic model. However, the model dynamics were based on a linear, single degree of freedom system, which these tests have shown is not the case. The localized screen oscillation and other non-linear effects made it impossible to sort out the coefficients for the model from the data acquired.

The investigation of the effects of vibration on surface tension devices should be continued. Two approaches are recommended. First, an empirical approach based on the hydrostatic model should be followed. This should be directed toward random vibration and typical surface tension devices. It should be established that test data can be gathered and applied to an actual surface tension device, installed in a tank.

The second approach is to continue to study the basic phenomena of the response of the screen to vibration. Basic specimens, similar to those tested under this program but free of the localized oscillation effects, should be tested and the verification of a dynamics model continued. Mass and flow effects need to be more extensively investigated. As confidence in the model is gained, the non-linear effects could then be considered.

Through these two approaches to the problem of screen vibration, reliable analytical methods of predicting the effects of vibration may then become available.

APPENDIX A

BUBBLE GROWTH MODEL

Presented in this appendix is a description of the bubble growth model and the development of this model that was performed under this program. The application of this model to the analysis of screen vibration is discussed in Chapter III.

The bubble growth model evaluates the response of the gas/liquid interface to pressure transients. Screen breakdown can be viewed as the growth and detachment of a gas bubble at a screen pore. The model is based on a theoretical derivation of the dynamic response of a gas bubble. Each aspect influencing the response of the screen can be incorporated into the analysis. A detailed description of the model can be found in Reference III-2. During this program the bubble growth model was refined and adapted to the specific conditions of interest.

The structural dynamics model (see Chapter III) is essential to the use of the bubble growth model. The time varying pressure of the liquid, as calculated by the structural dynamics model, is input to the bubble growth model.

A. SCREEN PARAMETERS

Parameters that account for the geometry of the screen are also input to the bubble growth model. The screen geometry determines the capillary pressure at a pore and the resistance to gas flow through the screen.

The capillary pressure at the pore must be defined as a function of the volume of the gas bubble. Only by simplifying the screen geometry, as shown in Figure A-1, can this capillary pressure be calculated.

The gap between the wires is the pore radius, which is derived from the bubble point of the screen (see Appendix C for a list of symbols).

$$r = \frac{2\sigma}{\Delta P_c} \qquad (1)$$

The radius of the wire is the average of the warp and shute wire radii.

The contact angle is assumed to be zero, as it is for most propellants. Contact angles other than zero could be considered. Since the pores are very small, capillary forces will dominate gravity forces, even

125

OF POOR QUALITY

ORIGINAL PAGE IS
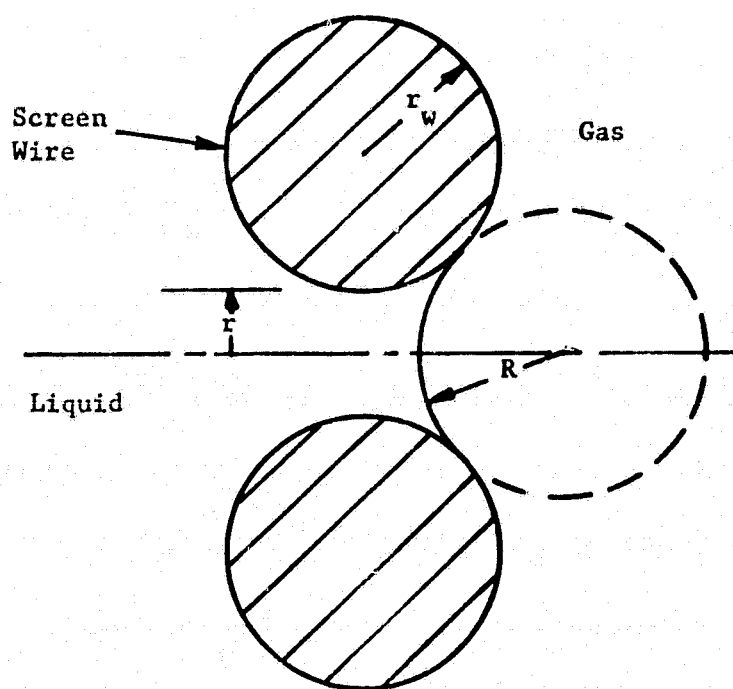
Figure A-1. Simplified Screen Pore

in one-g, so a zero-g interface can be assumed*. Therefore the interface at the pore is a segment of a sphere with radius R, tangent to the wires. The capillary pressure across the interface can be expressed as

$$\Delta P = \frac{2\sigma}{R} \ . \tag{2}$$

In a dimensionless form, based on the minimum pore radius, the equation becomes

$$\frac{\Delta P r}{\sigma} = \frac{2r}{R} \ . \tag{3}$$

Using the flat interface, having a capillary pressure of zero as a reference, the volume of the gas bubble can be calculated based on the defined screen geometry.

The parameters necessary to calculate the capillary pressure for each of the screens to be evaluated under this program are listed in Table A-1. The calculated variation of capillary pressure with bubble volume is shown in Figure A-2. The bubble volume (∀) is also placed in dimensionless form.

In this dimensionless form all of the screens have a curve of the same basic shape. The relative size of the screen pore and the wires causes the differences between the curves. Some interesting results can be noted in the figure. The progression of the curves from left to right is not the same order as based on increasing bubble point. The 50 x 250 and 200 x 1400 screen are the most obvious exceptions. This may be an indication of the relative capability of the screens in response to vibration.

Attempting to experimentally verify the curves in Figure A-2 would be difficult. Highly accurate measurements of the volume change related to a single pore would be required. There are factors that provide some confidence that the curves properly represent the capillary pressure. Obviously, the volume is zero when the capillary pressure is zero. The maximum capillary pressure is known from the bubble point.

The two dashed curves in Figure A-2 establish boundaries for the curves for any screen. One of the dashed curves is for a spherical

---

*For an extreme condition of oxygen (smallest kinematic surface tension of the liquids of interest), 200 x 200 screen (largest pore of the screens of interest), and a one-g acceleration, the Bond number based on the pore radius is 2×10^{-3}. The Bond number would have to be greater than 0.1 before there would be any significant change in the capillary pressure. Only when the gas bubble becomes very large would any influence of the acceleration be noted.

127

Table A-1. Screen Parameters

Screen (Wires per Inch)	Weave	Bubble Point with Isopropyl Alcohol cm. of H_2O (in. of H_2O)	Pore Radius, Microns (Inches)	Wire Diameter	
				Warp mm (in.)	Shute mm (in.)
325 x 2300	Dutch Twill	61.0 (24.0)	7.26 (2.86×10^{-4})	.038 (.0015)	.025 (.0010)
200 x 1400	Dutch Twill	41.4 (16.3)	10.7 (4.21×10^{-4})	.071 (.0028)	.041 (.0016)
165 x 800	Dutch Twill	19.6 (7.7)	22.7 (8.94×10^{-4})	.071 (.0028)	.051 (.0020)
165 x 800	Plain Dutch	24.1 (9.5)	19.1 (7.53×10^{-4})	.051 (.0020)	.036 (.0014)
80 x 700	Plain Dutch	15.5 (6.1)	28.5 (1.12×10^{-3})	.102 (.0040)	.076 (.0030)
50 x 250	Dutch Twill	8.9 (3.5)	51.8 (2.04×10^{-3})	.127 (.0050)	.114 (.0045)
850 x 155	Robusta	28.4 (11.2)	15.6 (6.13×10^{-4})	.030 (.0012)	.102 (.0040)
200 x 200	Square	9.7 (3.8)	45.5 (1.79×10^{-3})	.053 (.0021)	.053 (.0021)
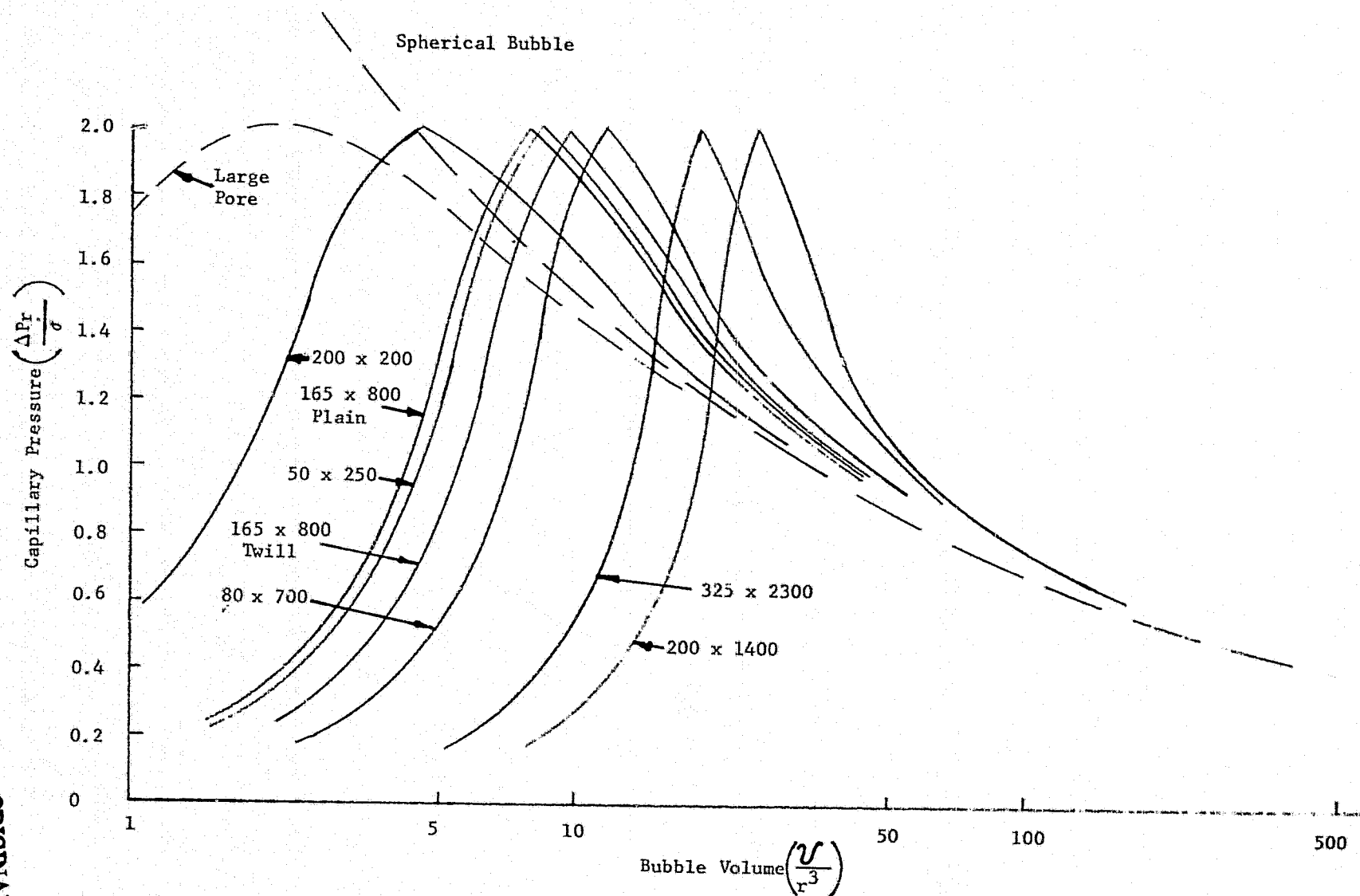
Figure A-2. Variation of Capillary Pressure with Bubble Volume

bubble, not attached to a surface. All the curves are asymptotic to the spherical bubble curve and have essentially converged after the capillary pressure ($\Delta P r/\sigma$) has fallen below about 0.6. A boundary for bubble volumes after the maximum capillary pressure is established by this curve. The dashed curve for a large pore is based on the limiting condition that the wire radius is negligible in comparison to the pore radius. All curves for a real screen must be shifted to the right of this curve.

Bubble growth after the bubble point of the screen has been exceeded is of prime interest, since this is the condition under which screen breakdown can occur. For that reason, the shape of the curve up to the bubble point is not critical.

Based on the above factors, the only uncertainty lies in the volume of the bubble at the maximum capillary pressure. If it was known, the entire curve would then be adequately defined.

The other geometric parameter is the coefficient that defines the resistance to gas flow through the screen. This flow resistance is one factor that limits the growth rate of the gas bubble due to an applied pressure differential. Based on Reference A-1, the flow resistance for a screen can be expressed as

$$\Delta P_f = n\rho V^2 + K\mu V \; . \tag{4}$$

This approach to characterizing the flow resistance has been widely used and verified.

For the screens, fluids and flow velocities of interest, the ρV^2 term is negligible in comparison to the μV term.

Therefore,

$$\Delta P_f = K\mu V \; . \tag{5}$$

However, the equations in Reference A-1 apply to an area of screen. To apply the expression to a single pore a pressure balance:

$$\Delta P_f = K\mu V = K_p \mu V_p \tag{6}$$

(where the subscripted variables are for the screen pore) and continuity:

$$\rho A V = \rho A_p V_p N \tag{7}$$

(where N is the number of pores in area A) must be considered. From the above two expressions

$$\frac{K_p}{K} = \frac{A_p N}{A} \; . \tag{8}$$

By definition the righthand side of the equation, is the void fraction, ϵ. Therefore

$$\Delta P_f = \epsilon K \mu V_p \; . \tag{9}$$

The flow velocity can be expressed as a function of the bubble volume

$$V_p = \frac{1}{A} \frac{d\mathcal{V}}{dt} \tag{10}$$

where A is now the orifice area.

Using expressions for $\mathcal{V}$ and A, based on the pore and bubble geometry, the velocity is

$$V_p = 4 \left(\frac{R}{r}\right)^2 \frac{dR}{dt} \; . \tag{11}$$

Therefore

$$\Delta P_f = 4 \epsilon K \mu \left(\frac{R}{r}\right)^2 \frac{dR}{dt} \; . \tag{12}$$

The values of K and ϵ can be calculated using equations provided in Reference A-1. Values of these coefficients for the screens of interest are listed in Table A-2. Equations for a Robusta weave are not provided in Reference A-1, so the equations for a plain Dutch screen were used, reversing the identification of the warp and shute wires (i.e., the 850 x 155 Robusta weave was assumed to be a 155 x 850 plain Dutch weave).

The accuracy of the coefficients in the bubble growth model were evaluated in detail to establish the best approach to adjusting the model in the process of correlation with test data. The most uncertainty resides in the curve for the capillary pressure of a pore versus the bubble volume.

If the maximum capillary pressure (bubble point) and the general form of the curve are held constant, the curve can be shifted by varying the volume of the bubble at the maximum capillary pressure. A number of trial cases were computed to establish the influence of that volume on the response of the pore. The response of the screen is defined in terms of an effective pressure, which is a steady pressure that produces the same effect on the screen retention as the transient applied pressure. The change in the effective pressure was less than 0.5% of the bubble point for an increase in 100% of the calculated volume. These results indicate that variations of this volume, over a reasonable range, does not provide a means of varying the response of the pore.

131

Table A-2. Coefficients for Flow Loss

Screen (wires per inch)	Weave	Void Fraction ϵ	Coefficient K 1/cm (1/in.)
325 x 2300	Dutch Twill	0.297	1.16×10^6 (2.94×10^6)
200 x 1400	Dutch Twill	0.267	9.49×10^5 (2.41×10^6)
165 x 800	Dutch Twill	0.430	1.77×10^5 (4.51×10^5)
165 x 800	Plain Dutch	0.598	5.08×10^4 (1.29×10^5)
80 x 700	Dutch Twill	0.368	2.09×10^5 (5.32×10^5)
50 x 250	Plain Dutch	0.616	1.41×10^4 (3.58×10^4)
850 x 155	Robusta	0.503	7.70×10^4 (1.96×10^5)
200 x 200	Square	0.642	1.60×10^4 (4.08×10^4)

The coefficient for the flow loss through the screen pore should be used to achieve correlation. This was the approach used when predictions from this model were compared with the response of a screen to pulsed flow (Ref. III-2). The coefficient is based on the work of Armour and Cannon (Ref. A-1). Our experience, including recent tests as part of the Space Shuttle Reaction Control System Tank Program, has indicated that the Armour and Cannon relations are at most about 30% conservative (i.e., predicts a pressure differential greater than measured). Data from another experimental program covering a wide range of screen meshes tends to substantiate that result (Ref. A-2).

Therefore a certain range of variation of this coefficient is permissible. Since the coefficient has been modified to account for a single pore, further uncertainty has been introduced. This coefficient is the only means of adjusting the model so it will inherently account for any other inaccuracies in the model, thus becoming more than a specifically identified orifice coefficient. After correlation has been achieved, the coefficient will correct the screen response, as analytically defined, to the actual physical case.

B. BUBBLE INERTIA

From the previous development of the bubble growth model (Ref. III-2), the inertia of the liquid interface was described using the basic Rayleigh equation for a spherical bubble in an infinite liquid. The kinetic energy of the liquid mass for spherical bubble growth is represented as (Ref. A-3):

$$\text{Kinetic energy} = 2\pi\rho \left(\frac{dR}{dt}\right)^2 R^3. \tag{13}$$

Equating the total kinetic energy to the work done by the liquid, yields the Rayleigh equation.

The bubble growth problem being analyzed here can be more accurately described by a spherical bubble attached to a flat surface. In this case, the kinetic energy has been calculated to be (Ref. A-4):

$$\text{K.E.} = 9.35\rho \left(\frac{dR}{dt}\right)^2 R^3. \tag{14}$$

Therefore, the Rayleigh equation is modified by a coefficient to account for the presence of the surface.

$$\Delta P_d = 1.49\rho \left[\frac{3}{2}\left(\frac{dR}{dt}\right)^2 + R\,\frac{d^2R}{dt^2} \right] \tag{15}$$

where ΔP_d = pressure differential due to inertia. This improvement has been incorporated into the model.

133

C. STATIC CONDITIONS

Consideration was also given to incorporating all the variables that would be encountered during the testing into the model. Under non-flow conditions, an input steady pressure differential accounts for the hydrostatic pressure due to one-g. When flow takes place, this same term can account for the sum of the steady pressure differentials acting at a screen pore. The magnitude of this differential is input to the model, based on a measured value or a separate calculation.

The thermodynamic state of the liquid is primarily accounted for by its pressure and temperature, and the saturation temperature at that pressure. Under non-equilibrium thermal conditions, vaporization of the liquid could contribute to the growth of a bubble at the screen pore. However, our primary interest here is in various conditions of liquid subcooling with thermal equilibrium. It was expected that the degree of subcooling would not strongly influence the point of first breakdown of the screen, but could significantly effect the screen response following initial breakdown. Once gas is on both sides of the screen pore, dryout may rapidly take place if there is little subcooling.

D. SAMPLE CASES

Some trial cases were analyzed with the model, using the coefficients derived in the above. It was assumed that a sinusoidal vibration produced a sinusoidal variation of the liquid pressure adjacent to the screen. A 200 x 1400 Dutch twill screen and isopropyl alcohol liquid were selected. For this analysis the retention of the screen was based on either a stable or unstable response of the bubble growth at a screen pore. A stable response occurs as a periodic growth and collapse of the bubble, with no net increase in size. For now, it will be assumed that detachment of the bubble does not occur during a stable response.

An unstable response is the continued growth of the bubble. A typical unstable response is shown in Figure A-3. With each cycle of the pressure the bubble radius undergoes a net increase. Detachment of the bubble is inevitable in this case, so an unstable response always leads to screen breakdown.

An effective pressure was calculated for an applied peak pressure over a range of frequencies. The results for two values of peak pressure, referenced to the bubble point, are shown in Figure A-4. These analytical results indicate that even at frequencies as low as 10 Hz, the screen does not respond to the peak pressure of the transient. As frequency increases, the effective pressure continues to decrease. The difference between the effective pressure and the bubble point is the maximum amount of steady pressure differential that can be applied in conjunction with the vibration, without causing screen breakdown.
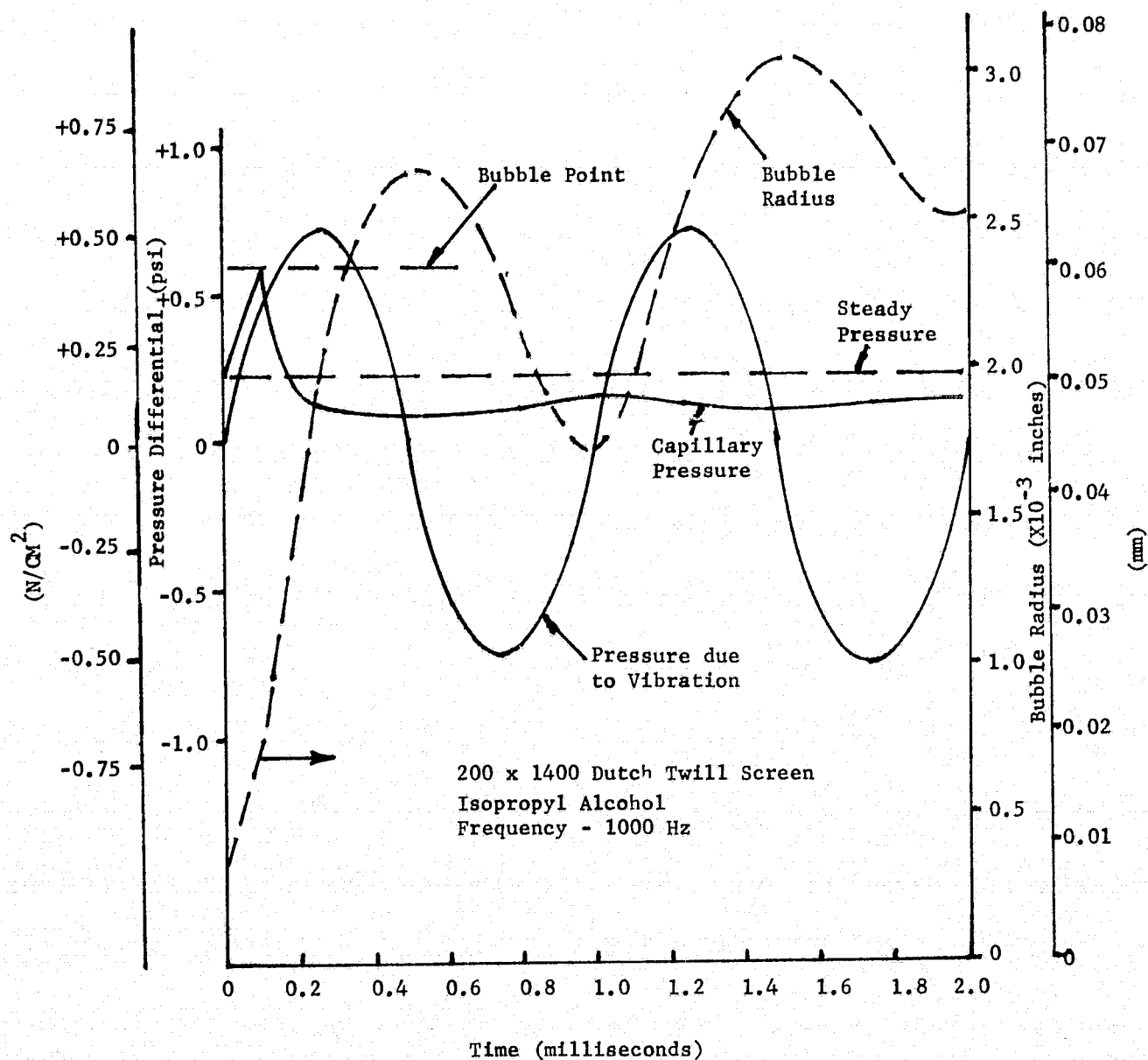
Figure A-3. Unstable Response to Sinusoidal Pressure Variation

135
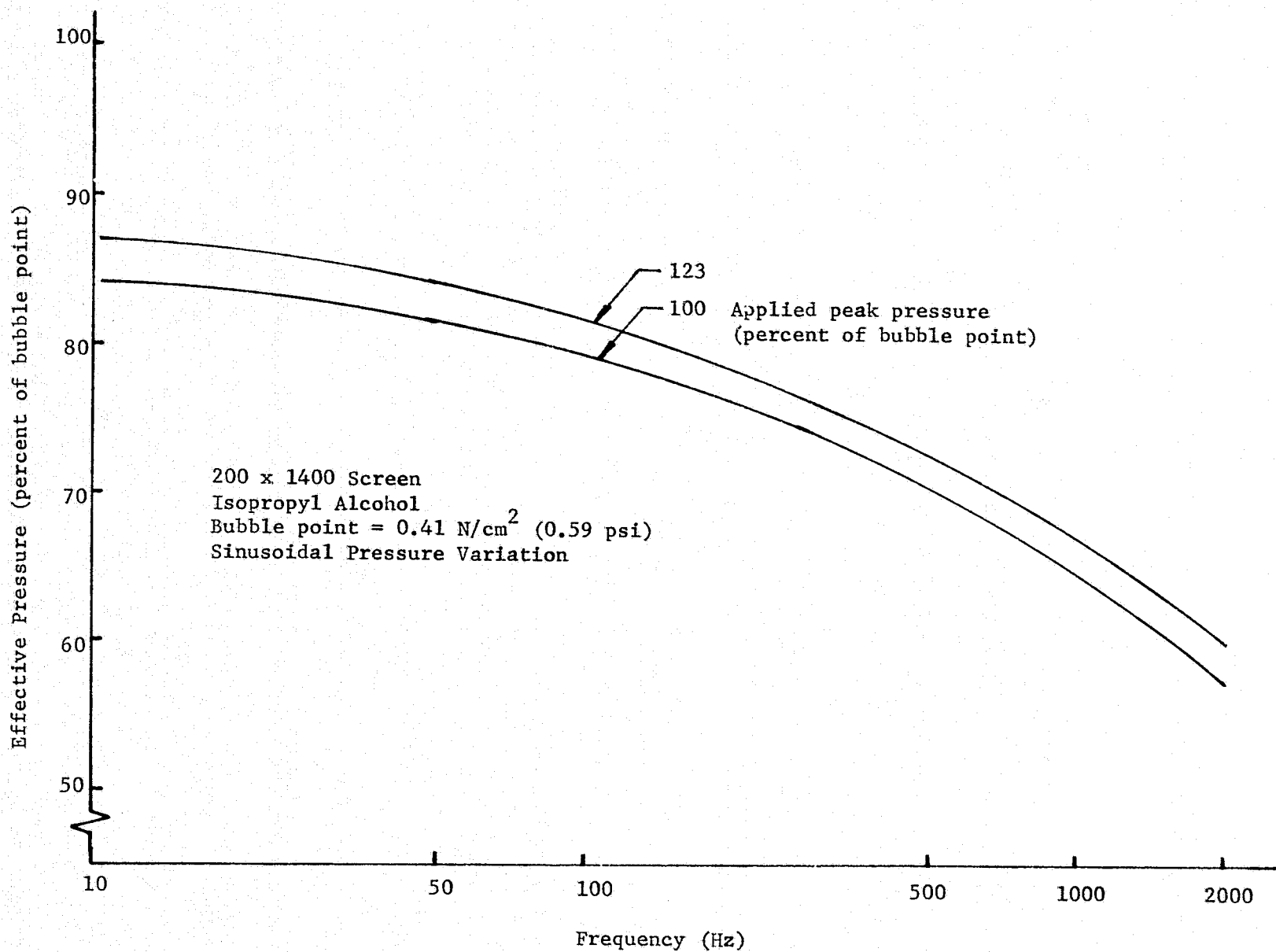
Figure A-4.   Effective Pressure for Sinusoidal Pressure Variation

136

The actual passage of gas through the screen occurs when the gas bubble is detached from the screen pore. As discussed above, if the response is unstable, the bubble continues to grow and detachment (screen breakdown) is inevitable. If the growth of the bubble is stable, this does not necessarily mean that screen retention is maintained. During the stable response the bubble may reach a size such that the forces acting on the bubble will cause detachment.

E. BUBBLE DETACHMENT

The growth of a gas bubble at the screen pore, in response to a pressure transient, can be either stable or unstable. Unstable growth implies that the applied pressures will continue to cause a net increase in the bubble size with time. The actual passage of gas through the screen (screen breakdown) occurs when the gas bubble is detached from the screen pore. If the bubble growth response is unstable, the continued growth makes detachment inevitable. During the stable response of the gas bubble, detachment may or may not occur depending on the forces acting on the bubble.

In general, the interest is in the point of incipient screen breakdown, where only a few of screen pores have begun to break down. For this regime it can be assumed that there will be no influence from adjacent pores and the forces on the bubble produced by the dynamic interaction of the bubble and the surrounding liquid are negligible.

1. Non-flow Condition

Under non-flow conditions, gravity forces are the prime means of causing bubble detachment. The mass of liquid displaced by the bubble produces a buoyant force that is opposed by the surface tension force where the bubble contacts the screen. A balance of forces, making use of the defined bubble geometry yields the following expression for the radius at which the bubble will detach due to buoyancy:

$$R = \left[\frac{3}{2} \frac{R_o}{Bo} \right]^{1/3} \tag{16}$$

where R_o is the radius of the line of contact between the bubble and the screen.

The variables R and R_o are dimensionless, being referenced to the minimum pore radius (r). The Bond number is also referenced to the minimum pore radius as follows:

$$Bo = \frac{\rho a r^2}{\sigma} \tag{17}$$

The radius of the line of contact is defined as:

137

$$R_o = \frac{R(1 + R_w)}{R_w + R}$$ (18)

where R_w is the dimensionless wire radius.

The possibility of bubble detachment due to buoyancy is evaluated by considering the maximum radius achieved by the bubble during a stable response. The value of R_o is calculated for the maximum bubble radius using equation (18). A value for R is then calculated using equation (16) and is compared to the original value for R. If the value from equation (16) is the smaller, the bubble does detach due to buoyancy. Screen breakdown does not occur as long as the maximum size of the bubble does not exceed the value given by equation (16).

The gravity force can also oppose the surface tension force at the interface of the bubble, if the direction of the acceleration tends to cause flow of liquid through the pore. If the gravity force exceeds the surface tension force along the interface, the interface of the bubble will collapse upon itself, causing detachment. This mechanism of detachment was evaluated by calculating the shape of the interface at the pore, as influenced by gravity forces, and establishing a limit for the existence of the interface. It was found that for a given liquid and acceleration level, buoyancy will cause detachment before that limit is reached.

The bubble radius for buoyant detachment was evaluated for a one-g acceleration. Of the typical propellants, liquid oxygen presents the worst case because of its low kinematic surface tension (Freon 11, one of the test liquids, has similar properties). Three screens, representing the span of meshes being considered, were evaluated. The parameters calculated are listed in Table A-3. The point of detachment is best represented by calculating the capillary pressure of the bubble at the point of detachment and comparing it to the bubble point of the screen. The values for capillary pressure listed in Table A-3 are relatively low. For such values of capillary pressure to be reached during stable bubble growth, the static pressure applied to the system would have to be of similar magnitude and the peak pressure of the transient would have to be much larger than the bubble point. Under low-g conditions it can be seen that buoyant detachment becomes much less significant.

2. Flow Condition

When there is liquid flow, parallel to the screen surface within a surface tension device, the shear force acting on the bubble can cause detachment. A surface tension force again opposes the shear so the balance of forces yields:

$$R = \left[\frac{4\,R_o}{C_D\,We}\right]^{1/2}$$ (19)

138

Table A-3. Bubble Detachment for Liquid Oxygen

Buoyancy	Screen Mesh		
	325x2300 Dutch Twill	165x800 Dutch Twill	200x200 Square Weave
Bond Number for one-g	4.39×10^{-5}	4.30×10^{-4}	1.73×10^{-3}
R	47.8	20.1	11.1
Percent of Bubble Point	2.09	4.97	8.99

Shear

	325x2300 Dutch Twill	165x800 Dutch Twill	200x200 Square Weave
Weber Number for U = .3 m/sec (1ft/sec)	0.0574	0.179	0.359
R	21.1	10.2	5.95
Percent of Bubble Point	4.74	9.78	16.8

The Weber number is referenced to the minimum pore radius.

$$We = \rho \frac{U^2 r}{\sigma} \tag{20}$$

where the flow velocity (U) is parallel to screen.

The drag coefficient (C_D) is a function of the Reynolds number of the bubble and can be found in most fluid mechanics text books (e.g., Ref. A-5).

The value of U can cover a wide range, dependent on the flow rate from the tank and the configuration of the surface tension device. A value of 0.3 m/sec (1.0 ft/sec) was selected as a representative upper limit for the flow velocity. Having picked a velocity, oxygen would again give the worst case condition due to its small kinematic surface tension. The calculated values are again presented in Table A-3. At large flow velocities, shear is the more likely cause of bubble detachment. Liquid flow in a high-g environment would require the valuation of the combined effects of shear and buoyancy.

The theory upon which the above described bubble detachment is based can be found in the literature regarding gas bubble generators (e.g., Ref. A-6 and A-7), and has been well verified with experimental data.

APPENDIX B

TEST DATA

The following table is a compilation of the measured data from selected vibration tests. These tests were selected from Table IV-4 as being representative of the total test program. All of these selected tests were performed using the single element model and there was no outflow. The model was installed in orientation 1 on the shaker unless otherwise noted in the table. Most of the listed tests were performed using isopropyl alcohol as the test liquid, except for tests 62 (Freon 113) and 63 (Freon 11). Presented in this table are the specific conditions of each vibration test. The results of the test that are presented are the frequency and peak positive amplitude of the pressure differential due to vibration at the first harmonic of the system, and the occurrence of screen breakdown is noted along with the degree of breakdown.

Test No.	Screen Specimen	Type of Vibration			Acceleration g Peak for Sine gRMS for Random	Ullage Height cm(in.)	Peak ΔP N/cm² (psi)	Frequency Hz	Breakdown	Remarks
		Sine								
		Sweep	Dwell	Random						
7	4	X			0.3	30.5 (12.0)			No	ΔP not recorded
			X		0.3	30.5 (12.0)	.14 (.20)	15	No	ΔP at top of model
			X		0.3	30.5 (12.0)	.11 (.16)	15	No	ΔP 2.5 cm (1.0 in) down
			X		0.3	30.5 (12.0)	.10 (.15)	15	No	ΔP 5.1 cm (2.0 in) down
			X		0.3	30.5 (12.0)	.08 (.12)	15	No	ΔP 10.2 cm (4.0 in) down
			X		0.3	30.5 (12.0)	.07 (.10)	15	No	ΔP 15.2 cm (6.0 in) down
			X		0.3	30.5 (12.0)	.06 (.08)	15	No	ΔP 19.1 cm (7.5 in) down
		X			0.3	30.5 (12.0)	.17 (.25)	16	No	
		X			0.5	20.3 (8.0)	.23 (.33)	20	No	
		X			1.0	30.5 (12.0)			Excessive	Break started at 8 Hz
		X			1.0	20.3 (8.0)			Significant	ΔP not recorded
		X			1.0	20.3 (8.0)	.43 (.62)	14	Significant	ΔP at top of model
		X			1.0	20.3 (8.0)	.32 (.47)	8	Significant	ΔP 10.2 cm (4.0 in) down
			X		1.0	20.1 (7.9)	.28 (.40)	20	Significant	ΔP 10.2 cm (4.0 in) down
			X		1.0	20.1 (7.9)	.49 (.71)	20	Significant	ΔP at top of model
			X		1.0	20.1 (7.9)	.25 (.36)	20	Significant	ΔP 10.2 cm (4.0 in) down
			X		1.0	19.1 (7.5)	.19 (.28)	25	Significant	ΔP 10.2 cm (4.0 in) down
			X		1.0	19.1 (7.5)	.76 (1.1)	25	Significant	ΔP at top of model
			X		1.0	19.1 (7.5)	.76 (1.1)	25	Significant	ΔP at top of model
			X		1.0	19.1 (7.5)	.26 (.38)	25	Significant	ΔP 10.2 cm (4.0 in) down
			X		1.0	20.3 (8.0)	.15 (.22)	30	Significant	ΔP 10.2 cm (4.0 in) down
			X		1.0	20.3 (8.0)	.39 (.57)	30	Significant	ΔP at top of model
			X		1.0	20.3 (8.0)	.14 (.20)	30	Significant	ΔP 10.2 cm (4.0 in) down
8	5	X			0.3	30.5 (12.0)	.16 (.23)	15	No	
		X			1.0	20.3 (8.0)			Significant	No good
			X		1.0	22.9 (9.0)	.41 (.60)	20	Significant	
			X		1.0	20.6 (8.1)	.24 (.35)	25	Significant	
			X		1.0	21.3 (8.4)	.22 (.32)	25	Significant	
			X		1.0	21.8 (8.6)	.26 (.37)	30	Significant	
		X			1.0	20.3 (8.0)	.45 (.65)	8	Significant	
				X	1.1	29.2 (11.5)			Slight	Flat 8 to 500 Hz spectrum
				X	1.2	33.0 (13.0)			Slight	
				X	1.3	31.8 (12.5)			Significant	

142

Test No.	Screen Specimen	Type of Vibration			Acceleration g Peak for Sine gRMS for Random	Ullage Height cm(in.)	Peak ΔP N/cm² (psi)	Frequency Hz	Breakdown	Remarks
		Sine		Random						
		Sweep	Dwell							
8	5			X	1.4	30.5 (12.0)			Significant	
				X	1.6	27.4 (10.8)			Significant	
				X	1.8	26.2 (10.3)			Significant	
				X	2.0	24.1 (9.5)			Significant	
				X	2.3	20.3 (8.0)			Significant	
				X	2.5	17.8 (7.0)			Significant	
				X	2.8	15.2 (6.0)			Significant	
				X	3.3	15.2 (6.0)			Significant	
				X	3.7	10.2 (4.0)			Significant	
				X	4.1	8.9 (3.5)			Significant	
				X	4.6	8.9 (3.5)			Significant	
14	6	X			2.0	20.3 (8.0)	.45 (.65)	33	Slight	
		X			2.0	30.5 (12.0)	.41 (.60)	29	Significant	
		X			2.0	25.4 (10.0)			Significant	ΔP not recorded
		X			2.0	15.2 (6.0)			No	
		X			2.0	30.5 (12.0)	.41 (.60)	50	Significant	
			X		2.0	22.4 (8.8)	.47 (.68)	35	Significant	
			X		2.0	27.9 (11.0)	.43 (.62)	30	Significant	
			X		2.0	38.1 (15.0)	.30 (.43)	20	No	
		X			1.0	20.3 (8.0)	.31 (.45)	75	No	
		X			1.0	30.5 (15.0)	.45 (.65)	40	Significant	
			X		1.0	29.2 (11.5)	.43 (.62)	40	Significant	
		X			2.0	25.4 (10.0)			Significant	ΔP not recorded
			X		2.0	Drain		35	Significant	ΔP not recorded
		X			1.0	25.4 (12.0)			Significant	ΔP not recorded
				X	0.4	38.1 (15.0)			No	Flat 8 to 500 Hz spectrum
				X	0.6	38.1 (15.0)			No	
				X	1.0	38.1 (15.0)			No	
				X	1.5	31.8 (12.5)			Significant	
				X	1.7	30.5 (12.0)			Significant	
				X	1.9	27.9 (11.0)			Significant	
				X	2.2	26.7 (10.5)			Significant	
				X	2.4	24.1 (9.5)			Significant	
				X	2.7	17.8 (7.0)			Significant	

Test No.	Screen Specimen	Type of Vibration			Acceleration g Peak for Sine gRMS for Random	Ullage Height cm(in.)	Peak ΔP N/cm² (psi)	Frequency Hz	Breakdown	Remarks
		Sine		Random						
		Sweep	Dwell							
14	6			X	3.0	16.5 (6.5)			Significant	
				X	3.4	14.0 (5.5)			Significant	
				X	3.8	10.2 (4.0)			Significant	
				X	4.5	6.4 (2.5)			Significant	
17	7	X			2.0	20.3 (8.0)			Excessive	ΔP not recorded
		X			2.0	15.2 (6.0)			Significant	ΔP not recorded
		X			2.0	20.3 (8.0)			Excessive	ΔP not recorded
			X		2.0	20.3 (8.0)		15	Significant	ΔP not recorded
			X		2.0	20.3 (8.0)		20	Significant	ΔP not recorded
		X			1.0	20.3 (8.0)			Slight	ΔP not recorded
		X			1.0	25.4 (10.0)			Slight	ΔP not recorded
		X			1.0	30.5 (12.0)			Excessive	ΔP not recorded
		X			1.0	20.3 (8.0)	.62 (.90)	17	Slight	
		X			1.0	25.4 (10.0)	.69 (1.0)	16	Slight	
		X			2.0	15.2 (6.0)			Slight	No good
		X			1.0	25.4 (10.0)	.69 (1.0)	16	Slight	Reference line disconnected
			X		2.0	20.3 (8.0)		15	Significant	Reference line disconnected
			X		2.0	20.3 (8.0)		15	Significant	
				X	0.3	38.1 (15.0)			No	Flat 8 to 500 Hz spectrum
				X	0.4	26.7 (10.5)			Slight	
				X	0.7	33.0 (13.0)			Significant	
				X	1.0	26.2 (10.3)			Significant	
				X	1.3	26.2 (10.3)			Significant	
				X	1.6	22.9 (9.0)			Significant	
				X	2.0	15.2 (6.0)			Significant	
				X	2.5	14.0 (5.5)			Significant	
				X	3.1	12.2 (4.8)			Significant	
				X	3.6	8.9 (3.5)			Significant	
19	8	X			2.0	20.3 (8.0)			Excessive	ΔP not recorded
		X			2.0	15.2 (6.0)			No	ΔP not recorded
		X			1.0	20.3 (8.0)			No	ΔP not recorded
		X			1.0	30.5 (12.0)			Excessive	ΔP not recorded
		X			1.0	25.4 (10.0)			Excessive	ΔP not recorded
		X			1.0	20.3 (8.0)	.41 (.60)	6.5	No	
		X			2.0	15.2 (6.0)	.45 (.65)	13	No	

144

145

Test No.	Screen Specimen	Type of Vibration			Acceleration g Peak for Sine gRMS for Random	Ullage Height cm(in.)	Peak N/cu (psi)	Frequency Hz	Breakdown	Remarks
		Sine		Random						
		Sweep	Dwell							
19	8		X		2.0	32.5 (12.8)	.22 (.32)	15	Significant	
			X		2.0	38.1 (15.0)		20	No	ΔP not recorded
		X			2.0	15.2 (6.0)	.43 (.62)	13	No	Reference line disconnected
		X			0.5	20.3 (8.0)	.21 (.30)	7	No	
		X			0.5	30.5 (12.0)	.43 (.63)	10	Slight	
				X	0.2	38.1 (15.0)			No	Flat 8 to 500 Hz spectrum
				X	0.4	38.1 (15.0)			No	
				X	0.6	38.1 (15.0)			No	
				X	0.9	38.1 (15.0)			No	
				X	1.0	38.1 (15.0)			No	
				X	1.3	38.1 (15.0)			No	
				X	1.5	35.6 (14.0)			Significant	
				X	1.7	34.3 (13.5)			Significant	
				X	2.0	31.5 (12.4)			Significant	
				X	2.3	30.5 (12.0)			Significant	
				X	2.5	27.9 (11.0)			Significant	
				X	2.8	27.4 (10.8)			Significant	
				X	3.1	27.4 (10.8)			Significant	
				X	3.1	26.7 (10.5)			Significant	
				X	3.5	25.4 (10.0)			Significant	
				X	3.5	26.7 (10.5)			Significant	
				X	3.9	19.1 (7.5)			Significant	
				X	4.4	14.0 (5.5)			Significant	
20	9	X			2.0	20.3 (8.0)			Excessive	ΔP not recorded
		X			2.0	15.2 (6.0)			Excessive	ΔP not recorded
		X			2.0	10.2 (4.0)			Significant	ΔP not recorded
		X			1.0	20.3 (8.0)			Excessive	ΔP not recorded
		X			1.0	15.2 (6.0)	.55 (.80)	8	Slight	
			X		1.0	15.2 (6.0)	.55 (.80)	15	Significant	
			X		1.0	15.0 (5.9)	.24 (.35)	20	Significant	
			X		1.0	15.0 (5.9)	.09 (.13)	40	Significant	
		X			0.5	20.3 (8.0)	.21 (.30)	20	Slight	
				X	0.2	38.1 (15.0)			No	Flat 8 to 500 Hz spectrum
				X	0.4	38.1 (15.0)			No	
				X	0.6	38.1 (15.0)			No	

Test No.	Screen Specimen	Type of Vibration Sine Sweep	Dwell	Random	Acceleration g Peak for Sine gRMS for Random	Ullage Height cm(in.)	Peak ΔP N/cm² (psi)	Frequency Hz	Breakdown	Remarks
20	9			X	1.0	34.3 (13.5)			Significant	
				X	1.3	31.8 (12.5)			Significant	
				X	1.5	27.9 (11.0)			Significant	
				X	1.8	25.4 (10.0)			Significant	
				X	2.0	21.6 (8.5)			Significant	
				X	2.3	19.1 (7.5)			Significant	
				X	2.5	14.0 (5.5)			Significant	
				X	2.8	12.7 (5.0)			Significant	
				X	3.1	11.4 (4.5)			Significant	
				X	3.5	10.2 (4.0)			Significant	
				X	4.0	7.9 (3.1)			Significant	
21	10	X			2.0	20.3 (8.0)			Excessive	ΔP not recorded
		X			2.0	15.2 (6.0)			Excessive	ΔP not recorded
		X			2.0	10.2 (4.0)			Excessive	ΔP not recorded
		X			1.0	20.3 (8.0)			Excessive	ΔP not recorded
		X			1.0	15.2 (6.0)	.48 (.70)	40	Significant	
			X		1.0	9.1 (3.6)	.17 (.25)	40	Significant	
			X		1.0	19.1 (7.5)	.50 (.73)	20	Significant	
		X			0.5	20.3 (8.0)			No	
		X			1.0	20.3 (8.0)				ΔP not recorded
		X			1.0	15.2 (6.0)				ΔP not recorded
			X		1.0	Drain		40		ΔP not recorded
				X	0.2	38.1 (15.0)			No	Flat 8 to 500 Hz spectrum
				X	0.4	38.1 (15.0)			No	
				X	0.6	38.1 (15.0)			Slight	
				X	0.8	38.1 (15.C)			Significant	
				X	1.0	31.8 (12.5)			Significant	
				X	1.3	29.2 (11.5)			Significant	
				X	1.5	17.8 (7.0)			Significant	
				X	1.7	16.5 (6.5)			Significant	
				X	1.9	12.7 (5.0)			Significant	
				X	2.1	11.4 (4.5)			Significant	
				X	2.4	9.7 (3.8)			Significant	

Test No.	Screen Specimen	Type of Vibration Sine Sweep	Dwell	Random	Acceleration g Peak for Sine gRMS for Random	Ullage Height cm(in.)	Peak ΔP N/cm² (psi)	Frequency Hz	Breakdown	Remarks
24	11	X			0.5	20.3 (8.0)	.17 (.25)	18	No	
		X			0.5	30.5 (12.0)	.23 (.33)	20	Significant	
		X			1.0	20.3 (8.0)	.24 (.35)	14	Slight	
		X			1.0	25.4 (10.0)	.28 (.40)	10	Excessive	
		X			1.0	15.2 (6.0)	.28 (.40)	27	Slight	
26	12	X			0.5	20.3 (8.0)			Excessive	Break at 5 Hz
		X			0.5	15.2 (6.0)	.21 (.30)	43	Significant	
		X			0.5	15.2 (6.0)			Slight	Continue to 500 Hz
			X		0.5	12.7 (5.0)	.13 (.19)	50	Significant	
			X		0.5	12.7 (5.0)	.14 (.20)	50	Significant	
			X		0.5	14.7 (5.8)	.13 (.19)	60	Significant	
			X		0.5	21.6 (8.5)	.08 (.12)	40	Significant	
28	13	X			0.5	15.2 (6.0)	.13 (.19)	13	Excessive	Break at 5 Hz
			X		0.5	16.5 (6.5)	.08 (.11)	20	No	
			X		0.5	17.8 (7.0)	.08 (.11)	20	Excessive	
			X		0.5	19.1 (7.5)	.07 (.10)	30	No	
			X		0.5	Drain		30	Excessive	
			X		0.5	26.2 (10.3)	.07 (.10)	40	Significant	
			X		0.5	28.7 (11.3)	.06 (.08)	50	Slight	
		X			0.8	15.2 (6.0)	.19 (.27)	7	Significant	
		X			0.8	10.2 (4.0)	.21 (.30)	18	Significant	
34	18	X			0.5	6.4 (2.5)	.02 (.03)	5	No	
		X			0.5	20.3 (8.0)	.10 (.15)	22	Significant	
			X		0.5	20.3 (8.0)	.08 (.12)	20	Significant	
			X		0.5	21.1 (8.3)	.08 (.11)	30	Significant	
			X		0.5	23.6 (9.3)	.06 (.09)	40	Significant	
		X			0.8	15.2 (6.0)	.10 (.15)	19	No	
		X			0.8	25.4 (10.0)			Excessive	Break at 5 Hz
		X			0.8	20.3 (8.0)			Excessive	Break at 5 Hz
		X			0.8	17.8 (7.0)			Excessive	Break at 5 Hz
		X			0.8	17.8 (7.0)			Excessive	Break at 5 Hz
36	26	X			0.5	10.2 (4.0)			No	No first mode
		X			0.5	12.7 (5.0)			Slight	No first mode
		X			0.8	10.2 (4.0)			Excessive	Break at 5 Hz

Test No.	Screen Specimen	Type of Vibration			Acceleration g Peak for Sine gRMS for Random	Ullage Height cm(in.)	Peak ΔP N/cm^2 (psi)	Frequency Hz	Breakdown	Remarks
		Sine		Random						
		Sweep	Dwell							
43 (Orientation 5)	14	X			0.5	15.2 (6.0)			No	ΔP not recorded
		X			1.0	15.2 (6.0)	.03 (.04)	5	No	
		X			2.0	15.2 (6.0)			Excessive	
		X			2.0	10.2 (4.0)	.06 (.08)	7.5	No	
		X			2.0	12.8 (5.0)	.06 (.09)	9.5	No	
		X			2.0	15.2 (6.0)	.06 (.08)	12	Significant	
		X			3.0	10.2 (4.0)	.07 (.10)	13	No	
		X			3.0	12.7 (5.0)	.08 (.12)	10	No	
			X		2.0	16.0 (6.3)	.04 (.06)	20	Significant	
			X		2.0	Drain		20		
			X		2.0	15.2 (6.0)		20		Move ΔP
46 (Orientation 5)	15	X			1.0	5.1 (2.0)	.03 (.05)	6	No	
		X			2.0	5.1 (2.0)	.05 (.07)	8	No	
		X			2.0	10.2 (4.0)	.04 (.06)	6	Excessive	Break at 6.5 Hz
		X			2.0	7.6 (3.0)	.10 (.15)	18	Slight	
			X		2.0	7.6 (3.0)	.05 (.07)	20	No	
			X		2.0	8.4 (3.3)	.05 (.07)	20	Significant	
			X		2.0	7.6 (3.0)	.02 (.03)	30	No	
			X		2.0	9.9 (3.9)	.08 (.11)	30	No	
			X		2.0	10.2 (4.0)	.08 (.11)	30	Excessive	
47 (Orientation 5)	17	X			1.0	7.6 (3.0)	.05 (.07)	7	Slight	
		X			1.0	8.9 (3.5)	.03 (.05)	7	Excessive	
		X			1.0	8.9 (3.5)	.05 (.07)	15	Excessive	
		X			2.0	7.6 (3.0)			Excessive	ΔP erratic
		X			2.0	5.1 (2.0)			Significant	ΔP erratic
			X		1.0	7.6 (3.0)		20	No	ΔP amplitude too low
			X		1.0	8.4 (3.3)		20	Significant	and erratic
			X		1.0	10.2 (4.0)		30	Excessive	
			X		1.0	9.7 (3.8)		30	Slight	
49	16	X			0.5	30.5 (12.0)			Excessive	Break at 5 Hz
		X			0.5	20.3 (8.0)	.17 (.25)	21	Excessive	
		X			0.5	15.2 (6.0)	.21 (.30)	42	Slight	
			X		0.5	24.4 (9.6)	.12 (.18)	15	Significant	
			X		0.5	24.9 (9.8)	.12 (.18)	20	Significant	

Test No.	Screen Specimen	Type of Vibration			Acceleration g Peak for Sine gRMS for Random	Ullage Height cm(in.)	Peak ΔP N/cm^2 (psi)	Frequency Hz	Breakdown	Remarks
		Sine		Random						
		Sweep	Dwell							
49	16		X		0.5	19.8 (7.8)	.16 (.23)	25	Significant	
			X		0.5	30.5 (12.0)	.08 (.12)	30	Significant	
			X		0.5	29.2 (11.5)	.08 (.11)	30	Significant	
			X		0.5	14.7 (5.8)	.21 (.31)	40	Significant	
			X		0.5	18.5 (7.3)	.17 (.25)	50	Significant	
			X		0.5	Drain		30		
		X			0.8	15.2 (6.0)	.19 (.27)	35	Excessive	
		X			0.8	10.2 (4.0)	.26 (.37)	29	Significant	
62 (Freon 113)	11	X			1.0	15.2 (6.0)			Excessive	ΔP not recorded
		X			1.0	10.2 (4.0)			Significant	ΔP not recorded
		X			1.5	10.2 (4.0)			Excessive	ΔP not recorded
63 (Freon 11)	11	X			1.0	15.2 (6.0)			Excessive	ΔP not recorded
		X			1.0	10.2 (4.0)			Significant	ΔP not recorded
		X			1.5	10.2 (4.0)			Excessive	ΔP not recorded

APPENDIX C

SYMBOLS

A	Area - m^2 (ft^2)
a,b	Screen dimensions - m (ft)
A,B	Model dimensions - m (ft)
Bo	Bond number
c	System damping - N sec/m (lbf sec/ft)
C_D	Drag coefficient
C_X, C_Y, C_Z	Flow amplification factors
f	Frequency - Hz
F	Force - N (lbf)
g	Acceleration - m/sec^2 (g)
g_{rms}	Overall gRMS level of random vibration - m/sec^2 (g)
h	Height - m (ft)
h_s	Height of screen exposed to ullage - m (ft)
k	System stiffness - N/m (lbf/ft)
L	Characteristic flow length - m (ft)
m	System mass - Kg (lbm)
M_{eff}	System effective mass - Kg (lbm)
n,K	Geometric coefficients for a particular screen
N	Number of pores
ΔP	Pressure differential - N/m^2 (lbf/ft^2)
ΔP_c	Screen bubble point with test liquid - N/m^2 (lbf/ft^2)
ΔP_d	Pressure differential due to inertia - N/m^2 (lbf/ft^2)
ΔP_f	Pressure differential due to flow - N/m^2 (lbf/ft^2)
ΔP_s	Hydrostatic pressure due to bulk liquid - N/m^2 (lbf/ft^2)

151

ΔP_t	Total pressure differential - N/m^2 (lbf/ft^2)
ΔP_v	Pressure differential due to vibration - N/m^2 (lbf/ft^2)
q	Displacement coordinate - m (ft)
q_o	Screen center displacement coordinate - m (ft)
q_1	Oscillatory vibration response coordinate - m (ft)
q_2	Liquid outflow coordinate - m (ft)
q_3	Orifice flow coordinate - m (ft)
Q	Dynamic amplification factor
r	Minimum pore radius - m (ft)
r_w, R_w	Wire radius - m (ft)
R	Bubble radius - m (ft)
R_o	Radius of the line of contact between the bubble and the screen - m (ft)
t	Time - sec
t_s	Screen thickness - m (ft)
T	Kinetic energy - Kg m^2/sec^2 (lbm ft^2/sec^2)
U	Liquid flow velocity - m/sec (ft/sec)
V	Gas flow velocity - m/sec (ft/sec)
$\mathcal{V}$	Bubble volume - m^3 (ft^3)
We	Weber number
$\ddot{X}$, $\ddot{Y}$, $\ddot{Z}$	Sinusoidal vibration input modulii - m/sec^2 (ft/sec^2)
ρ	Liquid density - Kg/m^3 (lbm/ft^3)
σ	Liquid surface tension - N/m (lbf/ft)
μ	Gas viscosity - Kg/msec (lbm/ft sec)
ω_o	System natural frequency - radians/sec
λ	Length - m (ft)
ϵ	Void fraction

APPENDIX D

REFERENCES

I-1   George F. Orton: <u>Simulated Flight Vibration Testing of a Surface Tension Propellant Expulsion Screen</u>. Master's Thesis, Saint Louis University, 1971.

I-2   G. W. Burge and J. B. Blackmon: <u>Study and Design of Cryogenic Propellant Acquisition Systems, Final Report, Volume II - Supporting Experimental Program</u>. MDC G5038. McDonnell Douglas Astronautics Company, Huntington Beach, California, December 1973.

I-3   G. R. Page: <u>Acquisition/Expulsion System for Earth-Orbital Propulsion System Study, Final Report, Volume III - Cryogenic Test</u>. MCR-75-171. Martin Marietta Corporation, Denver, Colorado, October 1973. (Contract NAS9-12182)

I-4   D. A. Fester: <u>SS/RCS Surface Tension Propellant Acquisition/ Expulsion Tankage Technology Final Report</u>. MCR-75-171. Martin Marietta Corporation, Denver, Colorado, August 1975. (Contract NAS9-13709)

I-5   J. R. Tegart: <u>The Effect of Vibration on Surface Tension Devices</u>. R-74-48602-001. Martin Marietta Corporation, Denver, Colorado, June 1974.

I-6   R. P. Warren: <u>Acquisition System Environmental Effects Study</u>. MCR-75-21. Martin Marietta Corporation, Denver, Colorado, May 1975. (Contract NAS8-30592)

II-1   D. A. Hess and G. F. Orton: <u>Space Shuttle OMS Propellant Acquisition</u>. Proceedings of the JANNAF 1975 Propulsion Meeting, Volume III, pp. 429-453.

II-2   <u>Tank Propellant - Reaction Control System</u>. MC282-0061C, Rev. D. Rockwell International Space Division, 8 June 1975 (Space Shuttle RCS Tank Specification)

II-3   C. D. Brown: <u>Viking Orbiter 1975, Propellant Management Device, Final Report</u>. SE010-47-01. Martin Marietta Corporation, Denver, Colorado, May 1973.

II-4   S. C. DeBrock and R. K. Grove: "Capillary Propellant Management for Integrated Primary and Secondary Propulsion Systems." <u>Journal of Spacecraft and Rockets</u>, May 1975, pp. 261-270.

II-5   L. T. Park and J. D. Corbin: Titan Transtage Spacecraft Propulsion System. AIAA Paper 73-1210. Presented AIAA/SAE 9th Propulsion Conference, Las Vegas, Nevada, November 1973.

II-6   M. H. Blatt and M. D. Walter: Centaur Propellant Acquisition System Study. NASA CR-134811. General Dynamics Convair Division, San Diego, California, June 1975.

II-7   R. L. Chase, M. J. Cook and D. L. Young: Planetary Mission Applications for Space Storable Propulsion. AIAA Paper 74-1178, presented AIAA/SAE 10th Propulsion Conference, San Diego, California, October 1974.

II-8   J. R. Tegart and D. A. Fester: "Space Storable Propellant Acquisition System." Journal of Spacecraft and Rockets, Vol. 12, No. 9, September 1975.

II-9   G. R. Page: Acquisition/Expulsion Orbital Propulsion System Study, Volume II, Cryogenic Design. MCR-73-97. Martin Marietta Corporation, Denver, Colorado, October 1973.

II-10 G. W. Burge, et al.: Design of Propellant Acquisition Systems for Advanced Cryogenic Space Propulsion Systems. AIAA Paper 73-1287, presented at AIAA/SAE 9th Propulsion Conference, Las Vegas, Nevada, November 1973.

II-11 J. R. Owens: Intelsat Satellite Onboard Propulsion Systems, Past and Future. AIAA Paper 76-289. Presented AIAA/CASI 6th Communications Satellite Systems Conference, Montreal, Canada, April 1976.

II-12 Baseline Space Tug Configuration Definition. MSFC 68M00039-2, NASA George C. Marshall Space Flight Center, July 15, 1974.

II-13 G. R. Page: Acquisition/Expulsion System for Earth Orbital Propulsion System Study, Volume II, Cryogenic Design. MCR-73-97, Martin Marietta Corporation, Denver, Colorado, October 1973.

II-14 G. W. Burge and J. B. Blackmon: Study and Design of Cryogenic Propellant Acquisition Systems, Volume I. Design Studies. MDC G5038, McDonnell Douglas Astronautics Company, Huntington Beach, California, December 1973.

II-15 J. F. Nichols: Study of Liquid Oxygen/Liquid Hydrogen Auxiliary Propulsion Systems for the Space Tug. NASA CR-134790, Rockwell International Corporation, Seal Beach, California, June 1975.

II-16 S. C. DeBrock: Development and Flight Experience with a Capillary Propellant Management System for a Three Axis Stabilized Vehicle. AIAA Jet Propulsion Specialists Conference, November 1972.

II-17   D. L. Balzer, et al.: The Monopropellant Hydrazine Reaction
          Control System for the RCA Globcom/RCA Alascom Communication
          Satellite (RCA Satcom). AIAA Paper 76-631, presented AIAA/SAE
          12th Propulsion Conference, Palo Alto, California, July 1976.

II-18   H. Himelblau, C. M. Fuller and T. D. Scharton: Assessment of
          Space Vehicle Aeroacoustic - Vibration Prediction, Design and
          Testing. NASA CR-1596. McDonnell Douglas Astronautics
          Company, Huntington Beach, California, July 1970.

II-19   Functional Requirement Viking Orbiter 1975 Environmental Design
          Criteria. VO75-3-240. Jet Propulsion Laboratory, Pasadena,
          California, 29 February 1972.

II-20   Rocket Engine Assembly, RCS. PD5000007. Martin Marietta
          Corporation, Denver, Colorado, July 1972 (Specification for
          Viking Lander Attitude Control Rocket Engine).

II-21   General Environmental Test Specification for Spacecraft
          Components. S-320-G-1. NASA Goddard Space Flight Center,
          Greenbelt, Maryland.

II-22   C. J. Beck, Jr. and D. N. Caba: "Vibration and Acoustic Environ-
          ment Characteristics of the Saturn V Launch Vehicle." Shock and
          Vibration Bulletin, No. 39, Part 6, March 1969.

II-23   Agena Payload Users Handbook. LMSC-A981500. Lockheed Missiles
          and Space Company, Sunnyvale, California, 1 March 1971.

II-24   F. L. Marks: Titan III Common Core Environmental Specifications.
          Martin Marietta Corporation, Denver, Colorado, January 5, 1967.

II-25   D. E. Newbrough, et al.: "Development and Verification of the
          Apollo Lunar Module Vibration Test Requirements." Shock and
          Vibration Bulletin, No. 37, Part 5, January 1968.

II-26   L. R. Pendleton: "Sinusoidal Vibration of Poseidon Solid
          Propellant Motors." Shock and Vibration Bulletin, No. 42,
          Part 3, January 1972.

II-27   J. R. Fowler and J. S. Rosenthal: Missile Vibration Environment
          for Solid Propellant Oscillatory Burning. AIAA Paper No. 71-756,
          presented AIAA/SAE 7th Propulsion Joint Specialist Conference,
          Salt Lake City, Utah, June 1971.

II-28   J. A. Schoenster and H. B. Pierce: Effects of Experimentally
          Measured Pressure Oscillations on the Vibration of a Solid
          Rocket Motor. NASA TN D6931, NASA Langley Research Center,
          Hampton, Virginia, November 1972.

II-29   Communication Technology Satellite, Qualification Test Report.
         Thiokol Corporation, Elkton, Maryland, July 30, 1975.

II-30   E. M. Landsbaum: Solid Motor Spacecraft Interfaces. AIAA Paper
         No. 74-1051, presented AIAA/SAE 10th Propulsion Conference, San
         Diego, California, October 1974.

II-31   Private Communication with Oren B. Phillips, Manager, Space
         Systems, Thiokol Corporation, Elkton, Maryland, June 28, 1976.

II-32   B. A. Conway and T. C. Henricks: A Summary of the Skylab Crew/
         Vehicle Disturbances Experiment T-013. NASA TN D-8128, NASA
         Langley Research Center, Hampton, Virginia, March 1976.

II-33   F. T. Dodge, et al.: Fluid Physics, Thermodynamics, and Heat
         Transfer Experiments in Space. NASA CR-134742, Southwest
         Research Institute, San Antonio, Texas, January 1975.

II-34   E. C. Cady: Effect of Transient Liquid Flow on Retention
         Characteristics of Screen Acquisition Systems. NASA-CR-135218,
         McDonnell Douglas Astronautics Co., Huntington Beach, California,
         April 1977. (Contract NAS3-19719)

II-35   J. A. Stark: Low-G Fluid Transfer Technology Study. NASA
         CR-134911, General Dynamics Corporation, San Diego, California,
         May 1976.

II-36   Ivan Bekey and Harris Mayer: "1980 - 2000, Raising Our Sights
         for Advanced Space Systems." Astronautics and Aeronautics,
         July/August 1976, pp. 34-63.

II-37   Outlook for Space. NASA SP-386, National Aeronautics and Space
         Administration, January 1976.

III-1   R. P. Warren: Acquisition System Environmental Effects Study.
         MCR-72-21, Martin Marietta Corporation, Denver, Colorado, May
         1975.

III-2   J. R. Tegart: Influence of Pressure Transients on the Performance
         of Capillary Propellant Acquisition Systems. AIAA Paper 76-597,
         presented AIAA/SAE 12th Propulsion Conference, Palo Alto,
         California, July 1976.

V-1   W. Lauterborn: "Numerical Investigation of Nonlinear Oscillations
         of Gas Bubbles in Liquids," J. Acoust. Soc. Am., Vol. 59, No. 2,
         February 1976, pp. 283-293.

V-2   E. C. Cady: Effect of Transient Liquid Flow on Retention
         Characteristics of Screen Acquisition Systems. Ninth Monthly
         Report, McDonnell Douglas Astronautics Company-West, Huntington
         Beach, California, April 1976. (Contract NAS3-19719)

V-3   G. R. Page, et al. <u>Acquisition/Expulsion System for Earth Orbital Propulsion System Study. Volume III, Cryogenic Test.</u> MCR-73-97, Martin Marietta Corporation, Denver, Colorado, October 1973. (Contract NAS9-12182)

V-4   <u>Freon Product Information.</u> B-2, E. I. duPont deNemours and Co., Wilmington, Delaware, 1969.

V-5   E. C. Cady: <u>Design and Evaluation of Thermodynamic Vent/Screen Baffle Cryogenic Storage System.</u> NASA CR-13480, McDonnell Douglas Astronautics Co., Huntington Beach, California, June 1975.

V-6   P. E. Bingham and J. R. Tegart: <u>Wicking in Fine Mesh Screens.</u> AIAA Paper 77-849, presented AIAA/SAE 13th Joint Propulsion Conference, Orlando, Florida, July 1977.

A-1   J. C. Armour and J. N. Cannon: "Fluid Flow through Woven Screens." <u>AIChE Journal</u>, Vol. 14, No. 3, May 1968, pp 415-420.

A-2   E. C. Cady: <u>Study of Thermodynamic Vent and Screen Baffle Integration for Orbital Storage and Transfer of Liquid Hydrogen.</u> NASA CR-134482, McDonnell Douglas Astronautics Company, Huntington Beach, California, August 1973.

A-3   B. B. Mikic, W. M. Rohsenow and P. Griffith: "On Bubble Growth Rates." <u>Int. J. Heat Mass Transfer</u>, Vol. 13, pp 657-666, 1970.

A-4   C. P. Nitze, V. E. Schrock and P. L. Chambre: "Flow about a Growing Sphere in Contact with a Plane Surface." <u>Int. J. Heat Mass Transfer</u>, Vol. 11, pp 1637-1652, 1968.

A-5   H. Schlichting. <u>Boundary Layer Theory.</u> McGraw-Hill Book Company, 1960, page 16.

A-6   D. W. VanKrevelen and P. J. Hoftijzer: "Studies of Gas Bubble Formation." <u>Chemical Engineering Progress</u>, Vol. 46, No. 1, 1950, pp 29-35.

A-7   E. Silberman: <u>Production of Bubbles by the Disintegration of Gas Jets in Liquid.</u> Proceedings of the Fifth Midwestern Conference on Fluid Mechanics, University of Michigan Press, April 1957.